Selection of the Liquid Desiccant in a Run-Around Membrane Energy Exchanger

A Thesis Submitted to the College of

Graduate Studies and Research

In Partial Fulfillment of the Requirements

For the Degree of Master of Science

In the Department of Mechanical Engineering

University of Saskatchewan

Saskatoon

By

Mohammad Afshin

Permission to Use

In presenting this thesis in partial fulfillment of the requirements for a Postgraduate degree from the University of Saskatchewan, I agree that the Libraries of this University may make it freely available for inspection. I further agree that permission for copying of this thesis in any manner, in whole or in part, for scholarly purposes may be granted by the professor or professors who supervised my thesis work or, in their absence, by the Head of the Department or the Dean of the College in which my thesis work was done. It is understood that any copying or publication or use of this thesis or parts thereof for financial gain shall not be allowed without my written permission. It is also understood that due recognition shall be given to me and to the University of Saskatchewan in any scholarly use which may be made of any material in my thesis.

Requests for permission to copy or to make other use of material in this thesis in whole or part should be addressed to:

Head of the Department of Mechanical Engineering

University of Saskatchewan

Saskatoon, Saskatchewan (S7N 5A9)

ABSTRACT

In this thesis, several possible liquid desiccants (aqueous solutions of LiCl, LiBr, $MgCl_2$ and $CaCl_2$) are investigated to find the most appropriate working fluid to be used in a run-around membrane energy exchanger (RAMEE). The liquid desiccant is one of the main components of the RAMEE and indirectly conditions the outdoor ventilation air by using the energy of the exhaust air, significantly reducing the building energy consumption.

Numerical simulations, in this thesis, show that the total effectiveness of the RAMEE changes less than 0.5% when different salt solutions are used. However, the capital and operational costs of the RAMEE are significantly different for different desiccants. $MgCl_2$ is the most inexpensive among the selected salt solutions and is followed by $CaCl_2$, LiBr and LiCl. The price of a LiCl solution in the RAMEE is almost 20 times more than the price of $MgCl_2$ solution. Different thermo-physical properties of the salt solutions result in different pumping energy consumptions for each specific salt solution. For example, the pumping energy consumption for a $MgCl_2$ solution is 3.5 times more than for a LiBr solution in the RAMEE. The change in the volume of the liquid desiccant throughout a year is another characteristic which depends on the thermo-physical properties of the salt solution. Solutions with larger volume expansion require larger storage tanks and will experience longer transient delays. The difference between the volume expansions of different salt solutions is less than 5% of the total solution volume. $MgCl_2$ solution expands more than 17% throughout a yearly operation of the system in Saskatoon.

Crystallization of the salt solution is another important parameter in the selection of the liquid desiccant. Simulations show that, for a specific indoor and outdoor operating condition the risk of crystallization is greatest for $MgCl_2$, followed by $CaCl_2$, LiCl and LiBr. The risk increases as the supply or exhaust airstreams become dryer. For a cross flow RAMEE with a total effectiveness of 55% (NTU=10 and Cr*=3) operating in a building with indoor RH of 50%, the critical outdoor humidity below which crystallization will begin to occur is 28% RH for $MgCl_2$, 20% for $CaCl_2$ and 0%RH for LiCl and LiBr. According to the simulations, all four investigated salt solutions can be used in North America (except the states of Nevada, Arizona, New Mexico and parts of Texas) with no risk of crystallization when the indoor humidity is 50% RH. However, with indoor humidity of 30% $MgCl_2$ and $CaCl_2$ solutions will have risk of crystallization for a large number of hours in a year in most of the central western United States. A mixture of 50% LiCl and 50% $MgCl_2$ solution is suggested to be used when the cost-effective $MgCl_2$ solution cannot be used due to crystallization issues. The price of this newly suggested mixture is 30% less than that of a pure LiCl solution and can be used in all North American climates with very small risk of crystallization.

ACKNOWLEDGEMENTS

I would like to thank my supervisors, Prof. Simonson and Prof. Besant for their support and guidance. I also wish to thank Dave Deutscher and Rick Retzlaff for their help in the experiments of this project.

I would like to acknowledge the financial support from the Natural Sciences and Engineering Research Council of Canada (NSERC) and Venmar CES, Saskatoon.

DEDICATION

I dedicate this thesis to my family that never stopped their support.

TABLE OF CONTENTS

Page

LIST OF TABLES

Table **Page**

LIST OF FIGURES

Figure **Page**

NOMENCLATURE

Acronyms

AHRI	Air-Conditioning, Heating and Refrigeration Institute
ASHRAE	American Society of Heating, Refrigerating and Air-Conditioning Engineers
CRD	Collaborative Research and Development
ERV	energy recovery ventilator
HRV	heat recovery ventilator
HVAC	Heating, Ventilating and Air-Conditioning
IAQ	indoor air quality
LAMEE	Liquid-to-Air Membrane Energy Exchanger
LDAC	Liquid Desiccant Air Conditioner
NFPA	National Fire Protection Agancy
NSERC	National Science and Engineering Research Council of Canada
RAHE	Run-Around Heat Exchanger
RAMEE	Run-Around Membrane Energy Exchanger
RH	Relative Humidity

English Symbols

A	membrane surface area, m^2
C_{Sol}	heat capacity rate of the salt solution, W/K
C_{Air}	heat capacity rate of the air, W/K
C_p	specific heat capacity, J/(kg·K)
C_{p0}	specific heat capacity of water, J/(kg·K)
Cr*	ratio of solution to air heat capacity rates
C	concentration of salt solution (kg of salt per kg of solution), %

D	diffusion coefficient, m^2/s
D_0	self diffusion coefficient of water, m^2/s
D_h	hydraulic diameter, m
D_p	pipe diameter, m
Dev	deviation between experimental and calculated values
d_{Air}	air channel thickness, m
d_{Sol}	solution channel thickness, m
h_{Air}	convective heat transfer coefficient between the air and membrane, $W/(m^2 \cdot K)$
h_{fg}	heat of vaporization, J/(kg)
h_m	convective mass transfer coefficient, $kg/(m^2 \cdot s)$
$h_{m,Sol}$	convective mass transfer coefficient between the membrane and the solution, $kg/(m^2 \cdot s)$
h_{Sol}	convective heat transfer coefficient between the solution and the membrane, $W/(m^2 \cdot K)$
k	thermal conductivity, $W/(m \cdot K)$
k_0	thermal conductivity of water, $W/(m \cdot K)$
k_f	thermal conductivity of fluid, $W/(m \cdot K)$
k_m	membrane water vapor permeability, $kg/(m \cdot s)$
L_p	pipe length, m
$\dot{m}$	mass flow rate, kg/s
$\dot{m}''$	mass flux rate of water, $kg/(m^2 \cdot s)$
NTU	number of transfer units
P	pressure, kPa
P_{atm}	atmospheric pressure, kPa
$\dot{q}''$	heat flux rate, W/m^2

T	bulk mean temperature, K
$T_{Sol,Mem}$	temperature of the solution at the membrane surface, K
t	temperature, ˚C
U	overall heat transfer coefficient, $W/(m^2 \cdot K)$
U_m	overall mass transfer coefficient, $kg/(m^2 \cdot s)$
u	velocity in the x direction, m/s
v	velocity in the y direction, m/s
VP	Vapor Pressure, kPa
W_{Air}	air humidity ratio, $kg_{water}/kg_{dry\ air}$
$W_{Sol,Mem}$	humidity ratio of the air that is in equilibrium with the solution at the membrane surface, $kg_{water}/kg_{dry\ air}$
W_{cr}	critical humidity ratio at which a specific salt solution crystallizes, $g_{water}/kg_{dry\ air}$
x,y,z	coordinates,m
x_0,y_0,z_0	exchanger dimensions, m
x_i	size of salt solution inlet and outlet header, m
X_{Sol}	solution mass fraction (kg of water per kg of salt), kg/kg
$X_{Sol,Mem}$	solution mass fraction at the membrane surface, kg/kg

Greek Symbols

Δ	difference (change in)
δ	membrane thickness, m
ε	effectiveness
μ	viscosity, Pa·s
μ_0	viscosity of pure water, Pa·s
ρ	density, kg/m^3
ρ_0	density of pure water, kg/m^3

ρ_{salt}	density of pure salt, kg/m^3
ρ_{sol}	density of solution, kg/m^3
ψ	stream function

Subscript

Air	air stream
cal	calculated data
E	exhaust
exp	experimental data
In	inlet
Lat	latent
Mem	membrane
O	overall
Out	outlet
Outdoor	outdoor air conditions
S	supply
Salt	pure salt
Sen	sensible
Sol	solution
SS	steady state
Tot	total

CHAPTER 1

INTRODUCTION

1.1 Overview of Ventilation in Buildings

Fresh ventilation air is essential to maintain acceptable Indoor Air Quality (IAQ) in buildings. Recent research has shown that higher ventilation rates can significantly improve the health and productivity of occupants (Fanger 2006; Seppanen et al. 2006). Reducing the ventilation outdoor air in dwellings has been found to increase the risk of high occupant absenteeism or sick building syndrome (SBS) (Engvall et al. 2005; Wargocki et al. 2000) and the risk of strong allergic symptoms among children (Bornehag et al. 2004).

Building ventilation rates are selected to follow international standards. These standards have had their minimum recommended ventilation rates for buildings revised from time to time. For example, when the ASHRAE ventilation standard was revised in 1989, the minimum recommended ventilation rate was increased from 2.5 L/s per person (ASHRAE 1981) to 10 L/s per person (ASHRAE 1989). This four times increase in the minimum ventilation rate was intended to dramatically reduce the growing fraction of buildings with significant IAQ problems caused by the 1981 standard which had reduced the value to respond a rapid rise in the cost of energy supplied to buildings. The most recent ASHRAE Standard 62.1 (2004) recommends a minimum ventilation rate of about 8.5 L/s per person for a typical office building (ASHRAE 2004). This minimum

ventilation rate is based partly on the building materials and partly on the occupancy per unit floor area.

1.2 Air-to-Air Heat/Energy Exchangers

Although higher ventilation rates improve IAQ, replacing a part of the air from the building with unconditioned outdoor air increases the energy consumption and costs of the building. Eto and Meyer (1988) investigated the HVAC capital costs and energy consumption imposed by increased ventilation rates. They reported a 0 to 20% increase in the chiller capacity and 0 to 10% increase in the boiler capacity (depending on the severity of the climate) by increasing ventilation rates from 2.5 L/s per person to 10 L/s per person. They also showed that annual heating and cooling energy consumption increased by a maximum of 8% and 14% respectively.

The increasing price of energy has drawn attention to energy recovery technologies to reduce the additional costs imposed by ventilation. Air-to-air energy recovery systems use waste energy from the airstream leaving the building (i.e., exhaust air) to pre-condition the outdoor ventilation air and can significantly reduce the HVAC life-cycle costs of buildings (Fauchoux et al. 2007 and 2009; Asiedu et al. 2005). Energy recovery may reduce, on average, one third of the total annual energy costs of a building (Zhang et al., 2000; and Dieckmann, 2008). Besant and Simonson (2003) also showed that the annual cooling and heating energy consumption can be reduced by 31% and 64%, respectively, by using energy recovery systems in an example building in Chicago.

Air-to-air recovery systems can be categorized into two major groups based on their ability to transfer sensible or latent heat: (1) devices only capable of transferring

sensible heat or heat recovery ventilators (HRVs), and (2) devices which can transfer both moisture and heat (i.e., enthalpy), also known as energy recovery ventilators (ERVs). Flat plate heat exchangers, heat pipes, heat wheels, run-around coil-to-coil loops, and thermosiphons are common commercially available HRVs and energy (enthalpy) wheels, hygroscopic fixed-plate exchangers and twin tower enthalpy recovery loops are the major ERVs available in the market.

Larson (2006) classified heat and energy recovery systems based on the type of heat or energy exchanged and the location of the supply and exhaust ducts. Heat and energy devices that require adjacent supply and exhaust ducts (e.g. fixed plate exchangers and energy wheels), are well suited to most new buildings, while other exchangers that allow the ducts to be located remotely (e.g. twin tower enthalpy loops and run-around heat exchangers) may be better suited to retro-fit existing buildings and for new buildings where contaminant control is very important (e.g. hospitals and laboratories).

1.2.1 Ideal Air-to-Air Energy Exchangers

An ideal air-to-air energy exchanger is the one that allows temperature driven heat transfer between the supply and exhaust airstreams as well as partial pressure driven moisture transfer between the two airstreams and also minimizes the cross leakage (cross-contamination) from the exhaust to supply stream (ASHRAE, 2008). Cross-contamination needs to be avoided specially in applications, such as hospitals, laboratories and clean rooms where it may cause severe health problems to the occupants or damage to the materials being processed in the clean rooms. In addition, an ideal energy recovery device should allow the supply and exhaust air ducts to be

located remotely. Devices with remote supply and exhaust exchangers may be utilized in retro-fit applications with minimal re-ducting expenses. Retro-fit applications could be a large growth area for the energy exchanger market since the replacement rate of buildings is typically less than 3% for the entire building stock in North America.

Heat/energy exchangers available in the market, each have specific advantages and disadvantages and have to be selected carefully according to the application requirements. Currently available energy exchangers as well as their advantages and disadvantages are presented in the following sections.

1.2.2 Fixed-Plate Exchangers

Fixed-plate exchangers consist of a series of flat plates that are arranged to form air channels as shown in Figure 1.1. Supply and exhaust airstreams flow in a cross-flow pattern through adjacent channels separated by thin plates. Plates that separate the airstreams are either smooth or made from corrugated materials (Kakac and Liu 2002). Plate spacing varies from 2.5 mm to 12.5 mm depending on the size of the exchanger, flow requirements and applications of the system (ASHRAE 1996). Aluminum and polymer plastics are the most commonly used materials for the plates in these heat exchanger. The separating plates may be chosen from micro-porous permeable polymer materials so moisture as well as heat can be transferred between the airstreams. Such hygroscopic membranes are hydrophilic so they can diffuse both liquid water and vapor across the membrane. They are chosen to maximize moisture transfer and minimize the air transfer due to air pressure differences across the membrane. This type of membrane will have somewhat different air transfer properties when the membrane is dry due to dry air inlet conditions than when it is wet due to high inlet air humidities. Suitable

membranes include cellulose, polymer and other synthetic materials such as hydrophilic electrolytes (ASHRAE 2008).

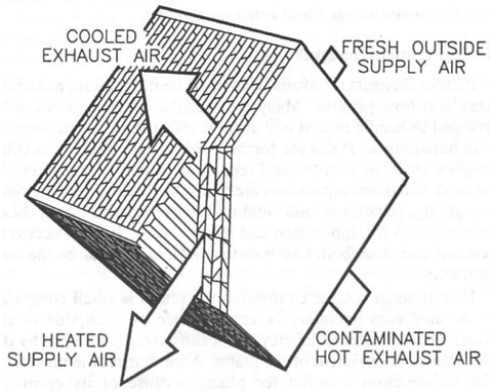

Figure 1.1: Fixed-plate heat exchanger ("Copyright©2010, ASHRAE (www.ashrae.org)" used with permission)

In a fixed-plate heat exchanger, heat transfers only through a primary membrane surface area so the total heat transfer resistance between the two airstreams is due to the membrane and the boundary layers in the supply and exhaust airstreams. Therefore, the sensible energy exchange effectiveness of such exchangers can be high (e.g. up to 75% for a cross-flow exchanger).

While fixed-plate exchangers with impermeable plates (e.g. aluminum) can only transfer heat, exchangers with hygroscopic membranes transfer both heat and moisture. Hygroscopic plate exchangers may recover almost 6 times more waste energy than sensible fixed-plate exchangers during hot and humid weather conditions (Niu and Zhang 2001). However, cross-contamination of the supply air may increase by up to 5% when hygroscopic membranes are used in place of impermeable membranes.

The supply and exhaust air ducts need to be adjacent to each other in a fixed plate heat exchanger. Also the pressure difference across the exchanger membranes has to be limited for some designs, especially if the membranes are hydrophilic.

1.2.3 Heat and Energy Wheels

Heat and energy wheels are rotating air-to-air energy exchangers that transfer heat/energy between two different airstreams. A schematic of a typical energy wheel is shown in Figure 1.2(a). Supply and exhaust airstreams, each flow through one-half of the wheel core, known as the wheel matrix (shown in Figure 1.2(b)), in a counter-flow configuration. Aluminum is the most commonly used material to make the wheel matrix, however, other materials such as, ceramics, plastic, paper and synthetic fiber may also be used for specific applications (Simonson 2007). The wheel matrix is often made of corrugated materials, as shown in Figure 1.2(b), to form small (1.5 to 2 mm) air channels and increase the heat/mass transfer surface area (ASHRAE 1996). A typical heat/energy wheel has 3000 to 4500 m^2 of contact surface area per m^3 of the wheel (Shang and Besant 2008). In an energy wheel, matrix materials are coated with desiccants (such as, zeolite, molecular sieve, silica gel and activated alumina) so moisture is transferred between the airstreams as well as heat.

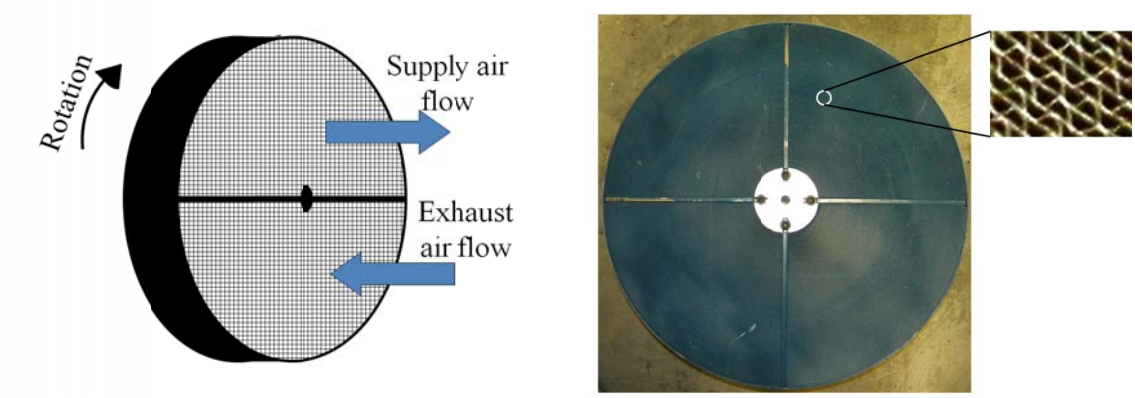

(a) (b)

Figure 1.2: (a) Schematic of a heat/energy wheel, and (b) picture of a wheel matrix.

In heat wheels, heat is transferred from the high temperature airstream to the matrix material in one-half of the wheel. As the wheel rotates, in the other half, the cool

air flows through the matrix resulting in the rejection of heat to the cool airstream. Energy wheels operate very similar to the heat wheels with the difference that they also transfer moisture between the airstreams. In an energy wheel, moisture is transferred from the humid airstream to the desiccant coating of the matrix and is later removed by the dry airstream on the other side. Energy wheels are the most commonly used energy exchangers in buildings because of their high effectiveness. Effectiveness of the energy wheels for commercial use ranges from 50 to 85% (Simonson 2007).

One of the main disadvantages of heat/energy wheels is that they transfer some air between the supply and exhaust airstreams. Air transfer occurs due to air leakage around seals and carryover of the air contained in the wheel as it rotates from the exhaust airstream to the supply airstream (ASHRAE 1996). However, carryover may be reduced significantly by installing a purge section on the wheel (ASHRAE 2008). Another disadvantage of heat/energy wheels is that supply and exhaust ducts need to be adjacent to each other. Therefore, heat/energy wheels are not ideal for retro-fit applications.

1.2.4 Run-Around Heat Exchangers

Run-around heat exchangers (RAHEs) comprise of two or more liquid-to-air heat exchangers which are thermally connected by a glycol-water solution (Gabriel 2007). Supply and exhaust heat exchangers may be placed in different locations in a RAHE which allows this device to be utilized in retro-fit applications or where complicated ducting systems are required (e.g. large buildings). Having completely separate heat exchangers in a RAHE also eliminates the chances of cross-contamination of the supply air.

The performance of a RAHE depends on several parameters such as the design and geometry of the exchangers, liquid and air flow rates and thermal characteristics of the coupling liquid (Gabriel 2007; Vali et al. 2009). The overall sensible effectiveness of a run-around heat recovery loop is typically between 45 to 65% (ASHRAE 2008). However, using two phase liquid-gas flow as the coupling fluid in the tubes is found to improve the heat transfer in the exchangers and increase the overall effectiveness of the system (Zeng et al. 1992).

RAHEs are only capable of transferring sensible heat between the airstreams since their heat exchangers are manufactured by impermeable materials (e.g. aluminum). In addition, the low sensible effectiveness of this type of heat exchangers compared to other energy exchangers limits their use in HVAC applications.

1.2.5 Thermosiphons and Heat Pipe Heat Exchangers

A typical thermosiphon loop (as shown in Figure 1.3) consists of a series of evacuated tubes, containing a small amount of a working liquid (e.g. water), connected with pipes. Hot air flows through one set of the tubes (evaporator) causing the liquid to evaporate and to move to the cold side (condenser) where it condenses. Condensed vapor, then, returns to the evaporator by gravity. A considerable amount of heat can be transferred between the two airstreams because of large latent heat of vaporization of the working fluid (Reay and Kew 2006).

Operation of the thermosiphons depends on nucleate boiling of the working fluid. Therefore, their performance is highly affected by the temperature difference between the two airstreams. However, their effectiveness is generally less than 60%. (ASHRAE 1996). One advantage of thermosiphon loops over other coil energy

recovery loops is that thermosiphons do not require pumps (external power) in order to circulate the working fluid.

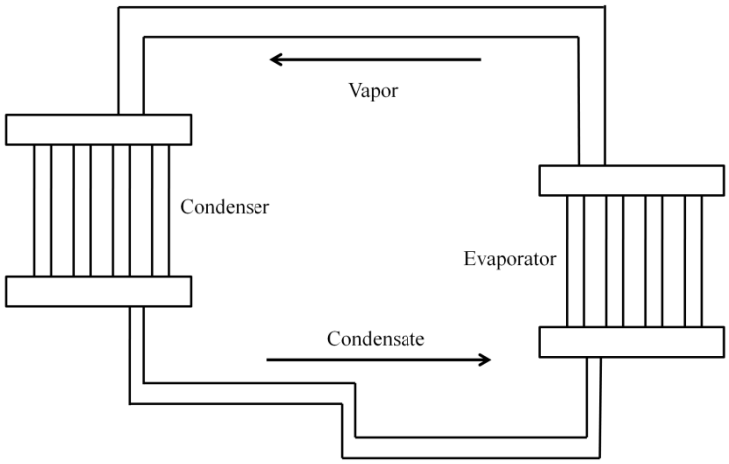

Figure 1.3: Schematic of a thermosiphon loop.

Heat pipes differ from thermosiphons only in a wicking structure, fixed to their inside surface. In heat pipes the condensate returns to evaporator through the wick by capillary forces. The performance of a heat pipe depends on the latent heat of evaporation, surface tension, thermal conductivity and dynamic viscosity of the working fluid and the type of the wick structure (Naterer 2007).

Low effectiveness and very high manufacturing costs of the thermosiphones and the heat pipe heat exchangers make them unlikely choices for energy recovery applications.

1.2.6 Twin Tower Enthalpy Recovery Loops

Similar to RAHEs, twin tower enthalpy recovery loops consist of two exchangers coupled with a working fluid. The main advantage of twin tower enthalpy systems over RAHE is their ability to transfer moisture. Liquids with hygroscopic

properties (i.e., liquid desiccants, such as LiCl-water solution) are used as the working fluid in a twin tower loop. In a twin tower enthalpy loop, the liquid desiccant is continuously pumped between two supply and exhaust contactor towers. In each contactor tower, the liquid desiccant comes in direct contact with the supply and exhaust airstreams so moisture and heat are transferred between the air and the liquid. Although direct contact between the air and liquid streams significantly enhances heat and moisture transfer (Ali et al. 2004; Masquita et al. 2006), the supply airstream may entrain small droplets of the liquid desiccant, resulting in reduced IAQ (Dieckmann, 2008) and corrosion problems in the downstream metallic ducts (Conde 2007).

The heat and moisture exchangers in twin tower enthalpy recovery systems are completely separated and can be placed remotely. This eliminates air leakage between the supply and exhaust airstreams. However, soluble gases in the liquid desiccant may be transferred between exhaust and supply airstream in very small quantities (ASHRAE 1996). Most sorbent solutions used in twin tower systems have antibacterial characteristics. Experiments on actual twin tower systems show that almost 94% of the atmospheric bacteria are removed in twin tower enthalpy loop exchangers by the liquid desiccant (ASHRAE 1996).

Although twin tower enthalpy recovery loops are the only recovery systems capable of transferring heat and moisture between two remotely located supply and exhaust exchangers, problems associated with direct contact between the airstreams and the liquid desiccant in such systems has limited their use in HVAC applications.

1.3 Run-Around Membrane Energy Exchanger (RAMEE)

The run-around membrane energy exchanger (RAMEE) is a novel energy exchanger developed to eliminate the disadvantages of other air-to-air exchangers. The RAMEE transfers heat and moisture between two different airstreams while allowing the supply and exhaust exchangers to be separated. This allows a RAMEE to be used in retro-fit applications and significantly reduces the risk of contaminant transfer between the supply and exhaust airstreams.

A schematic of a RAMEE system is shown in Figure 1.4. The main parts of a RAMEE are two liquid-to-air membrane energy exchangers (LAMEEs), two small centrifugal pumps, and two liquid desiccant storage tanks. Heat and moisture are transferred between the air and liquid streams in the LAMEEs. As shown in Figure 1.5, each LAMEE is made up of several air and liquid flow channels, separated by semi-permeable membranes. Semi-permeable membranes allow water vapor to transfer through the membrane but prevent liquid transfer (Larson et al. 2006).

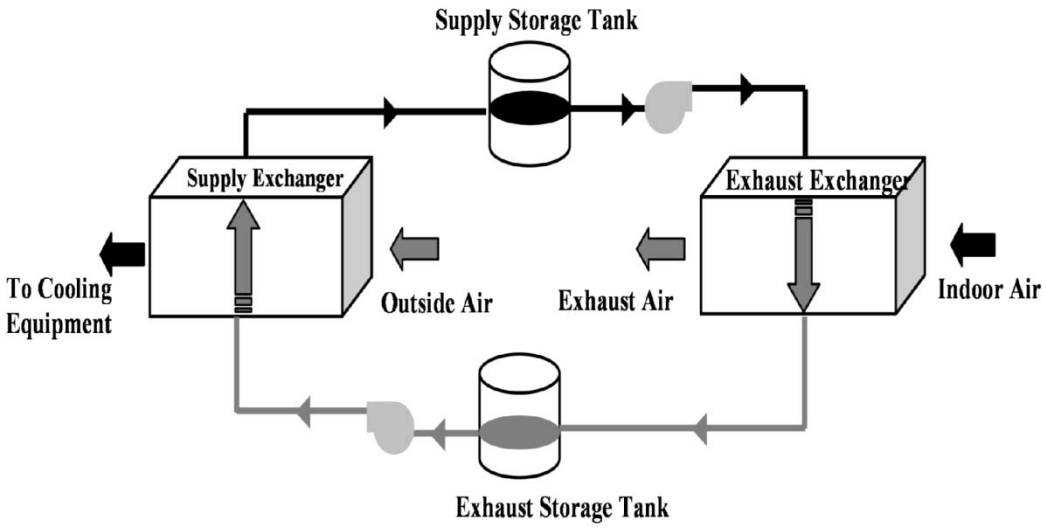

Figure 1.4: Schematic of a Run-Around Membrane Energy Exchanger (RAMEE) system.

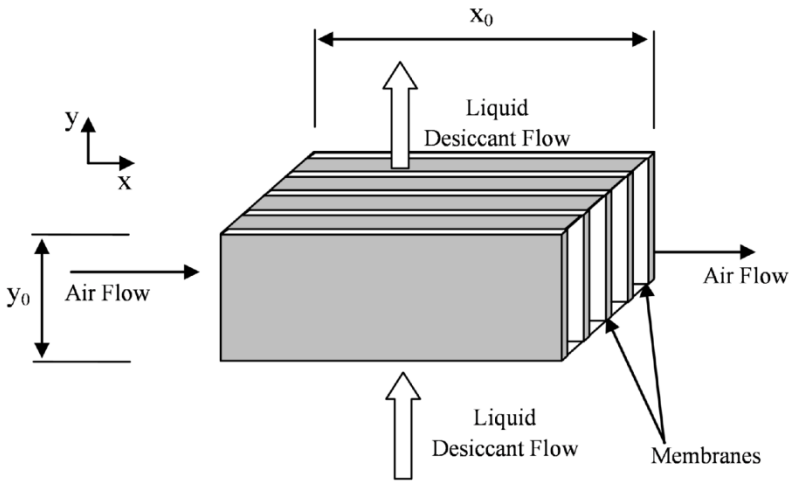

Figure 1.5: Schematic of a Liquid–to-Air Membrane Energy Exchanger (LAMEE).

During summer operating conditions, the desiccant in the supply LAMEE absorbs heat and moisture from the hot and humid outdoor ventilation air and leaves the supply exchanger as a warm and dilute solution. Therefore, the supply air becomes cooler and dryer as it flows through the exchanger. Warm and dilute liquid desiccant then flows to the supply storage tank where it is pumped to the exhaust LAMEE. In the exhaust exchanger, the desiccant solution loses heat and moisture to the cool and dry indoor air that is exhausted from the building. Therefore, the solution is regenerated (cooled and concentrated) in the exhaust exchanger. The loop repeats by pumping cool and concentrated liquid desiccant to the supply exchanger. A similar process happens during winter operating conditions with the difference that, during the winter, the outside air is dry and cold, so the liquid desiccant will lose moisture and heat in the supply exchanger and gain moisture and heat in the exhaust exchanger.

1.3.1 Background of the RAMEE Project

Several graduate students (6 completed and 6 current) have studied different design characteristics of the RAMEE system since Professors Simonson and Besant

were awarded an NSERC Collaborative Research and Development (CRD) grant to investigate this system in 2002. The following sections introduce the previous investigations done on the RAMEE system in this research group.

1.3.1.1 First RAMEE Numerical Simulation (Fan, 2005)

Fan (2005) simulated the RAMEE system with two cross flow energy exchangers coupled with a Lithium Bromide solution using the finite difference method. The temperature and humidity distributions in the air and liquid desiccant channels of the exchangers were determined as well as the latent and sensible effectivenesses. Simulations showed that a total effectiveness of 70% is achievable by the RAMEE.

1.3.1.2 Prototype I (Hemingson, 2005)

Based on the promising results of Fan (2005), Hemingson (2005) designed and built the first prototype in the thermal sciences laboratory at the University of Saskatchewan. Some design problems were noticed during the testing of this prototype, including deflection of the membrane and LAMEE structure, high air permeability and low liquid penetration pressure of the membrane. Deflection of the membrane resulted in blocking of some air flow channels at high liquid pressure. At low liquid pressures, however, the high air permeability of the membrane caused air flow to the liquid channels. The low liquid penetration pressure of the membrane caused the liquid desiccant to leak through the membrane and into the airstreams.

1.3.1.3 Membrane Research (Larson, 2006)

Larson (2006) investigated several available membranes to find a more appropriate membrane for the RAMEE. He measured some of the important membrane characteristics, such as, elastic properties, air and water vapor permeability and liquid

penetration pressure. His research led to the selection of Propore^{TM}, a vapor permeable but liquid resistant fabric laminated to a propylene non-woven layer. Larson's investigations also showed that the water vapor permeability values used by Fan et al. (2005) were much higher than the permeability of commercially available membranes resulting in over estimation of the effectiveness by Fan (2005).

1.3.1.4 Prototype II (Erb, 2006 and 2007)

The second RAMEE prototype was built by Erb (2006, 2007) with Propore^{TM} as the membrane and Magnesium Chloride as the coupling fluid. Prototype II had two LAMEEs with a cross-flow configuration (as did prototype I). An aluminum screen was used to support the membranes in the LAMEEs to reduce the deflection of the membrane as recommended by Larson (2006).

During testing, Erb found that the RAMEE system could take many hours to reach quasi-steady state. He also showed that the quasi-steady-state effectiveness of the system was influenced by number of transfer units (NTU) and ratio of solution and air heat capacity rates (Cr^*), as expected from the numerical results of Fan (2005). However, some discrepancies were found between the experimental and numerical results. For example, the numerical simulations showed that the effectiveness should increase as Cr^* is increased until $Cr^*=3$, where the maximum effectiveness occurs, and then decreases slightly to an asymptotic value for increasing Cr^*. However, the experimental effectivenesses increased continuously with increasing Cr^* to an asymptotic value and did not show the peak effectiveness at $Cr^*=3$.

1.3.1.5 Transient Modeling (Seyed Ahmadi, 2008)

Seyed Ahmadi (2008) numerically simulated the transient behavior of a RAMEE with two cross-flow LAMEEs and accumulated the time required for the RAMEE to return to steady state following a step change in the inlet air properties. Seyed Ahmadi found several factors which influence the transient performance of the RAMEE system. His research showed that increasing Cr^* decreases the transient time of the system, while increasing NTU increases the transient time. The volume of the liquid desiccant circulating in the system was also found to play a significant role on the transient time. The volume of the liquid desiccant in the system needs to be minimized to reduce the transient response delays. Seyed Ahmadi also showed that the heat transfer between the environment and the RAMEE system (exchangers, piping and storage tanks) could significantly change the quasi-steady-state effectiveness of the system. The initial concentration of the desiccant solution in the system is the other factor affecting the transient time of the system. Seyed Ahmadi recommended that the initial concentration of the liquid desiccant be selected very close to the expected steady-state value to reduce the transient response delays of the system.

Numerical results for the transient behavior of the RAMEE system were found to be in agreement with the experimental results of Erb (2009). The maximum average absolute differences between the numerical and experimental effectivenesses were found to be 7.5% and 10.3% for summer and winter operating conditions, respectively during the transient time duration of the experiments.

1.3.1.6 Counter/Cross-Flow LAMEEs (Vali 2009 and Mahmud 2009)

Although many of the problems with prototype I were fixed in the second RAMEE prototype, the effectiveness of the second prototype was lower than the desired effectiveness value (target of 55% to 65%). One way to enhance the effectiveness of the system is to change the flow configuration of the system (Vali, 2009). Possible flow patterns in a heat and mass exchanger are shown in Figure 1.6. RAMEE prototypes I and II were both constructed with liquid and air channels perpendicular to each other (i.e. cross-flow configuration, Figure 1.6(a)). However, studies show that exchangers with counter-flow configuration, in which, liquid and air streams flow along the same axis have better performance than the ones with cross-flow configuration. Although counter-flow exchangers perform the best, it would be very difficult, in a practical HVAC system, to separate the liquid and air streams at the ends of each counter-flow LAMEE. In order to avoid this problem, cross flow inlet and outlet headers were used on a counter/cross-flow configuration exchanger (see Figure 1.6(c)). Vali (2009) showed that using the counter/cross-flow configuration for exchangers in the RAMEE system typically would increase the effectiveness of the system by approximately 6% compared to systems with pure cross-flow LAMEEs.

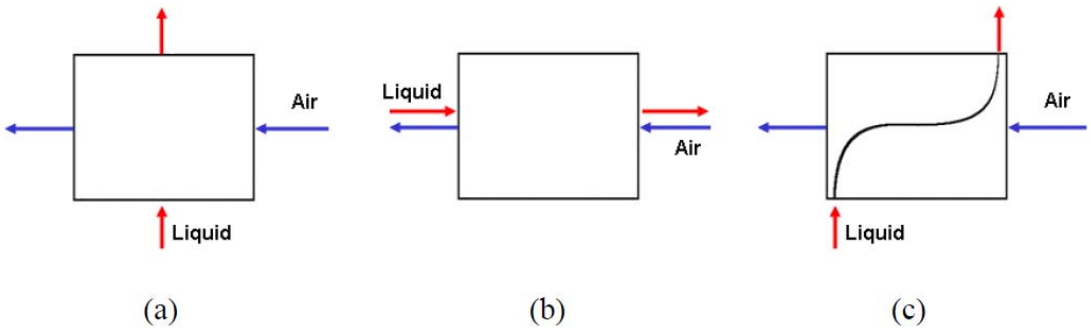

Figure 1.6: Possible air and liquid configurations in a LAMEE: (a) cross flow, (b) counter flow, and (c) counter/cross flow (Vali, 2009)

Mahmud (2009) designed, built and tested the third RAMEE prototype which consisted of two counter/cross-flow configuration LAMEEs. Discrepancies between the measured and simulated effectivenesses were between 1 to 7% (absolute) for the test data of Mahmud (2009) and the numerical simulations of Vali (2009) with the experimental data usually less than the simulated effectiveness. This RAMEE prototype with counter/cross-flow exchangers (prototype III) had a 10 to 20% higher effectiveness compared to the previous prototype (prototype II)).

1.3.1.7 Operational Control Strategies (Erb, 2009)

Erb (2009) investigated different control strategies to minimize the system transient delays during both RAMEE start-up and changing outdoor weather conditions. Both temperature and concentration control were investigated to reduce the transient delay. This control system would add water to the liquid desiccant when concentration of the coupling salt solution needed to be reduced (e.g. for the case when moisture should be added to the supply air). If the solution concentration needed to be increased, heat would be added to the desiccant in the exhaust storage tank to increase the moisture removal from the desiccant in the exhaust exchanger. This control system is expected to reduce the transient delay by up to 90% compared to a passive system with no control.

1.3.1.8 Liquid Desiccant Research

The RAMEE research group at the University of Saskatchewan has investigated many aspects of RAMEEs, such as membrane characteristics, flow configuration in the LAMEEs and transient and steady state behavior of the system. However, no detailed research has been done so far on the selection of the best liquid desiccant for the RAMEE system based on safety, system performance, capital costs, operating conditions and costs. Early RAMEE prototypes used LiBr solution as the coupling liquid desiccant (Hemingson, 2005), while later prototypes used $MgCl_2$ (Erb 2006; Mahmud 2009). The main reason for changing the liquid desiccant was to reduce cost since $MgCl_2$ has a lower price than LiBr. In addition to costs, there is a need to study the operational performance factors and limitations, disadvantages and advantages of different liquid desiccants which may be used in the RAMEE system. This matter will be the focus of this thesis.

1.4 Desiccants in Air Conditioning

Environmental and economical problems associated with conventional vapor compression air conditioning systems have significantly increased the use of desiccant-based air conditioning systems as a replacement. Nevertheless, desiccant air conditioning is only used in some specific applications, such as super markets, hospitals and applications where very dry supply air conditions are required, often in very humid climates (Dieckmann, 2005).

Desiccants are materials with high affinity for water vapor and water. The process of attracting water vapor by desiccants is described as either adsorption or absorption (ASHRAE 2005). During adsorption the desiccant does not chemically

change while water is added to its exposed surfaces. This process occurs in desiccants in the solid form (i.e., solid desiccants) and the desiccant remains solid while moisture is added in multi-layers of H_2O molecules on the solid surfaces. The adsorption of moisture occurs on the vast surface area of the solid desiccant. Some common solid desiccants are silica gel, activated alumina, molecular sieve (zeolite) and activated carbon.

Absorption, on the other hand, changes the desiccant as the water molecules are internally taken into the desiccant (ASHRAE, 2005). Absorption often occurs in materials called liquid desiccants. Liquid desiccants are categorized into two major groups in the dehumidification and air-conditioning industry: hygroscopic salt solutions and glycols. Hygroscopic salt solutions are mixtures of any hygroscopic salt, such as NaCl or LiCl, in water. Glycols, on the other hand, are organic compounds with a water absorption capacity. Unlike dry, solid hygroscopic salts, glycols are liquid at room temperature. Glycols have properties such as high viscosity and volatility and thus they will not be widely used in HVAC applications (Mei and Dai 2008). For example, triethylene glycol (TEG), which was once a common liquid desiccant, is now only used in very limited industrial applications as a hygroscopic solution.

Investigations into liquid desiccant-based air conditioners (LDACs) started in the 1930s and 1940s (Conde-Petit 2007). Figure 1.7 shows the schematic of one of the earliest open cycle absorption systems available in the literature (Bichowsky and Kelley, 1935). In this system the indoor air is dehumidified in a drying tower, where it is in contact with a concentrated LiCl solution. The salt solution is later pumped to a boiler where it loses moisture while being heated. Bichowsky and Kelley (1935) suggested the

use of LiCl and $CaCl_2$ solutions in open absorptive systems. Other possible desiccants such as, highly corrosive and toxic sulfuric acid would pose serious risk to the occupants of any building as well as increase the costs for corrosion protection.

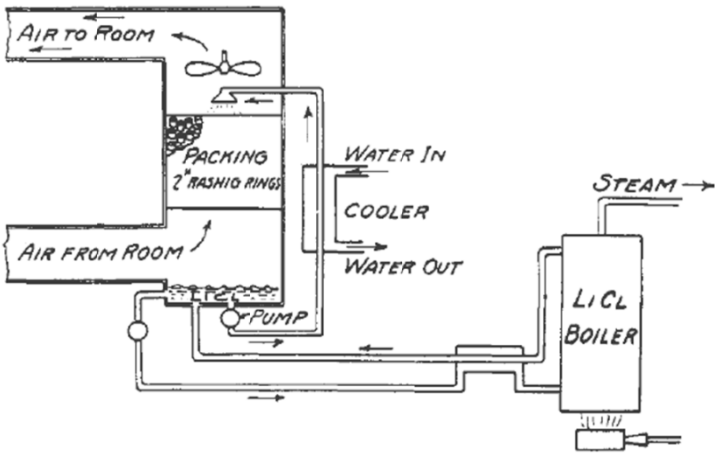

Figure 1.7: Liquid desiccant system proposed by Bichowsky and Kelley in 1935 (used with permission).

Nearly 80 years after the first investigations of liquid desiccant air conditioning systems, these systems still use the same salt solutions (Conde-Petit and Weber, 2006). However, researchers have sought to find liquid desiccants that perform better and cause less damage (e.g. corrosion) to the equipment.

1.4.1 Liquid desiccant properties

As mentioned previously, mixtures of hygroscopic salts and water are a major group of liquid desiccants and are used in HVAC applications. The addition of salt to water changes physical, thermodynamic, and transport properties of the water and these property relationships are required to investigate RAMEE performance.

Several investigations have been done to measure the properties of different salt solutions at various concentrations and temperatures. Horvath (1985) has listed several

reference books which provide the properties of aqueous electrolyte solutions. Zaytsev and Aseyev (1992) compiled values of several properties of different aqueous salt solutions such as density, viscosity, specific heat capacity, thermal conductivity, and diffusion coefficient from more than 400 previous investigations and developed correlations for some properties from experimental data. Extensive experimental and correlated data is available for thermodynamic properties of lithium halides (i.e., LiBr, LiCl, and LiI) because of their wide use in the absorption refrigeration systems (Wimbley and Berntsson 1994; Hellmann and Grossman 1996; McNeeley 1978).

Equilibrium vapor pressure at the solution-air interface is one of the most investigated properties of the salt solutions. In the RAMEE, the difference between the vapor pressure at the salt solution surface and the airstream is the reason for moisture transfer. Therefore, the equilibrium vapor pressure of a salt solution is perhaps its most important property for RAMEE research. Equilibrium vapor pressure data are available in the literature for some common absorption fluids (Boryta et al. 1975; Lenard et al. 1992; Patil et al. 1990). Cisternas and Lam (1991) developed correlations to predict the vapor pressure of aqueous and non-aqueous electrolytes. Their correlations are valid for 111 different electrolytes, and mixtures of these electrolytes in six different solvents for a range of concentrations and temperatures. Although their correlation includes almost every potential salt solution which may be used in the RAMEE system, the correlations for some of the salt solutions, such as $MgCl_2$ are limited to low concentrations. Concentration of the salt solution in the RAMEE may become very high (i.e., close to saturation) at some specific operating conditions, especially if less soluble salt solutions in water (such as $MgCl_2$ or $CaCl_2$) are used indicating a need for new research in this

area. Some other researchers have measured and correlated vapor pressure of some highly concentrated and saturated salt solutions using experimental data (Greenspan 1977).

Another important property of salt solutions is the solubility of the solute (i.e., salt) in the solvent (i.e., water). Solubility indicates the maximum amount of solute which can be dissolved in the solvent at a specific temperature and pressure. When the concentration of the salt solution equals this maximum amount, additional moisture removal causes crystallization of salt on nucleation surfaces such as salt particles and other solid surfaces. Crystallization has to be avoided in the RAMEE since salt crystals may block the solution pathways or reduce the moisture transfer and overall performance of the system. Liao and Radermacher (2007) investigated crystallization control strategies in an air-cooled absorption chiller and noted that high ambient temperatures may trigger crystallization in the system. Several researchers (Izquierdo et al. 2004; Kim and Infante Ferreira 2009) have investigated crystallization issues in solar absorption systems. Izquierdo et al. (2004) have concluded that crystallization occurs in a solar air-cooled absorptive system, with LiBr solution as the liquid desiccant, when the absorption temperature is higher than 50°C. Nonetheless, there is no specific research on the crystallization of salt solutions in membrane based HVAC units (e.g. RAMEE). In addition, operating conditions of the system play an important role on the crystallization of the salt solution in a liquid desiccant air conditioner (LDAC). Since the liquid desiccant in a RAMEE system operates in a completely different temperature range than solar absorptive systems or absorption chillers, crystallization limits will be very different for the RAMEE and need to be determined.

Mixing salt solutions is one way to get cost-effective liquid desiccants with better performance (Mei and Dai 2008). Ertas et al. (1992) investigated the properties of a mixture of Lithium Chloride and Calcium Chloride solutions and found the vapor pressure of the mixture to be lower than the vapor pressure of pure Calcium Chloride. They showed that the mixture had a 30% lower cost than a pure LiCl solution with the same equilibrium vapor pressure as a pure LiCl solution. Iyoki et al. (1990, 1993) reported thermodynamic properties of Lithium salt mixtures in water and developed correlations from experimental data. They suggested that $LiNO_3$ be added to the absorptive fluid of a chiller in order to reduce corrosion of the metallic parts, and Lithium Iodide be added for its high solubility in water. Koo et al. (1999) suggested a mixture of LiBr-$LiNO_3$-LiI-LiCl-water for small-scale absorption refrigeration systems. They also correlated density, viscosity and vapor pressure using their experimental data for the temperature range of 10-60°C. They simulated a double effect absorption chiller with their suggested solution mixture and reported no crystallization problems at higher absorption temperatures.

1.5 Thesis objectives

The main objective of this research is to identify the most appropriate liquid desiccant for the RAMEE based on a set of safety, performance and cost criteria. The following are detailed objectives of this thesis:

1- Modify the numerical model of Vali (2009) to calculate the temperature and humidity at the solution-membrane interface in the LAMEEs as this is most critical area for salt crystallization and investigate the impact of the

RAMEE operational and design characteristics on the risk of crystallization and recommend strategies to control crystallization.

2- Find the most accurate correlations available in the literature to calculate the properties of the liquid desiccants and compare the performance, initial and operational cost, and safety of different salt solutions.

3- Obtain new data for vapor pressure of mixtures of salt solutions (e.g. $MgCl_2$ and LiCl) to study the feasibility of using such salt mixtures in the RAMEE as cost-effective alternative liquid desiccant with good performance.

4- Recommend the best salt solution for a RAMEE system located in various typical cities with different climatic conditions.

1.6 Thesis overview

As mentioned in the previous sections, the RAMEE system with cross and counter/cross flow LAMEEs had been numerically simulated by other members of the research group (Vali 2009; Fan 2005). This numerical model is presented in chapter 2. The presented model is slightly modified to calculate the properties at the solution-membrane interface (**Objective 1**).

Available correlations to calculate physical and thermal properties of some selected salt solutions (LiCl, LiBr, $MgCl_2$ and $CaCl_2$) are introduced in chapter 3. Some of these correlations are compared to experimental measurements and the most accurate correlations are chosen to calculate the properties of the salt solution in the numerical model. In chapter 3, the effects of changing the salt solution on the effectiveness of the RAMEE system and operational costs (e.g. pumping power) are shown. The safety and cost of these salt solutions are also discussed in chapter 3 (**objective 2**).

The numerical model (introduced in chapter 2) is applied to investigate the risk of crystallization of the selected salt solutions in chapter 4 (**objective 1**). Different parameters affecting the risk of crystallization, such as operating conditions and design characteristics of the RAMEE system are also discussed.

Mixtures of the salt solutions are experimentally tested to measure the equilibrium relative humidity at their interface with air and the results are presented in chapter 5 (**objective 3**). Performance and cost of the mixtures are compared with single salt solutions in order to show if mixtures can be used in the RAMEE system as a cost-effective working fluid.

Finally, the research results are summarized and conclusions stated in chapter 6. Recommendations for future work are also included in chapter 6. Chapter 6 includes the final recommendations for the most appropriate salt solutions to be used in different climates in North America (**objective 4**).

CHAPTER 2

NUMERICAL MODEL

2.1 Introduction

The purpose of this chapter is to introduce the numerical model that is used in this thesis to simulate the RAMEE system. Heat and mass transfer governing equations, as well as assumptions and boundary conditions are fully described in this chapter for LAMEEs with cross and counter-cross flow configurations. The numerical model is then used to determine the temperature and humidity distributions in the air and at the solution-membrane interface in the flow channels of the LAMEEs. The temperature and humidity distributions are used in chapter 4 to predict the crystallization risk of the salt solution in the LAMEEs.

2.2 Mathematical Modeling of the RAMEE

The RAMEE system comprising two cross-flow exchangers was simulated numerically by Fan (2005). His numerical model was later modified to simulate LAMEEs with combined cross and counter flow configurations by Vali (2009). The numerical model used in this thesis to predict the crystallization of different salt solutions in the RAMEE is based on the numerical models of Fan (2005) and Vali (2009). The numerical model first finds the bulk mean flow distribution in the flow channels (for counter-cross flow configuration). The velocity distribution is then used to

calculate the temperature and humidity distributions in each liquid and air flow channel in the LAMEEs.

2.2.1 Assumptions

Several assumptions were made to reduce the complexity of the physical problem without affecting the accuracy of the calculations significantly (Vali 2009). These assumptions are as follows:

1. The liquid desiccant and air flows in the LAMEEs are assumed to be laminar, steady-state and fully developed.
2. Heat and mass transfer only occurs in the direction perpendicular to the membrane.
3. Condensation is neglected in the air channels.
4. Exchangers, storage tanks and connecting pipes are assumed to be sealed and perfectly insulated. Therefore, no heat transfer occurs between the system and the surroundings.
5. No evaporation occurs from the salt solution in the storage tanks. Mass transfer only occurs in the LAMEEs.
6. The heat of phase change of water in the exchangers is assumed to be delivered to or taken from the liquid in the exchangers.
7. All liquid and air channels in the LAMEEs are assumed to be identical. Only one air and liquid channel is simulated in this thesis for each exchanger. The effect of the channels located at the edges and malistribution of the salt solution and air flows in the exchangers are neglected.

8. The salt solution is well mixed in the storage tanks before entering each exchanger and is assumed to contain no other chemicals and impurities.
9. Heat and mass transfer properties of the membrane are independent of temperature and humidity.
10. The salt solution and the air are assumed to be in equilibrium at the solution-air interface which is located at the liquid-membrane interface.

The validity of the majority of these assumptions is discussed by Vali (2009) and Seyed Ahmadi (2008). The governing equations for solving the flow distribution, heat and mass transfer between the air and the salt solution were developed by Fan (2005) and Vali (2009) based on the assumptions listed above. Models of Fan (2005) and Vali (2009) calculate the properties of the bulk air and solution streams while the properties at the solution membrane interface are required to investigate the crystallization of salt in the system. The mathematical model described in the following sections is a modified version of Fan (2005) and Vali (2009) to calculate the liquid-membrane interface properties.

2.2.2 Flow Configurations of the LAMEEs

The flow configuration in the LAMEEs affects the heat and moisture transfer rates in the exchangers of a RAMEE which itself may affect the crystallization risk of the salt solutions in the LAMEEs. In this thesis, LAMEEs with both flow configurations are investigated for the crystallization risk in their liquid flow channels.

Figures 2.1 shows the flow distribution of the liquid desiccant in a cross flow and a counter-cross flow LAMEE. As seen in Figure 2.1(a), the liquid desiccant flows along the x-axis in a cross flow LAMEE, while the flow distribution is more complex in a

counter-cross flow LAMEE. The liquid desiccant enters the counter-cross flow LAMEE from the bottom header and leaves from the top header. The length of the headers is smaller than the total length of the exchanger. Therefore, the flow pattern is closer to counter-flow in the middle of the exchanger while it is more cross-flow close to the headers. Air flows only in the direction of y-axis in both cross flow and counter-cross flow LAMEEs to minimize the pressure drop in the airstream.

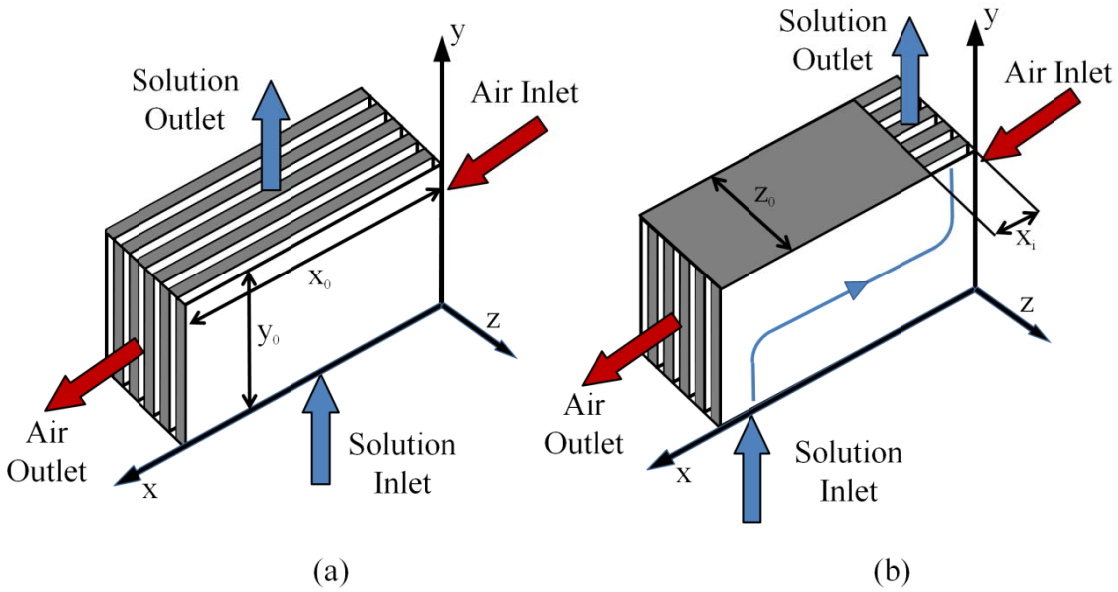

Figure 2.1: Schematic of a (a) cross flow and (b) counter-cross flow LAMEE

The velocity profile in the liquid desiccant has to be determined in order to solve the governing heat and mass transfer equations in the liquid and air channels of a LAMEE. In a cross flow configuration, the air and liquid flow through straight channels. Therefore, the streams may be considered as one dimensional flow. In the numerical model, constant velocities are inputted for the air and liquid streams and no solution is required to determine the velocity field. In a counter-cross flow LAMEE, on

the other hand, the salt solution has a two dimensional flow pattern and has to be determined numerically prior to the solution of the heat and mass transfer equations.

The salt solution flows with very low Reynolds numbers in narrow liquid channels of a counter-cross flow LAMEE. Therefore, the Navier-Stokes equations can be simplified to second order Laplace equation of the stream function (Vali 2009):

$$\frac{\partial^2 \psi}{\partial x^2} + \frac{\partial^2 \psi}{\partial y^2} = 0 \tag{2-1}$$

where ψ is the stream function. The bulk mean velocity of the salt solution may later be calculated by using the definition of the stream function:

$$u = \frac{\partial \psi}{\partial y} \tag{2-2}$$

$$v = -\frac{\partial \psi}{\partial x} \tag{2-3}$$

where u is the x component of the bulk mean velocity of the salt solution and v is the velocity component in the y direction.

2.2.3 Governing Equations of Coupled Heat and Mass Transfer in the LAMEEs

Figure 2.2 shows a control volume in a cross flow LAMEE. The control volume consists of an adjacent air and liquid channel with the separating membrane. The coordinate system is also shown in Figure 2.2. Coupled heat and mass transfer governing equations were derived using heat and mass balance equations in both air and liquid channels of the control volume shown in Figure 2.2 (Fan 2005 and Vali 2009).

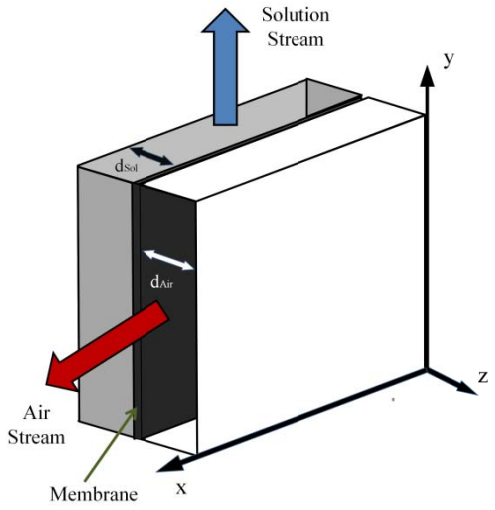

Figure 2.2: Control volume and coordinate system for the governing equations.

2.2.3.1 Conservation of Mass in the Air Channels

As air flows through the channels of a LAMEE, it transfers moisture with the adjacent liquid streams. The amount of moisture transferred through the membrane at any point (x,y) is balanced with the water vapor gain/loss in the air channel. Since the air flow distribution is the same for the LAMEEs with cross and counter-cross flow configurations, the governing equations in the air side of the channel would be the same for both flow configurations. Conservation of mass in the air channel may be expressed as:

$$\frac{2U_m y_0}{\dot{m}_{Air}}(W_{Air} - W_{Sol,mem}) = \frac{\partial W_{Air}}{\partial x} \tag{2-4}$$

where:

y_0 is the height of the LAMEE [m],

$\dot{m}_{Air}$ is the mass flow rate of the airstream in one channel [kg/s],

W_{Air} is the bulk mean humidity ratio of air at point (x,y) [kg/kg],

$W_{Sol,mem}$ is the humidity ratio of air at the solution-membrane interface [kg/kg], and

U_m is the mass transfer coefficient [kg/(m^2·s)].

The left hand side of Equation (2-4) calculates the water vapor transfer from the bulk airstream through the membrane to the solution-membrane interface. Therefore, the mass transfer coefficient may be defined as:

$$U_m = \left[\frac{1}{h_{m,Air}} + \frac{\delta}{k_m} \right]^{-1} \tag{2-5}$$

where:

$h_{m,Air}$ is the convective mass transfer coefficient of air [kg/(m^2·s)],

k_m is the water vapor permeability of the membrane [kg/(m·s)], and

δ is the thickness of the membrane [m].

Water vapor permeability (k_m) is a membrane property which depends on the shape, size and density of the membrane pores. Although the value of k_m is somewhat sensitive to temperature and humidity (Larson 2006), it was assumed to be constant in this thesis. The value of k_m used in this thesis is 1.66×10^{-6} kg/(m·K) which is based on Larson's measurements on Propore® membrane. The thickness of the membrane was also considered constant and equal to 2 mm in the numerical model.

The humidity ratio at the solution-membrane interface ($W_{Sol,mem}$) at each point (x,y) is a function of the temperature at the membrane surface and the concentration of the salt solution at that specific point:

$$W_{Sol,mem} = f(T_{Sol,mem}, C_{Sol,mem}) \tag{2-6}$$

where:

$C_{Sol,mem}$ is the concentration of the salt solution at the solution-membrane interface [$kg_{Salt}/kg_{Solution}$], and

$T_{Sol,mem}$ is the temperature at the solution-membrane interface [K].

The humidity ratio at the surface of a salt solution is one of its properties which will be discussed in detail in chapter 3 along with other properties of the salt solutions.

2.2.3.2 Conservation of Energy in the Air Channels

Similar to the conservation of mass, energy gain/loss in the air channel is balanced with the energy transfer rate through the membrane. The conservation of energy in the air channel may be expressed as:

$$\frac{2Uy_0}{C_{Air}}(T_{Air} - T_{Sol}) = -\frac{\partial T_{Air}}{\partial x} \tag{2-7}$$

where:

C_{Air} is the heat capacity rate of the air [J/(s.K)],

T_{Air} is the bulk mean temperature of air at point (x,y) [T],

T_{Sol} is the bulk mean temperature of the salt solution [K], and

U is the overall heat transfer coefficient [$W/(m^2.K)$].

The heat capacity rate of the airstream may be calculated using:

$$C_{Air} = \dot{m}_{Air}(C_{p,Air} + W_{Air}C_{p,vapor}) \tag{2-8}$$

where:

$C_{p,Air}$ is the specific heat capacity ratio of the air [J/(kg.K)], and

$C_{p,vapor}$ is the specific heat capacity ratio of the water vapor [J/(kg.K)].

The overall heat transfer coefficient accounts for the overall resistance of the air, membrane and the salt solution to the heat flux and therefore may be defined as:

$$U = \left[\frac{1}{h_{Air}} + \frac{\delta}{k} + \frac{1}{h_{Sol}} \right]^{-1} \tag{2-9}$$

where:

h_{Air} is the convective heat transfer coefficient of the air [W/(m^2.K)],

k is the membrane thermal conductivity [W/m·K], and

h_{Sol} is the convective heat transfer coefficient of the salt solution[W/(m^2.K)].

The temperature and humidity at the solution-membrane interface are calculated using the heat and mass flux balance in a control volume on the membrane surface, as shown in Figure 2.3 (Hemingson 2010). The heat balance may be expressed as:

$$\dot{q}" = \frac{T_{Air} - T_{Sol,mem}}{\left(h_{Air}\right)^{-1} + \left(\frac{k}{\delta}\right)^{-1}} + \frac{W_{Air} - W_{Sol,mem}}{\left(h_{m,Air}\right)^{-1} + \left(\frac{k_m}{\delta}\right)^{-1}} h_{fg} = h_{Sol}\left(T_{Sol,mem} - T_{Sol}\right) \tag{2-10}$$

The mass flux balance is based on the assumptions that porous membranes contain still air and that the solution-air interface is on the solution side of the membrane (i.e., at the solution-membrane interface):

$$\dot{m}'' = \frac{W_{Air} - W_{Sol,mem}}{\left(\frac{1}{h_{m,Air}}\right)^{-1} + \left(\frac{k_m}{\delta}\right)^{-1}} = h^{c}_{m,Sol}\left(C_{Sol} - C_{Sol,mem}\right) \tag{2-11}$$

where:

$\dot{m}"$ is the mass flux rate of water vapor through the membrane [kg/(m^2·s)],

$\dot{q}''$ is the heat flux rate through the membrane [W/m^2],

C_{Sol} is the bulk concentration of the solution [$kg_{Salt}/kg_{Solution}$],

h_{fg} is the heat of vaporization [m^2/s^2], and

$h^{c}_{m,\,Sol}$ is the convective mass transfer coefficient of solution based on concentration gradient [$kg/(m^2 \cdot s)$].

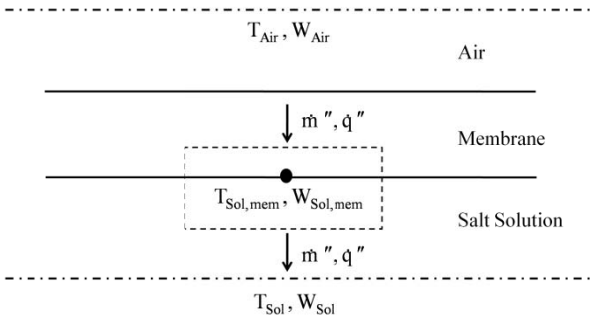

Figure 2.3: Control volume at the solution-membrane interface of two adjacent liquid and air channels.

Equations (2-4), (2-7), (2-10) and (2-11) are coupled and are solved iteratively to find the temperature and concentration at the solution-membrane interface. These values may be used in Equation (2-4) to find the humidity at the solution-membrane interface (Hemingson 2010).

In order to calculate the overall heat and mass transfer coefficients in equations (2-5) and (2-9), the convective heat and mass transfer coefficients (h and h_m) are required. The Nusselt number for laminar, fully developed flow between two infinite, rectangular parallel plates may be assumed constant and equal to 8.24 (Incropera and Dewitt 2002). Therefore the convective heat transfer coefficient may be found from the definition of Nusselt number:

$$Nu = \frac{h}{k_f D_h} = 8.24 \tag{2-12}$$

where:

k_f is the thermal conductivity of the fluid [W/(m·K)], and

D_h is the hydraulic diameter of the channel [m]

The convective mass transfer coefficient can also be found from an analogy between the heat and mass transfer coefficients (Incropera and Dewitt 2002):

$$\frac{h}{h_m} = \rho c_p Le^{2/3} \tag{2-13}$$

where Le is the Lewis number and is defined as the ratio of thermal diffusivity of the fluid to its mass diffusivity. From Equation (2-13), the $h^c_{m,Sol}$ becomes:

$$h^c_{m,Sol} = \rho h_{m,Sol} = c_p Le^{2/3} \tag{2-14}$$

2.2.3.3 Conservation of Mass in the Liquid Channels

The conservation of mass equation for the liquid stream is similar to the mass conservation equation for the airstreams. The change in the moisture content of the salt solution, flowing in one channel of a LAMEE, is equal to the moisture transfer through the membrane. The conservation of mass for the liquid stream in a LAMEE with cross flow configuration then becomes:

$$\frac{2U_m x_0}{\dot{m}_{Salt}}(W_{Air} - W_{Sol,mem}) = \frac{\partial X_{Sol}}{\partial y} \tag{2-15}$$

where:

$\dot{m}_{Salt}$ is the mass flow rate of the salt [kg/s],

x_0 is the total length of the exchanger [m], and

X_{Sol} is the mass fraction of the solution [kg_{Water}/kg_{Salt}]

The equation of the conservation of mass in a liquid channel of a counter-cross flow LAMEE may be expressed as:

$$2U_m(W_{Air} - W_{Sol,mem}) = \rho_{Salt} d_{Sol}(u_{Sol}\frac{\partial X_{Sol}}{\partial x} + v_{Sol}\frac{\partial X_{Sol}}{\partial y}) \quad (2\text{-}16)$$

where:

ρ_{Salt} is the density of the pure salt [kg/m^3],

d_{Sol} is the thickness of the liquid channel [m],

u_{Sol} is the x-component of the bulk mean velocity of the salt solution [m/s], and

v_{Sol} is the y-component of the bulk mean velocity of the salt solution [m/s].

The relation between the mass fraction of the salt solution (X_{Sol}) and the concentration of the salt in the solution may be expressed as:

$$C_{Sol} = \frac{1}{1 + X_{Sol}} \quad (2\text{-}17)$$

2.2.3.4 Conservation of Energy in the Liquid Channels

The energy transferred through the membrane is balanced by the heat gain/loss to/from the salt solution and the heat released due to the evaporation of water. The energy equation in a liquid channel of a cross flow exchanger then becomes:

$$\frac{2Ux_0}{(\dot{m}C_p)_{Sol}}(T_{Air} - T_{Sol}) + \frac{2U_m x_0}{(\dot{m}C_p)_{Sol}}(W_{Air} - W_{Sol,mem}) \cdot h_{fg} = \frac{\partial T_{Sol}}{\partial y} \quad (2\text{-}18)$$

where:

$C_{p,Sol}$ is the heat capacity rate of the salt solution [J/(s·K)]

For a liquid stream flowing in the channels of a counter-cross flow LAMEE, the flow distribution is two dimensional and the energy equation may be written as (Vali 2009):

$$2U(T_{Air} - T_{Sol}) + 2U_m(W_{Air} - W_{Sol,mem}) \cdot h_{fg} = (\rho C_p d)_{Sol}\left(u_{Sol}\frac{\partial T_{Sol}}{\partial x} - v_{Sol}\frac{\partial T_{Sol}}{\partial y}\right) \qquad (2\text{-}19)$$

where:

ρ_{Sol} is the density of the salt solution [kg/m^3]

The first term on the left hand side of Equations (2-18) and (2-19) is the energy transfer through the membrane and the second term is the latent heat of vaporization of water. The summation of these two terms is balanced by the change in the energy of the salt solution as it flows through the control volume (advection).

The simultaneous solution to the governing heat and mass equations as well as the heat and mass flux balance at the membrane surface gives the bulk mean temperature and humidity distributions in the air and solution channels and the temperature and humidity at the surface of the membrane (liquid-membrane interface). The temperature and humidity distributions at the solution-membrane interface will be used in chapter 4 to predict the crystallization of salt in the solution.

2.2.4 Boundary Conditions

Velocity Field at the Boundaries:

The salt solution is assumed to have a uniform velocity at the exchanger inlet headers. The velocity of the liquid desiccant at the headers of a counter-cross flow LAMEE may be found using the mass flow rate of the salt solution (Vali 2009):

$$\frac{\partial \psi}{\partial x} = -v_{Sol} = \frac{\dot{m}_{Sol}}{(\rho d)_{Sol}\, x_i} \quad \text{when } y=0 \text{ and } x_0-x_i<x<x_0 \text{ or } y=y_0 \text{ and } 0<x< x_i \tag{2-20}$$

Other walls of the liquid channels are assumed to be impermeable and, therefore, no flow passes through the walls which means that the value of the stream function is constant on the walls:

$$\psi = \text{constant} \quad \text{when} \quad x=0 \text{ and } 0<y<y_0 \text{ or } x=x_0 \text{ and } 0<y<y_0 \text{ or } y=0 \text{ and } 0<x<(x_0-x_i) \text{ or } y=y_0 \text{ and } x_i<x<x_0 \tag{2-21}$$

Temperature and Humidity at the Boundaries:

The temperature and humidity at the inlet of the supply exchanger are assumed to be constant and equal to the temperature and humidity of the outdoor air. The temperature and humidity at the inlet of the exhaust exchanger is the temperature and humidity of the air inside the building. On the liquid side, the temperature and concentration at the inlet of each exchanger is equal to the bulk average temperature and concentration at the outlet of the other exchanger. The exchanger walls are assumed to be perfectly insulated and therefore no heat transfer occurs through the external walls.

Figure 2.4 summarizes the boundary conditions for cross flow and counter-cross flow LAMEEs.

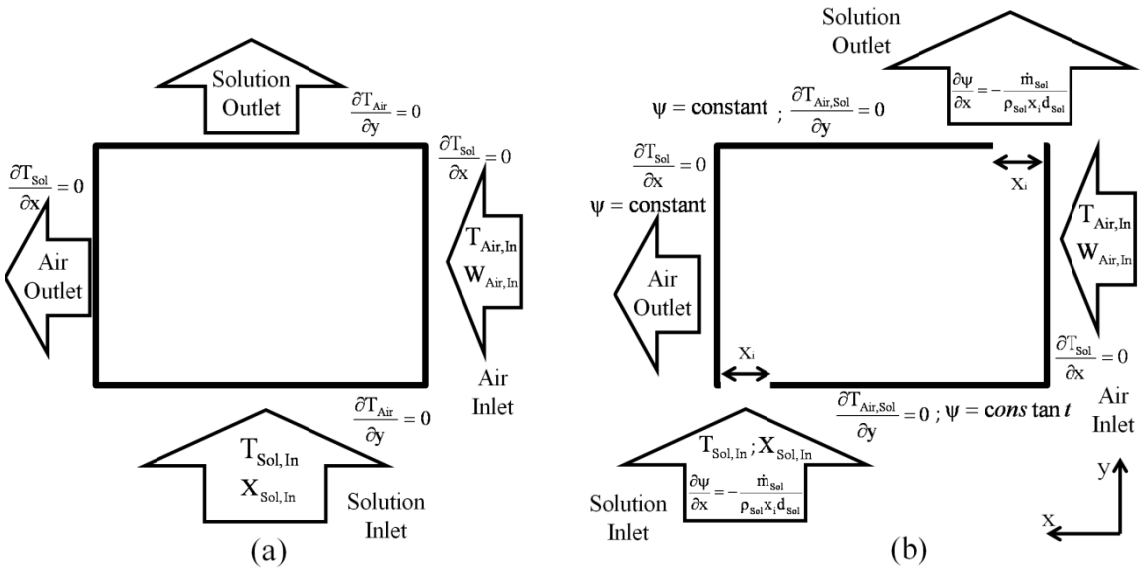

Figure 2.4: Boundary conditions of a (a) cross flow, and (b) counter-cross flow LAMEE.

2.2.5 Dimensionless Groups

Using dimensionless parameters is a common way to express the performance and design conditions of heat exchangers. The performance of an exchanger may be evaluated by dimensionless parameters of latent, sensible and total effectiveness. The effectiveness shows how the exchanger operates compared to an exchanger with the maximum possible heat, moisture or enthalpy transfer. The sensible, latent and total effectiveness of the RAMEE system are defined as:

$$\varepsilon_{Sen} = \frac{T_{Air,S,In} - T_{Air,S,Out}}{T_{Air,S,In} - T_{Air,E,In}} = \frac{T_{Air,E,Out} - T_{Air,E,In}}{T_{Air,S,In} - T_{Air,E,In}} \tag{2-22}$$

$$\varepsilon_{Lat} = \frac{W_{Air,S,In} - W_{Air,S,Out}}{W_{Air,S,In} - W_{Air,E,In}} = \frac{W_{Air,E,Out} - W_{Air,E,In}}{W_{Air,S,In} - W_{Air,E,In}} \tag{2-23}$$

$$\varepsilon_{Tot} = \frac{H_{Air,S,In} - H_{Air,S,Out}}{H_{Air,S,In} - H_{Air,E,In}} = \frac{H_{Air,E,Out} - H_{Air,E,In}}{H_{Air,S,In} - H_{Air,E,In}} \tag{2-24}$$

where subscripts:

"Sen" is for sensible,

"Lat" is for latent,

"Tot" is for total,

"Air" is for airstream,

"S" is for supply exchanger,

"E" is for exhaust exchanger,

"In" is for inlet,

"Out" is for outlet.

Since there is assumed to be no heat gain/loss to/from the exchangers and connecting piping, the effectiveness values are equal for both supply and exhaust exchangers at steady state.

The effectiveness of an exchanger may be expressed as a function of two other dimensionless groups (Incropera and Dewitt 2002):

$$\varepsilon = f(\mathrm{NTU}, \mathrm{Cr}^*) \tag{2-25}$$

where Cr^* is the ratio of the heat capacity rate of the salt solution to that of air (C_{Sol}/C_{Air}) and NTU is the number of heat transfer units and is defined as:

$$\mathrm{NTU} = \frac{2\mathrm{UA}}{\mathrm{C}_{\mathrm{Air}}} \tag{2-26}$$

where

A is the surface area of the membrane [m^2].

Similarly, the latent effectiveness may be expressed as a function of the number of mass transfer units (NTU_m) and the ratio of the mass flow rate of the salt to the air:

$$\varepsilon_{\mathrm{lat}} = f(\mathrm{NTU}_{\mathrm{m}}, \dot{m}_{\mathrm{Salt}} / \dot{m}_{\mathrm{Air}}) \tag{2-27}$$

where NTU_m may be defined as:

$$NTU_m = \frac{2U_m A}{\dot{m}_{Air}} \tag{2-27}$$

2.3 Design and Operating Conditions

The RAMEE system is simulated with several design parameters (i.e. NTUs and Cr*s) and operating conditions (i.e. indoor and outdoor temperatures and humidities) in chapter 4 to investigate the impact of design and operating conditions on the risk of crystallization. These conditions will be discussed in detail in section 4.2 in chapter 4.

The physical properties of the LAMEEs modeled in this thesis are shown in Table 2.1. Dimensions of the simulated LAMEEs are chosen so the values are close to the counter-cross flow RAMEE prototype III (Mahmud, 2009).

Table 2.1: Physical properties of the simulated LAMEEs (Mahmud, 2009).

Property	Symbol	Value
Exchanger Size	$x_0 \times y_0 \times z_0$	$1.8 \times 0.2 \times 0.075$ m
Entrance Length (Counter-Cross LAMEE)	x_i	0.076 m
Air Channel Thickness	d_A	4.4 mm
Liquid Channel Thickness	d_L	2.7 mm
Membrane Thickness	δ	0.2 mm
Thermal Conductivity of the Membrane	k	0.334 W/(m.K)
Mass Flow Rate of Solution (NTU=10, Cr*=3)	$\dot{m}_{Sol}$	0.03kg/s
Mass Flow Rate of Air (NTU=10, Cr*=3)	$\dot{m}_{Air}$	0.024 kg/s
Mass Conductivity of the Membrane	k_m	1.66×10^{-6} kg/(m.s)

The operating conditions under which the RAMEE system is simulated in this thesis are presented in Table 2.2. The system is mostly simulated for outdoor and indoor operating conditions as specified by AHRI Standard 1060 (AHRI 2005). However, other operating conditions were also used in the simulations to investigate the effect of changing indoor and outdoor conditions on the properties of the salt solutions.

Table 2.2: Selected indoor and outdoor operating conditions.

		Indoor			Outdoor		
		T	**Humidity Ratio**	**Relative Humidity**	**T**	**Humidity Ratio**	**Relative Humidity**
Summer	**AHRI Condition**	24 °C	9.3 g/kg	50%	35° C	17.5 g/kg	50%
					35° C	11.5 g/kg	33%
		24 °C	5.5 g/kg	30%	35° C	10.5 g/kg	30%
		24 °C	1.8 g/kg	10%	35° C	7.4 g/kg	21.2%
Winter	**AHRI Condition**	21 ° C	7.1 g/kg	46%	1.7° C	3.5 g/kg	82%
		21 ° C	4.6 g/kg	30%	-	-	-

2.4 Numerical Solution Method and Results

The first step in the solution algorithm is to generate rectangular grids in the liquid and air channels (201×201 grids according to Vali 2009) and assign an arbitrary initial value of temperature and humidity to each spatial node. The steady state temperature and humidity at each node is then evaluated by iteratively solving the coupled discretized governing equations (Vali 2009).

The iteration continues until the temperature and moisture content of the air and liquid streams reach the steady state condition (Vali 2009). The temperature and humidity distributions may later be used to determine the effectiveness of the system and the risk of crystallization.

2.5 Preliminary Results

The temperature and humidity distributions in the air stream and at the liquid desiccant-membrane interface of a supply LAMEE are shown in Figures 2.5 and 2.6 for a RAMEE system with cross flow exchangers. The distributions are shown for RAMEE systems operating during summer AHRI operating conditions with an NTU=10 and Cr^{*}=3. These results were validated and a grid sensitivity was presented by Vali (2009).

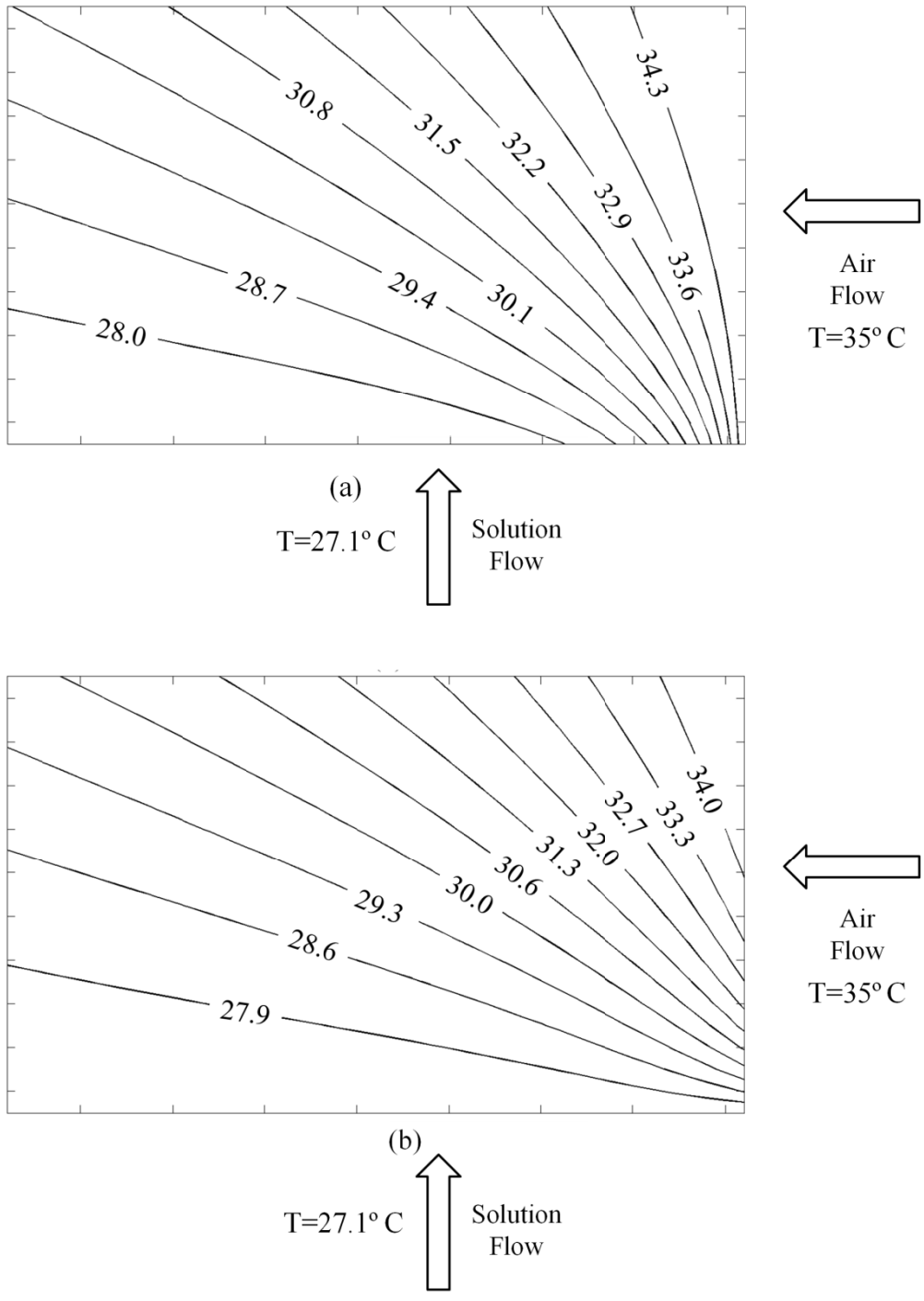

Figure 2.5: Temperature (˚C) distribution (a) in an air channel and (b) at the solution-membrane interface of a liquid channel in the supply LAMEE at AHRI summer conditions (NTU=10, Cr*=3).

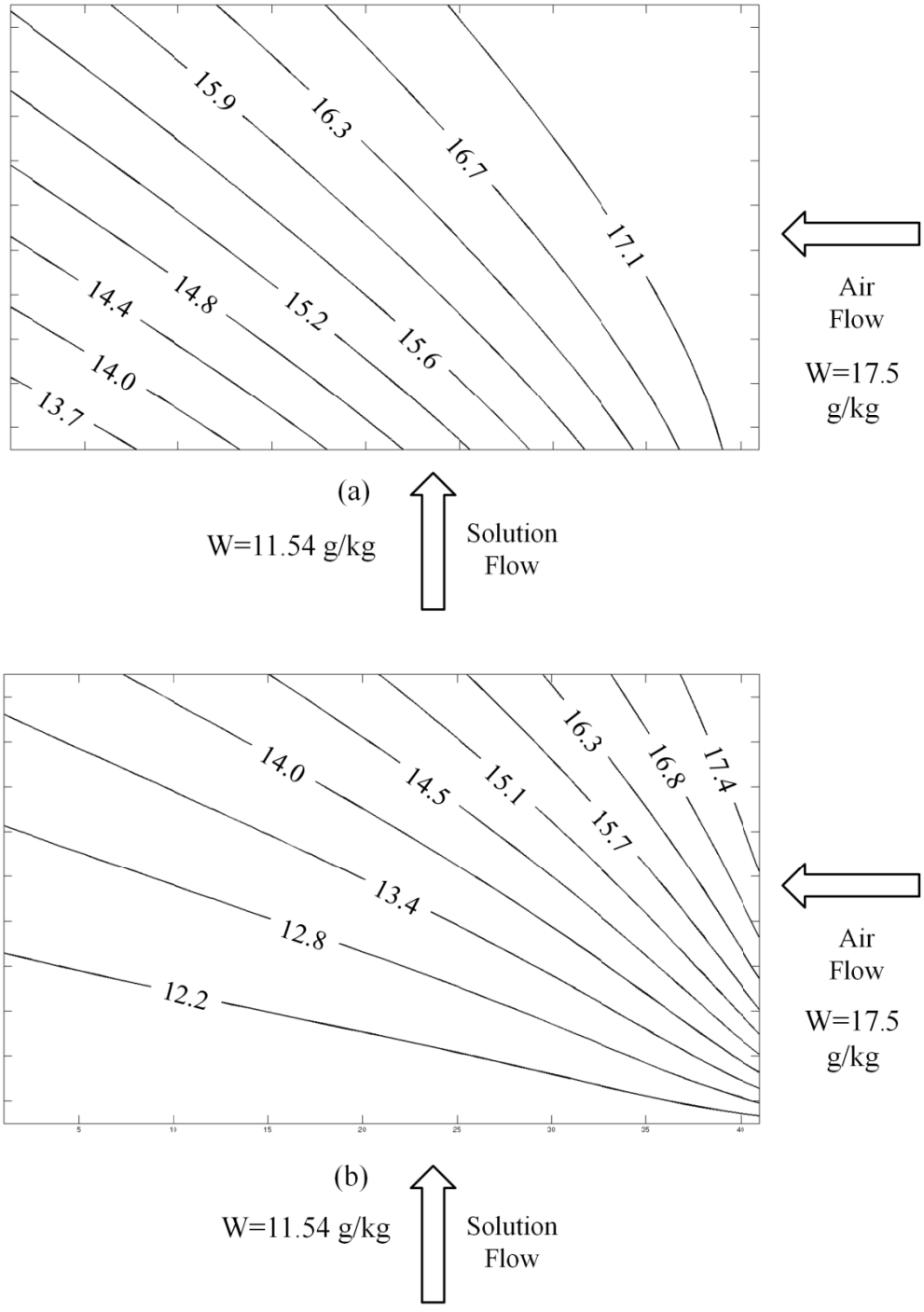

Figure 2.6: Humidity ratio (g/kg) distribution (a) in an air channel and (b) at the solution-membrane interface of a liquid channel in the supply LAMEE at AHRI summer conditions (NTU=10, Cr*=3).

Figures 2.7 and 2.8 show the temperature and humidity distributions of a supply exchanger in a RAMEE system with counter-cross flow exchangers with similar operating and design conditions as in Figures 2.5 and 2.6 (NTU=10, Cr*=3 and AHRI summer test conditions).

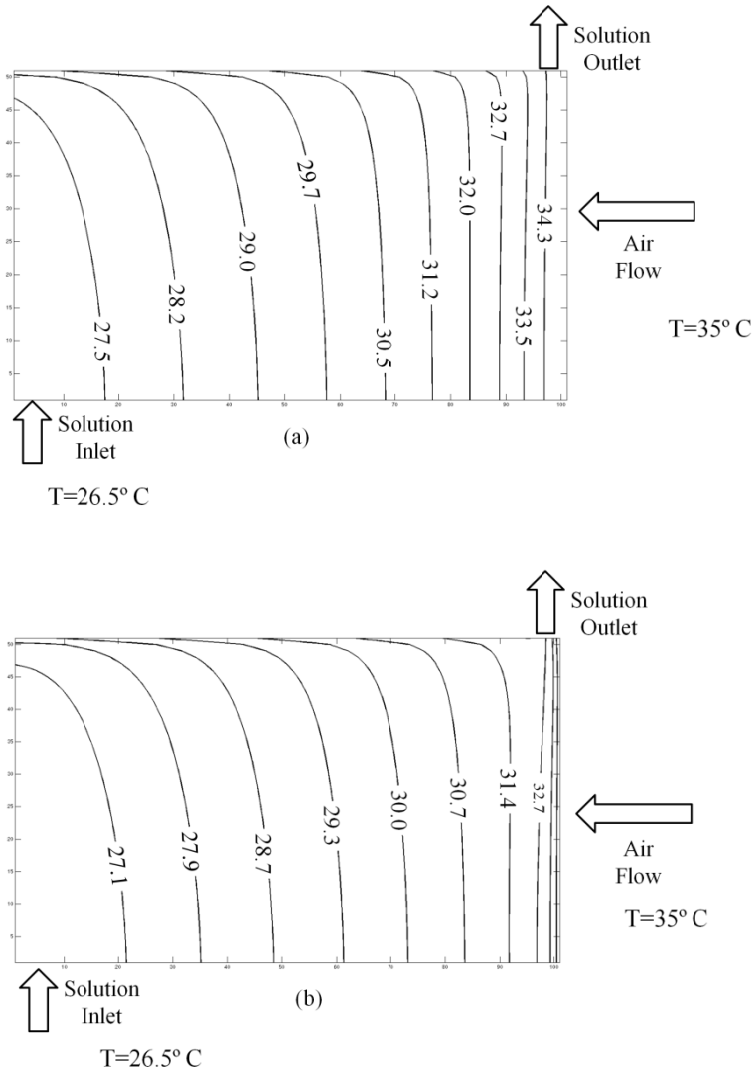

Figure 2.7: Temperature (˚C) distribution (a) in an air channel and (b) at the solution-membrane interface of a liquid channel in the supply LAMEE at AHRI summer conditions (NTU=10, Cr*=3).

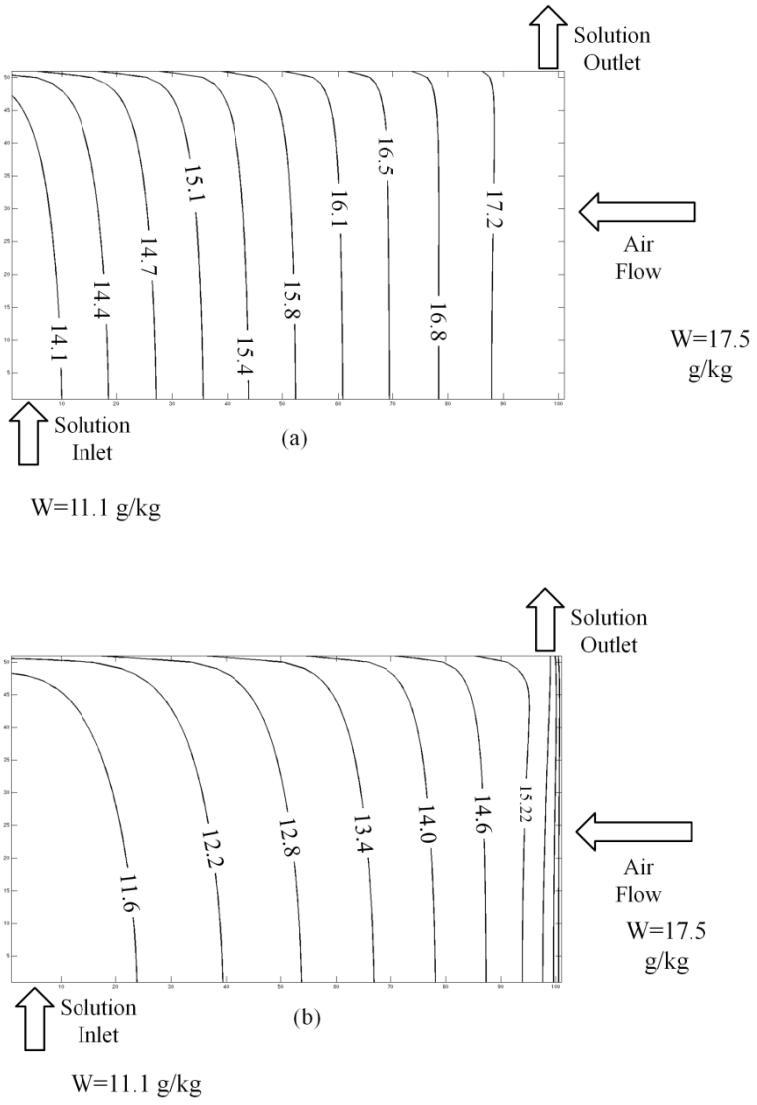

Figure 2.8: Humidity ratio (g/kg) distribution (a) in an air channel and (b) at the solution-membrane interface of a liquid channel in the supply LAMEE at AHRI summer conditions (NTU=10, Cr*=3).

As seen in Figures 2.5 to 2.8, the bulk air temperature and humidity decrease from the air inlet to the air outlet in the exchanger while the temperature and humidity at the liquid-membrane interface increase from the liquid outlet to the liquid inlet.

The temperature and humidity at the surface of the membrane (liquid side) may be used to investigate the crystallization risk of the salt in the solution. The method of

predicting the crystallization risk of the desiccant solution from the temperature and humidity distributions is described in chapter 4. The temperature and humidity distributions at the liquid-membrane interface may be affected by changing the design and operating conditions. This change in the temperature and humidity distribution eventually affects the risk of crystallization of salt on the membrane surface. The effect of outdoor and indoor operating conditions and also design properties of the LAMEEs on the risk of crystallization of the salt solution will be discussed in Chapter 4.

The performance of a RAMEE system is also a function of the design properties of the system (i.e., NTU and Cr^*). Therefore, RAMEE systems with different effectivenesses may have different temperature or humidity distributions in their LAMEE flow channels which will affect the concentration and crystallization risk of the liquid desiccant flowing in the system. Figure 2.9 shows the total effectiveness of RAMEE systems with cross flow and counter-cross flow configurations. The systems shown in Figure 2.9 have been simulated with NTU=10 and Cr^* values ranging from 0 to 6. The impact of changing the effectiveness of the RAMEE system on the risk of crystallization of the salt solution is another objective of this thesis which will be discussed in detail in Chapter 4. The numerical model introduced in this chapter is validated using experimental measurements of Mahmud (2009).

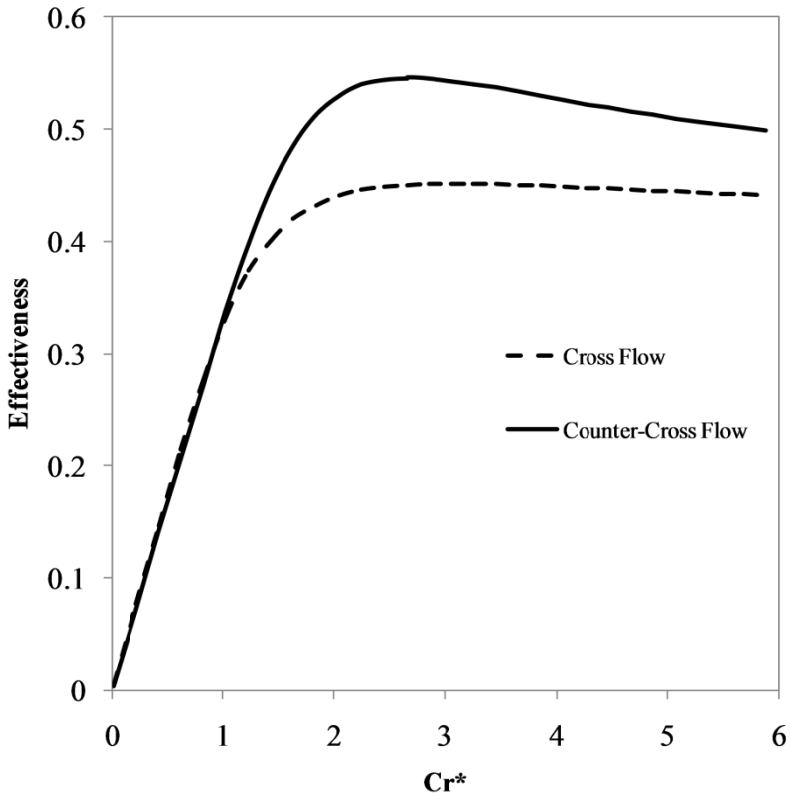

Figure 2.9: Effectiveness of cross and counter-cross flow RAMEEs with NTU=10.

2.6 Summary

In this chapter, a numerical model is described which can be used to calculate the temperature and humidity distributions in the liquid and air channels of a RAMEE system. The numerical model is applicable for both cross and counter-cross flow LAMEEs.

The numerical model solves the coupled heat and mass transfer equations in the flow channels using a finite difference method. In this model the temperature and humidity values are calculated at the solution-membrane interface where crystallization of the salt solution may occur. The temperature and humidity values at the salt solution-membrane interface will be used in chapter 4 to predict crystallization of the liquid

desiccant in the LAMEEs. In order to investigate the RAMEE systems with different design characteristics, several dimensionless parameters are also defined in this chapter.

CHAPTER 3

SALT SOLUTIONS

3.1 Introduction

The purpose of this chapter is to explain how liquid desiccants function and investigate the properties of some selected liquid desiccants which may be used in the RAMEE. The liquid desiccants investigated in this chapter are aqueous solutions of: LiCl, LiBr, $MgCl_2$ and $CaCl_2$. All of the aforementioned salt solutions except $MgCl_2$ are commonly used as liquid desiccants in commercial air conditioners and dehumidifiers. The properties studied in this chapter are:

- Vapor pressure
- Dynamic viscosity
- Density
- Thermal conductivity
- Specific heat capacity
- Binary diffusion coefficient
- Safety
- Cost

Finally, the cost to pump the desiccant and effectiveness of RAMEEs operating with different salt solutions in various operating conditions is compared in this chapter.

3.2 How Do Salt Solutions Work as Liquid Desiccants?

Liquid desiccants are primarily used in air conditioning systems because of their ability to dehumidify moist air. The attraction of water vapor is a result of the liquid desiccant creating a water vapor pressure at the interface between the liquid and surrounding. When a hygroscopic salt (e.g. NaCl or LiCl) is dissolved in water, the equilibrium vapor pressure (VP) at the liquid-air interface of the mixture decreases compared to the VP for pure water. The equilibrium VP is the pressure at which the vapor phase of a material is in equilibrium with its non-vapor phase. When the equilibrium VP at the liquid-air interface is higher than that of the air, moisture evaporates from the liquid and when the VP at the liquid-air interface is lower than that of air, moisture is transferred from the air to the liquid and the air is dehumidified. Figure 3.1 shows the equilibrium VP at the surface of a saturated LiCl-Water solution as well as the VP of pure water. As seen in Figure 3.1, by dissolving adequate LiCl in pure water and creating a saturated salt solution the vapor pressure may be reduced by 90%.

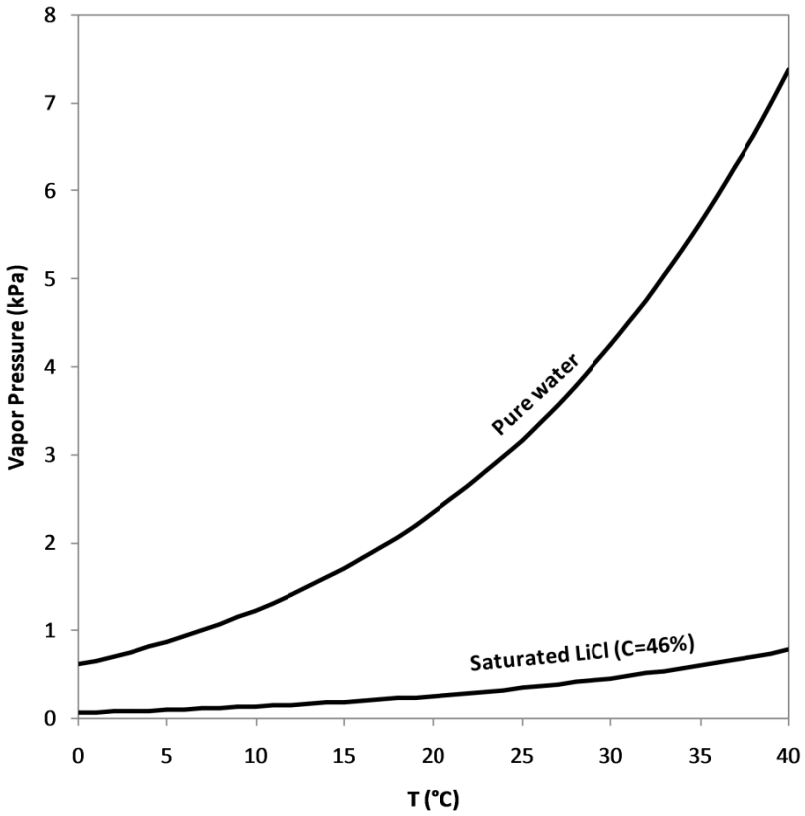

Figure 3.1: Equilibrium vapor pressure at the surface of pure water and saturated aqueous LiCl solution.

The equilibrium VP of liquid desiccants is typically very low. Therefore, the desiccant will dehumidify air even when the air is relatively dry. The humidity ratio at the surface of a salt solution, at a constant pressure, depends on the concentration and temperature of the solution. Figure 3.2 shows the humidity ratio lines at the liquid-air interface of a $MgCl_2$-Water solution for different concentrations, superimposed on a psychrometric chart. The humidity ratio at the solution-air interface increases as the solution temperature increases and decreases as concentration increases. As shown in Figure 3.2, when a 30% $MgCl_2$ solution is heated from 20°C to 30°C the surface humidity ratio increases from 7.9 to 14.7 g/kg dry air. The effect of increasing

concentration on humidity ratio at the surface of a $MgCl_2$ solution is also illustrated in Figure 3.2.

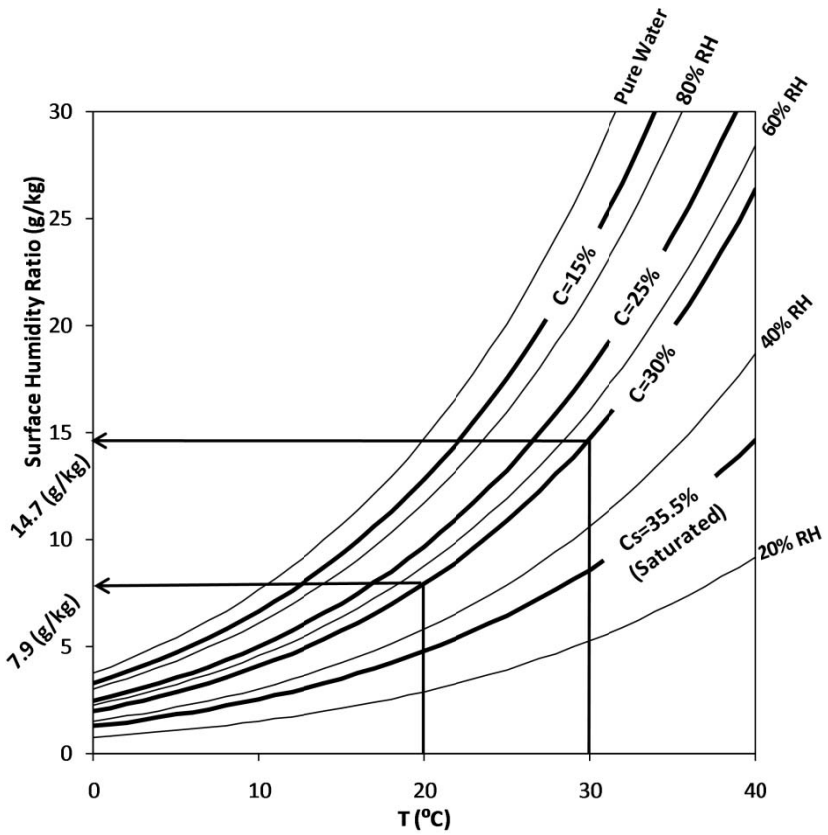

Figure 3.2: Equilibrium humidity ratio lines at the surface of a $MgCl_2$ solution at different concentrations.

From a different perspective, the equilibrium humidity ratio at the liquid-air interface of a salt solution, at a given concentration, changes in such a way that the relative humidity at the solution-air interface almost remains constant. For example, a 25% weight concentrated $MgCl_2$ solution will maintain the relative humidity close to 66% over a wide range of temperatures (see Figure 3.2).

In a LAMEE, each liquid desiccant channel is adjacent to two air channels. When the humidity of an airstream is higher than the equilibrium humidity ratio at the solution-membrane interface, moisture is absorbed by the solution and the airstream is

dehumidified. Conversely, if the airstream has a lower humidity ratio (i.e., drier) than the equilibrium humidity ratio at the solution-membrane interface, water evaporates from the salt solution and the airstream is humidified. Figure 3.3 shows the bulk humidity ratio of the airstream and at the solution-membrane interface at the inlet of the supply exchanger of a RAMEE with NTU=10 and Cr^*=3, operating during AHRI summer conditions.

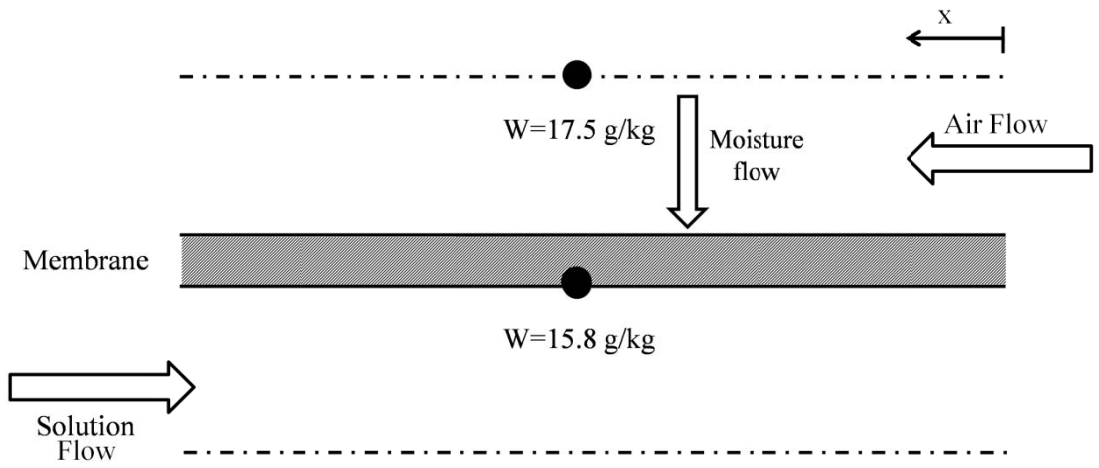

Figure 3.3: Humidity ratio at the liquid surface and in the bulk airstream.

As seen in Figure 3.3, the bulk humidity ratio of the airstream is higher than that at the liquid-membrane interface for this particular case. This gradient drives moisture from the airstream towards the liquid desiccant which eventually dries the supply air.

3.2.1 Desiccant cycle in the RAMEE

After a salt solution absorbs moisture, its water content increases. An increase in the water content of the salt solution makes the mixture more dilute. In other words, the concentration of the salt solution decreases as it gains moisture. As mentioned previously, the humidity ratio at the surface of a salt solution is inversely proportional to

the salt concentration. Meaning, as the concentration of the salt solution decreases the equilibrium humidity ratio increases, reducing the moisture transfer potential between the liquid and the airstream. Therefore, excessive moisture has to be removed from a dilute (weak) salt solution so the solution can absorb water vapor again. The process of removing moisture from a dilute salt solution is called regeneration or reactivation.

In a RAMEE system, absorption and regeneration occur in the LAMEEs. Consider a RAMEE system operating during summer conditions, when the outdoor air is hot and humid (Figure 3.4). During these operating conditions, the VP of the supply air is higher than the VP at the surface of the salt solution. Therefore, the desiccant solution attracts moisture from the air and its moisture content rises (i.e., concentration decreases). After exiting the supply LAMEE, the dilute salt solution has to be reactivated in order to be able to dehumidify supply air again. The reactivation of the salt solution occurs in the exhaust LAMEE during summer operating conditions. In the exhaust LAMEE, the salt solution comes into contact with the exhaust airstream. The condition of the exhaust air is closer to the desired supply condition (i.e., previously cooled and dehumidified). The relatively dry exhaust air contacts the dilute salt solution in the exhaust LAMEE regenerating the desiccant by evaporating moisture from the solution. The regenerated solution is pumped to the supply LAMEE when it can dry and cool the supply air again.

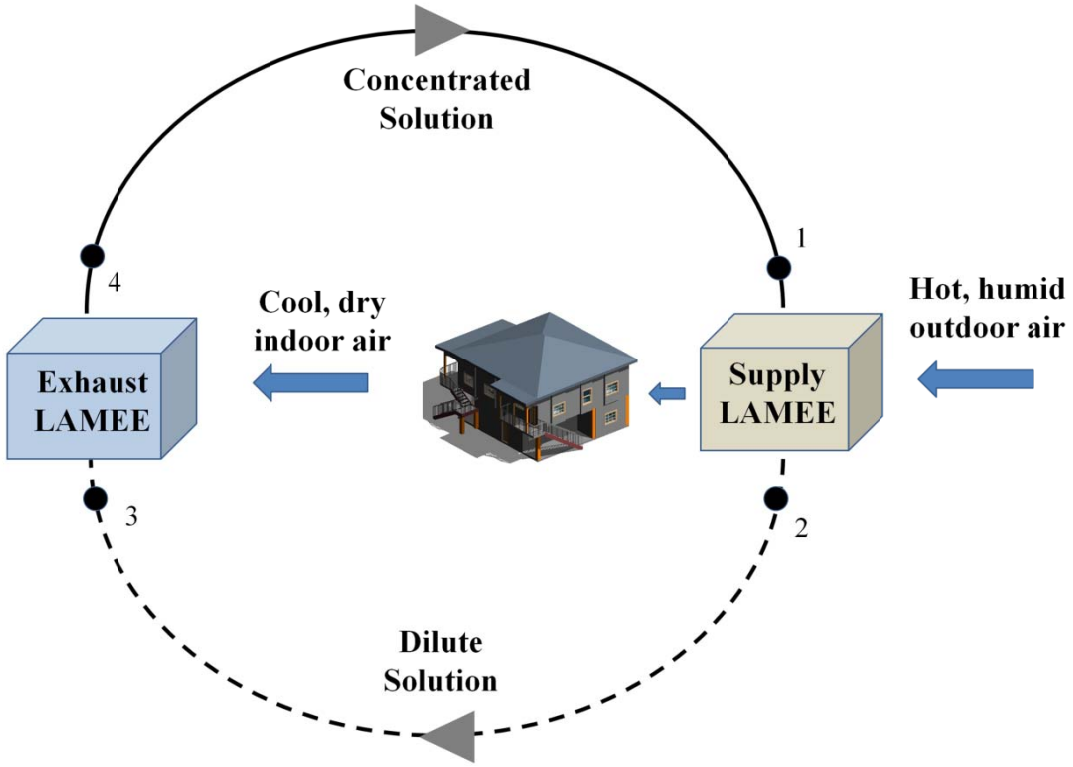

Figure 3.4: Change in the concentration of the salt solution in a RAMEE loop during summer operating conditions.

Figure 3.5 shows a complete cycle of the liquid desiccant in a typical RAMEE system, operating during summer AHRI conditions, superimposed on a psychrometric chart. Cool and concentrated salt solution enters the supply LAMEE (point 1 in Figure 3.5), where it absorbs heat and moisture from outdoor air. The salt solution leaves the supply LAMEE at point 2 and enters the exhaust LAMEE (point 3). Regeneration occurs in the exhaust exchanger, where the warm and dilute salt solution rejects heat and moisture to the exhaust airstream. The regenerated salt solution leaves the exhaust LAMEE at point 4 and is pumped to the supply exchanger, completing the recovery cycle (point 1). During this cycle, the supply air loses 4.7 g/(kg dry air) of moisture (in

a RAMEE with NTU=10, Cr*=3) and is cooled 7.5˚C, indirectly, by using the low temperature and humidity exhaust airstream as an energy sink.

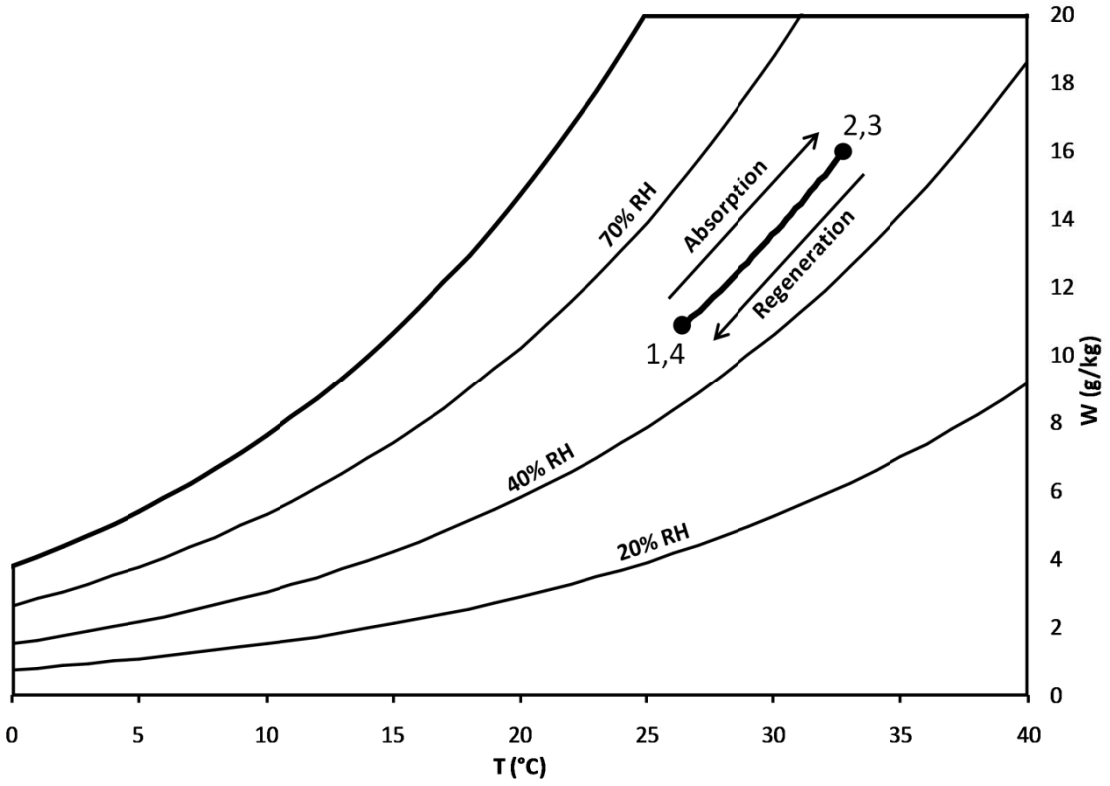

Figure 3.5: Absorption and regeneration processes in a RAMEE operating during summer.

3.3 Salt Solution Properties

This section presents the available correlations and experimental measurements of properties of the selected binary salt solutions. Most of these correlations are based on experimental measurements and are only valid for prediction of properties of dilute salt solutions. Each of the available correlations is valid for a specific range of temperatures and concentrations and, therefore, has to be carefully selected for use in the numerical simulation or further studies.

3.3.1 Equilibrium Vapor Pressure and Humidity Ratio

As mentioned earlier, the difference between the VP at the liquid desiccant-air interface and the surrounding air is the driving potential for moisture transfer between the air and the liquid desiccant. Therefore, the equilibrium VP of the salt solution has to be known in order to determine the mass transfer rate in the RAMEE. Equilibrium vapor pressure, similar to other properties of the mixtures, depends on temperature, pressure and concentration of the salt solution. Although extensive experimental data are available in the literature for the equilibrium VP at the surface of the salt solutions, no universal formulation exists that can be applied for every salt solution. Especially at high concentrations (i.e. close to saturation), the salt solutions exhibit complicated behaviors making VP prediction very difficult.

In this thesis, three different correlations are used to calculate the VP at the solution-air interface. The most general correlation is by Cisternas and Lam (1991) and may be applied to calculate the VP of all of the selected salt solutions. Another correlation is only valid for LiCl and $CaCl_2$ solutions (Conde 2003). The final correlation calculates the VP at the surface of saturated salt solutions (Greenspan 1977). The mathematical equations for these correlations are shown in Appendix A.

Figure 3.6 shows the vapor pressure at the solution-air interface of a LiBr solution calculated from the correlations proposed by Cisternas and Lam (1991) and Greenspan (1977) against some experimental measurements. The lines shown in this figure are the correlations and the data points are the experimental measurements. The literature sources used to create Figure 3.6 are Boryta (1975), Uemura et al. (1964), Lower (1961) and Patil et al. (1990). The deviation between the correlated and experimental data increase as the concentration and temperature of the solution increase

(see Figure 3.6). For example, the deviation is less than 7% for a LiBr-water solution with C=50% and T=25˚C (0.07 kPa absolute deviation) while the deviation is about 30% for a LiBr-water solution with C=60% and T=40˚C (0.21 kPa absolute deviation) where the percent deviation is defined as:

$$\%Dev = 100\left|\left(P_{\exp} - P_{cal}\right)/P_{\exp}\right| \tag{2-1}$$

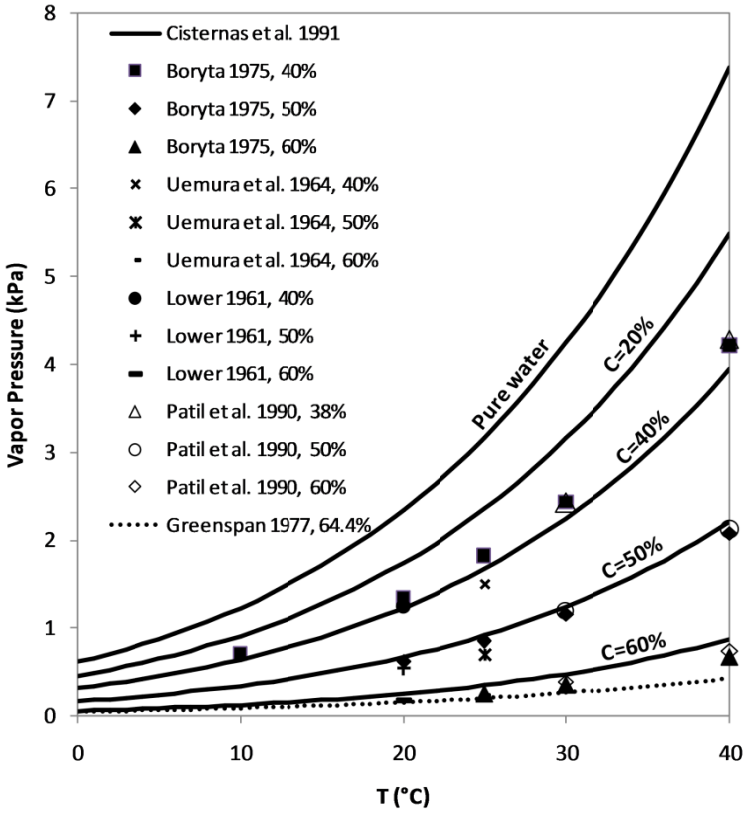

Figure 3.6: Vapor pressure at the surface of a LiBr solution for different concentrations.

Figures 3.7 and 3.8 show the VP at the solution-air interface of LiCl and $CaCl_2$ solutions respectively. These VP values are calculated using correlations of Conde (2004) and are compared with some experimental data. As seen in Figure 3.7 and 3.8, the correlation proposed by Conde (2004) predict the vapor pressure of highly concentrated LiCl and $CaCl_2$ solutions more accurately than correlation of Cisternas and

Lam (1991). In fact, correlation of Conde (2004) predicts the vapor pressures of solutions of LiCl-water and $CaCl_2$-water with less than 3% deviation from the experimental measurements for the whole range of concentrations (i.e., concentration changing from 0 to saturation) and temperatures ranging between 0 to 100 ˚C.

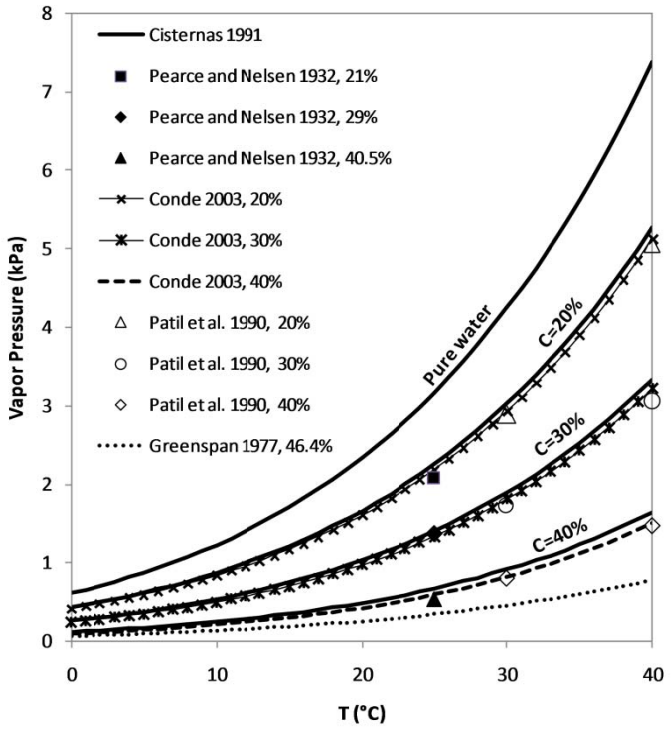

Figure 3.7: Vapor pressure at the surface of a LiCl solution for different concentrations.

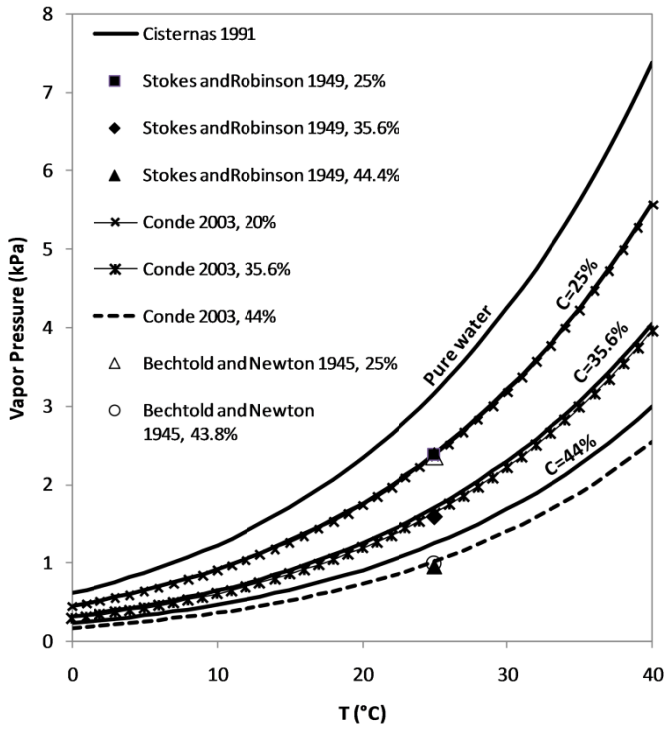

Figure 3.8: Vapor pressure at the surface of a $CaCl_2$ solution at different concentrations.

The equilibrium vapor pressure at the solution-air interface of $MgCl_2$ solution is shown in Figures 3.9. There are few experimental measurements available in the literature for the vapor pressure of $MgCl_2$ solutions. As seen in Figure 3.9, the correlation of Cisternas and Lam (1991) can predict the VP of a $MgCl_2$ solution very accurately up to 20% weight concentration. However as the concentration increases above 20%, the correlation becomes less accurate in predicting the vapor pressure (similar to LiBr solution).

In the current numerical model, the correlation of Conde (2004) is used to calculate the equilibrium VP of LiCl and $CaCl_2$ solutions (because of its higher accuracy compared to correlation of Cisternas and Lam (1991)). For the LiBr and $MgCl_2$ solutions, the correlation of Cisternas and Lam (1991) is used to calculate the VP. Although the correlation of Cisternas and Lam (1991) is not accurate at higher

concentrations, the effectiveness calculations of different salt solutions in section 3.5 and the temperature and humidity distributions show that the model can predict the solution conditions for outdoor humidities as low as 20% RH.

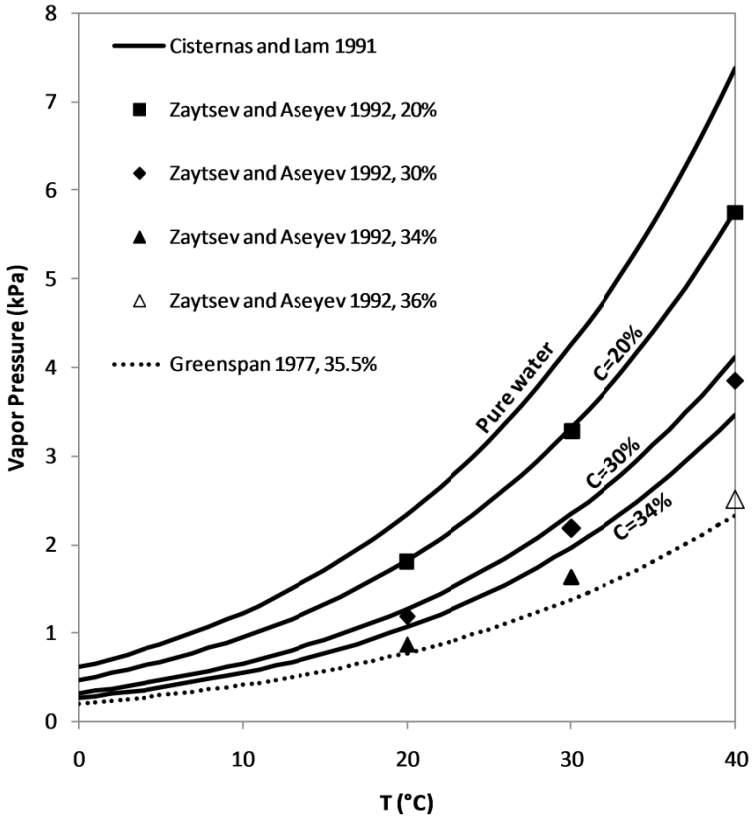

Figure 3.9: Vapor pressure at the surface of a $MgCl_2$ solution for different concentrations

The vapor pressure at the solution-air interface can be used to find the humidity ratio at the interface using (ASHRAE 2005):

$$W = \frac{0.62198VP}{P_{atm} - VP} \tag{3-2}$$

where

W is humidity ratio [kg_{H2O}/kg_{air}],

VP is vapor pressure of the salt solution [kPa], and

P_{atm} is the atmospheric pressure [kPa].

Figure 3.10 compares the humidity ratio at the surface of saturated salt solutions of LiBr, LiCl, $CaCl_2$, $MgCl_2$ and LiI, superimposed on a psychrometric chart. As seen in Figure 3.10, different saturated salt solutions create different equilibrium air relative humidities (RH) at saturation. For example, a saturated $MgCl_2$ solution produces an equilibrium air RH of 33%, while a saturated LiCl solution maintains an equilibrium RH of approximately 10%.

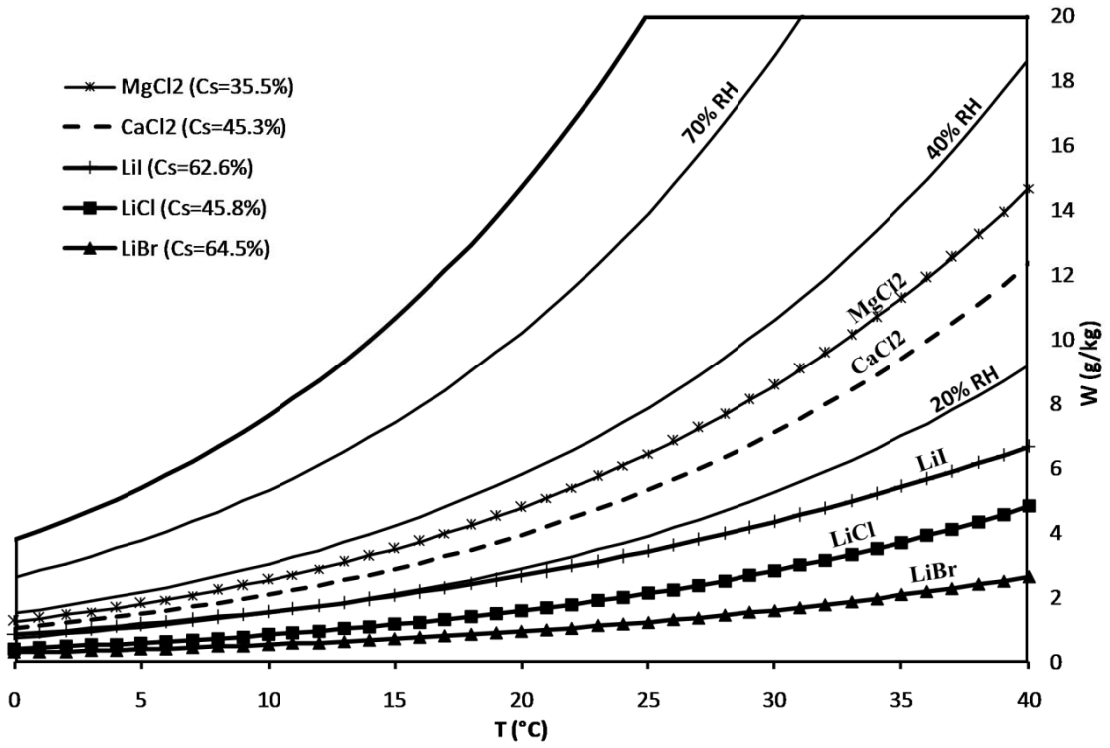

Figure 3.10: Equilibrium humidity ratio lines at the surface of some selected saturated salt solutions. Cs values indicate the saturation concentration of the salt solutions at 25 ˚C (Linke 1965; Stephen and Stephen 1963).

A salt solution with lower equilibrium humidity at saturation is able to dry the air more and is less likely to crystallize than a solution with high equilibrium humidity. Among the selected salt solutions, shown in Figure 3.10, LiBr is the strongest salt solution (i.e., lowers the air humidity the most) and $MgCl_2$ is the weakest (i.e., lowers

the air humidity the least). The importance of lowering the humidity ratio and avoiding crystallization will be discussed in detail in chapter 4.

3.3.2 Dynamic viscosity

Viscosity is a measure of fluid's resistance to the flow (White 2003). Thicker fluids (i.e., fluids with a higher viscosity) need more driving force and consequently require more pumping power to transfer them between the LAMEEs which increases the cost to operate the RAMEE.

Figure 3.11 compares the viscosity of LiCl-water and $CaCl_2$-water solutions calculated from the correlations of Zaytsev and Aseyev (1992) and Conde (2004) with some experimentally measured data (markers) from the literature (the correlation equations are presented in Appendix A). As seen in Figure 3.11, viscosity of the aqueous solution increases with concentration and may be 20 times higher than the viscosity of pure water (C=0%). The viscosity of the electrolyte solutions increases slightly with concentration at low concentrations; but increases significantly with concentration at higher concentrations. As seen in Figure 3.11, the correlation proposed by Zaytsev and Aseyev (1992) may only be used to predict viscosity values at low concentrations (i.e., concentrations less than 25% in the case of aqueous LiCl and $CaCl_2$ solutions), while the correlation of Conde (2004) is valid for concentrations up to saturation concentration for aqueous LiCl and $CaCl_2$ solutions.

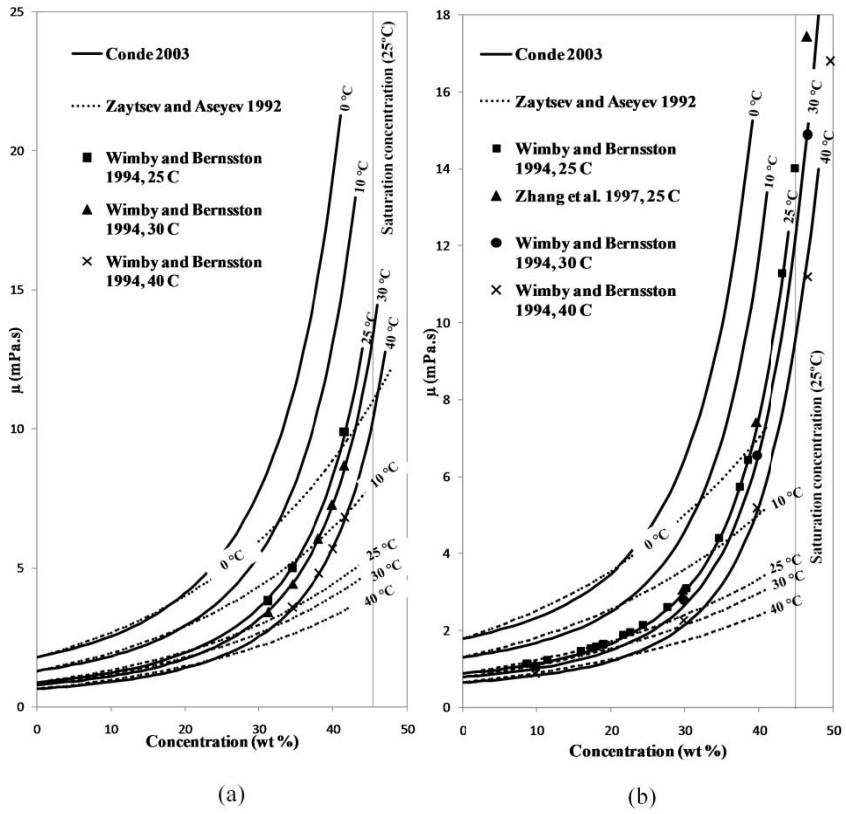

Figure 3.11: Dynamic viscosity of aqueous (a) LiCl and (b) $CaCl_2$ solutions.

Figure 3.12 shows the viscosity of aqueous solutions of $MgCl_2$ and LiBr. Correlations of Zaytsev and Aseyev (1992), Muhiuddin and Ismail (1983) and Lee et al. (1990) are used to calculate the viscosity of the $MgCl_2$ and LiBr solutions (see Appendix A for equations).

As seen in Figure 3.12, the correlation of Zaytsev and Aseyev (1992) only accurately predicts the viscosity of dilute solutions of $MgCl_2$ and LiBr. At higher concentrations, other empirical correlations have to be used to predict the viscosity of these salt solutions.

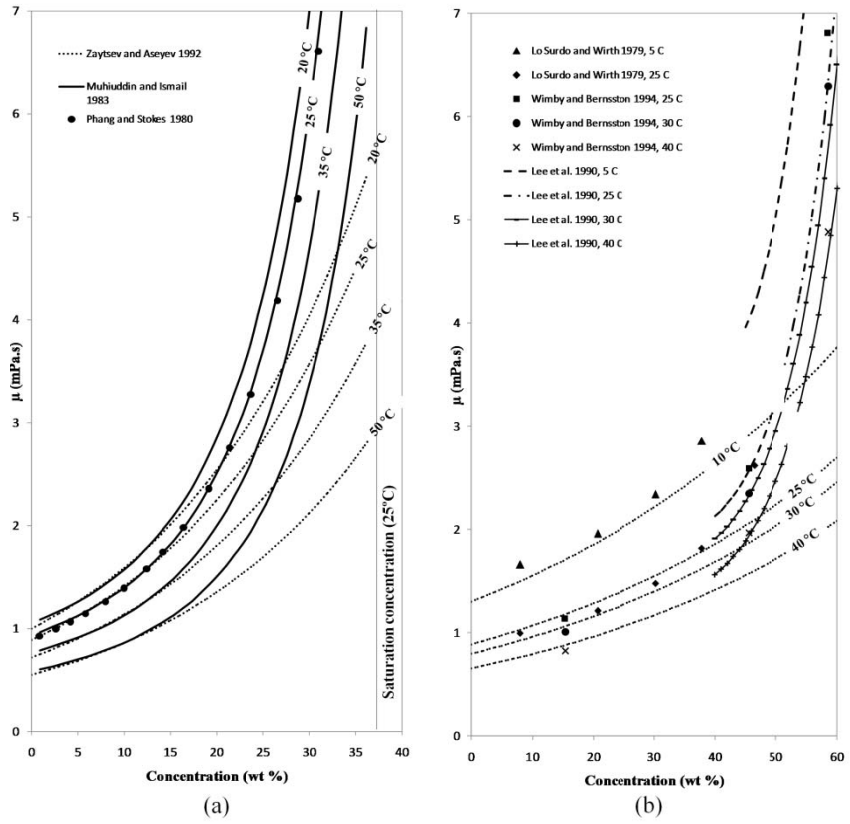

Figure 3.12: Dynamic viscosity of aqueous (a) $MgCl_2$ and (b) LiBr solutions.

Viscosities of $MgCl_2$ calculated from correlation of Muhiuddin and Ismail (1983) agree well with the experimental measurements of Phang and Stokes (1980) at 25˚ C.

To calculate the viscosity of LiBr solutions at concentrations higher than 40% the correlation of Lee et al. (1990) may be used. Their correlation is derived from measured viscosities at temperatures of 25 to 200˚C, but Phang and Stokes (1980) reported that this correlation may still be used at lower temperatures with fairly accurate results.

The correlation of Zaytsev and Aseyev (1992) may be used to calculate the viscosity of LiBr solutions with concentrations lower than approximately 30%, and $MgCl_2$ solutions with concentrations lower than 15%. Calculation of properties of

$MgCl_2$ solution close to saturation concentration is especially important since RAMEE systems operating with $MgCl_2$ solution mostly operate close to saturation condition.

In the current numerical model, the most accurate correlations (based on comparison with the experimental measurements) are chosen to calculate the viscosity of the salt solutions. The viscosity of the LiCl and $CaCl_2$ is calculated using correlation of Conde (2004). The correlation of Muhiuddin and Ismail (1983) is used to calculate the viscosity of $MgCl_2$ in the model. For LiBr solutions the correlation of Zaytsev and Aseyev (1992) is used for lower concentrations (C<40%) and correlation of Lee et al. (1990) is used for higher concentrations.

3.3.3 Density

The density of the salt solution is required to solve the conservation of energy in the liquid channels of a LAMEE (Equation (2-18) in chapter 2). The density also affects the pressure drop of the liquid through the LAMEEs and piping network that connects the LAMEEs in a run-around system.

As with the dynamic viscosity of the solutions, several correlations are available to calculate the density of an electrolyte mixture. Zaytsev and Aseyev (1992) have developed a general correlation with adjustable parameters which may be applied to calculate the densities of 133 different electrolytes. Conde (2004) reviewed the density measurements from 1850 to 2003 and suggested calculation methods for the density of LiCl and $CaCl_2$ solutions. Novotny and Sohnel (1988) also developed correlations that predict the density of 360 different salt solutions. The correlations used to calculate the density of the selected salt solutions are described in detail in Appendix A.

Figures 3.13 and 3.14 present the density of the salt solutions (LiCl, $CaCl_2$, $MgCl_2$ and LiBr) at different temperatures and concentrations. These figures show that there is a very good agreement between the different correlations for density. For example, the maximum difference between the densities predicted with correlation of Zaytsev and Aseyev (1992) and correlation of Conde (2004) for a LiCl solution is about 0.5%. This difference almost has no effect on the calculated temperature and humidity distributions in the LAMEEs by the numerical model. In the current numerical model, correlations of Zaytsev and Aseyev (1992) are used to calculate the density of the salt solution at different temperatures and concentrations.

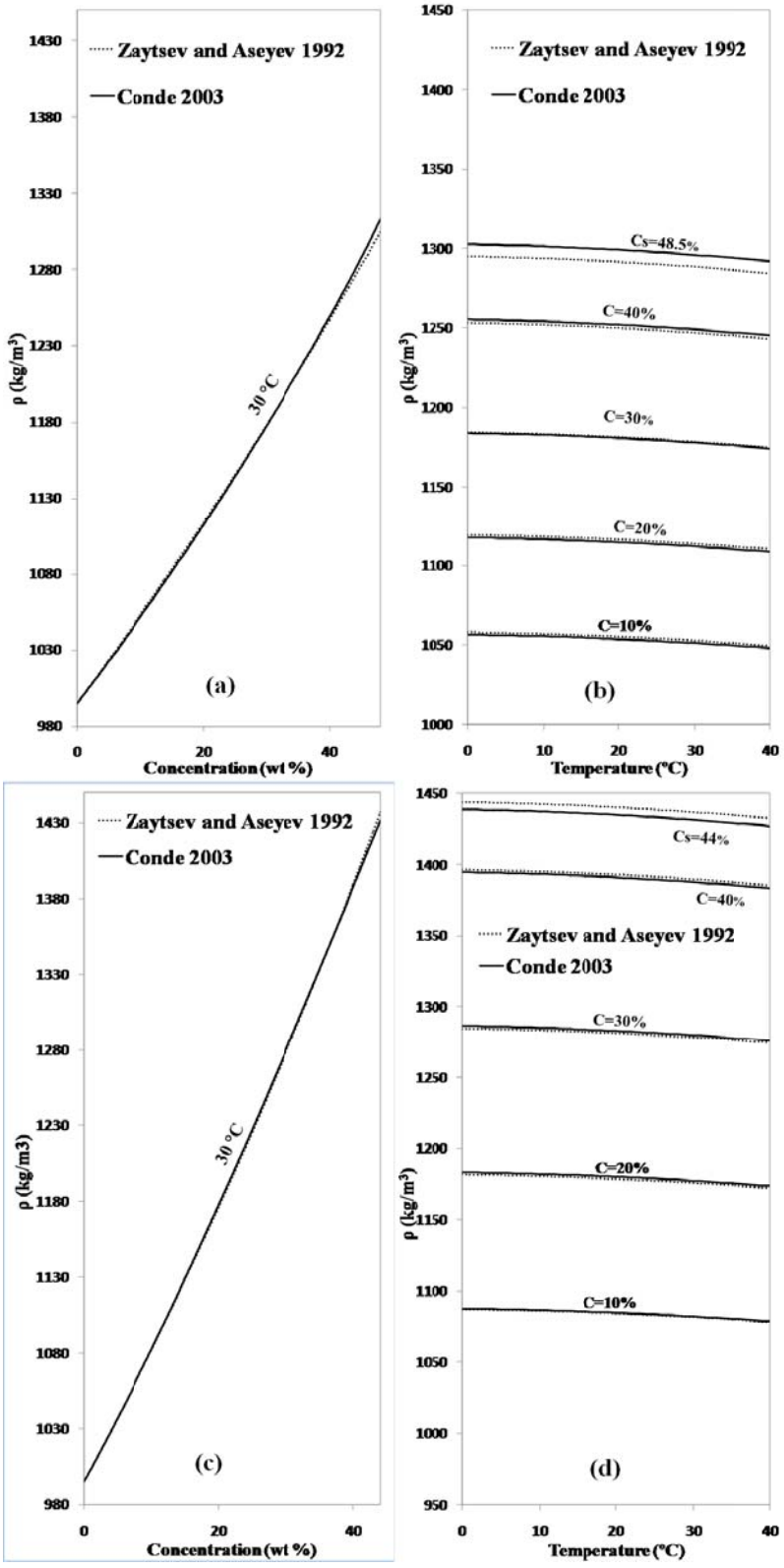

Figure 3.13: Density of a LiCl solution versus (a) concentration and (b) temperature and a $CaCl_2$ solution versus (c) concentration and (d) temperature.

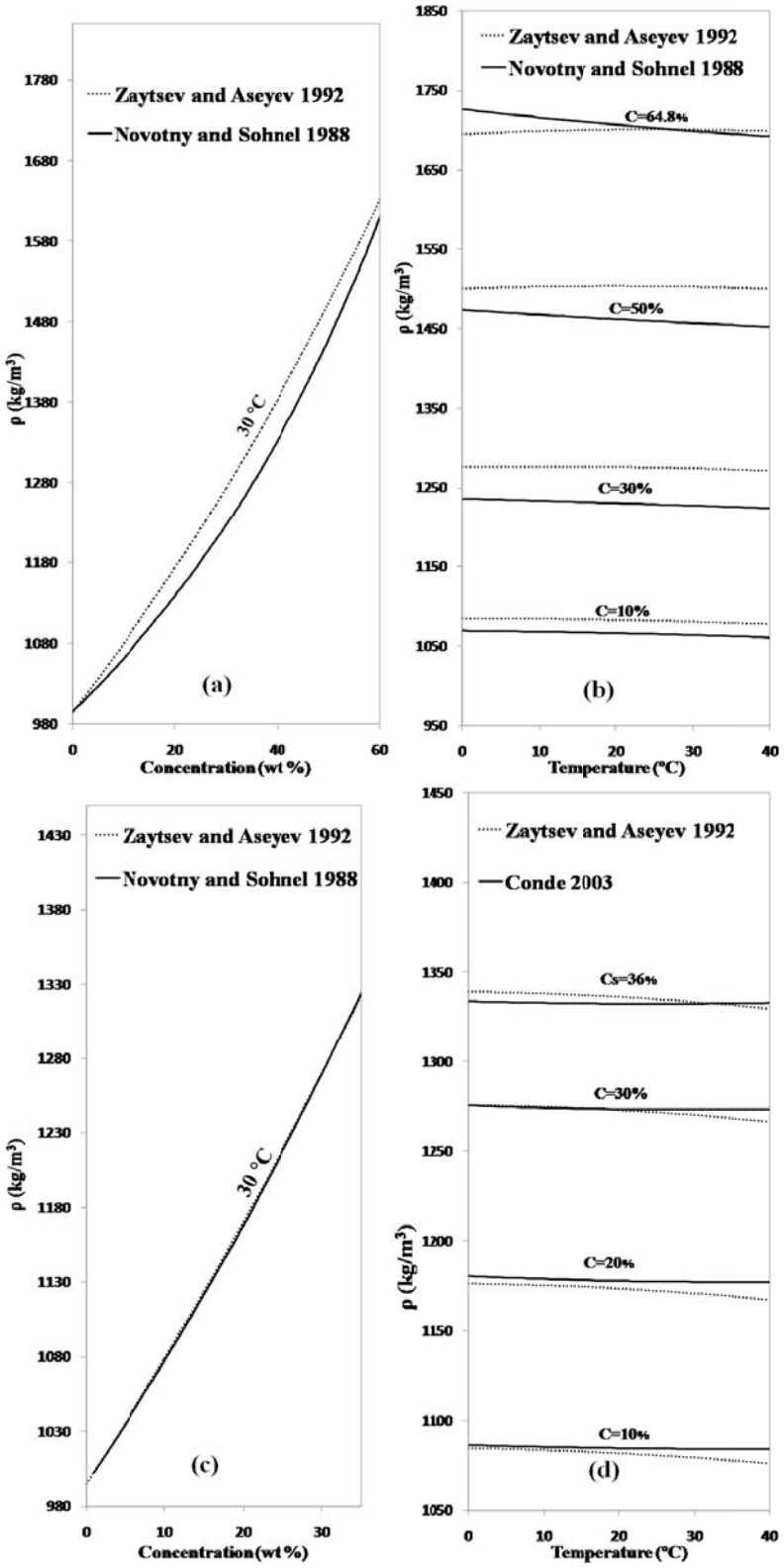

Figure 3.14: Density of a LiBr solution versus (a) concentration and (b) temperature and a $MgCl_2$ solution versus (c) concentration and (d) temperature

The density of the salt solutions changes very slightly as the temperature changes. For example, if the temperature of a 30% $MgCl_2$ is changed from 0 to 40 ˚C the density changes by only 0.08%. However, the concentration of the salt solution has a significant effect on the density of the mixture. This dramatic change in the density may cause a large change in the volume of the liquid desiccant in the system as the steady state concentration changes. Therefore storage tanks are needed in the RAMEE system to eliminate the possible damage to the system due to a change in volume of the salt solution. This issue is discussed in more detail in section 3.4.4, later in this chapter.

3.3.4 Specific Heat Capacity

Specific heat capacity is the amount of heat required to increase the temperature of a unit quantity of a substance by one degree. The specific heat capacity of the salt solutions is needed to calculate the change in temperature of the solution due to energy transfer as it flows through a liquid channel in a LAMEE. The specific heat capacity affects the temperature distribution in the liquid channels, the sensible effectiveness of the system and also affects the crystallization risk of the salt solution in the exchangers.

Results from the correlations of Zaytsev and Aseyev (1992), Conde (2004), and Chua et al. (2000) are compared in Figures 3.15 to 3.17 for the salt solutions of LiCl, $CaCl_2$, $MgCl_2$ and LiBr. The equations to calculate the specific heat of the selected salt solutions are given in Appendix A.

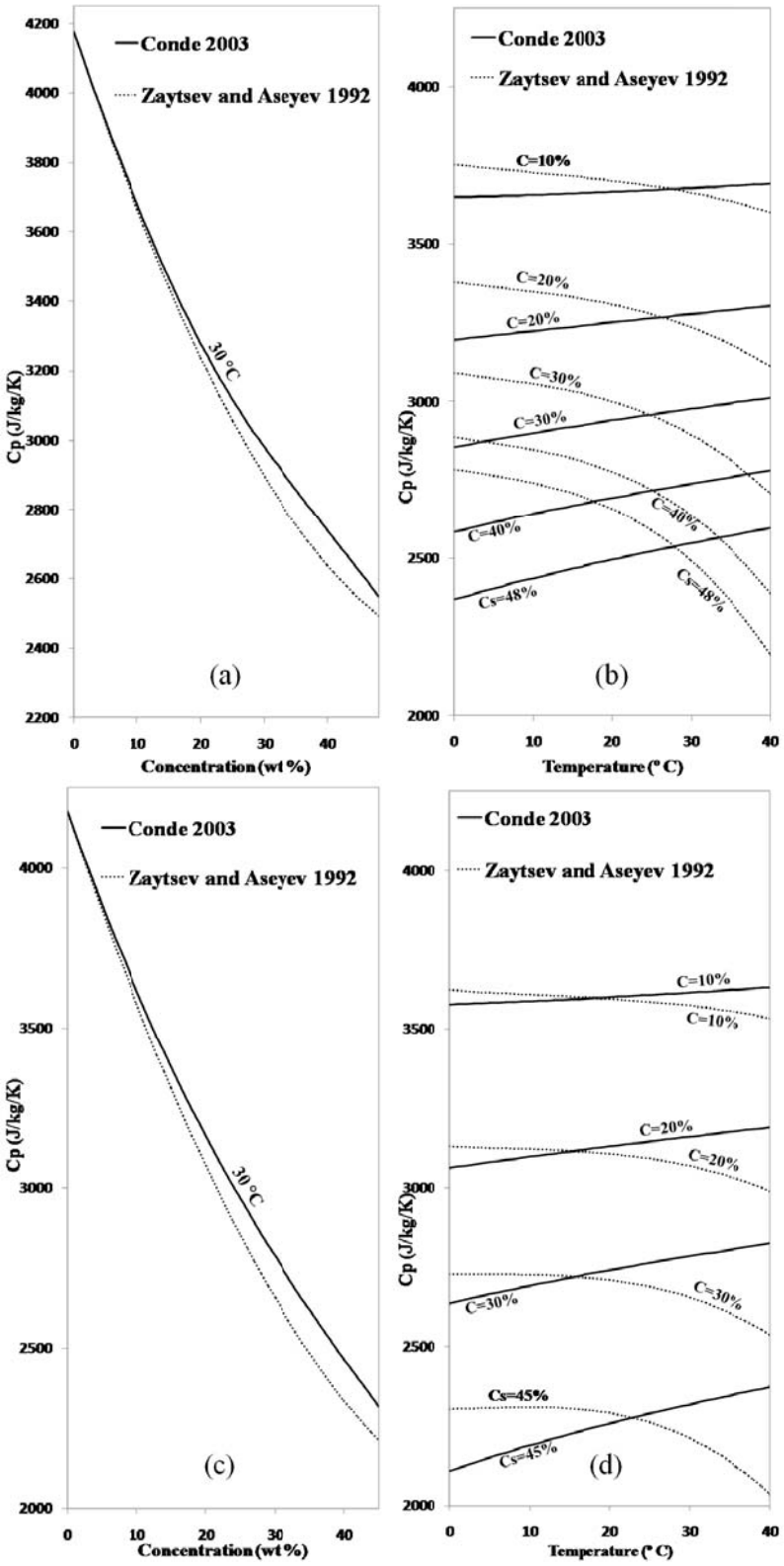

Figure 3.15: Specific heat capacity of a LiCl solution versus (a) concentration and (b) temperature and the specific heat capacity of a $CaCl_2$ solution versus (c) concentration and (d) temperature.

As seen in Figures 3.15 to 3.17, all correlations predict that the specific heat capacity of the salt solutions will decrease as the concentration of salt increases. The specific heat capacity of a saturated LiCl-water solution is 40% lower than that of pure water at 30 ˚C. The correlation of Zaytsev and Aseyev (1992) predicts that the specific heat capacity would decrease with temperature. However, correlations of Conde (2004) and Chua (2000) predict an increase in heat capacity as the temperature increases. Unfortunately not enough experimental data are available in the literature to compare with the correlations. The correlation of Conde (2004) was validated by comparing to previous measurements in his research paper, therefore, correlation of Conde is used in the current model to calculate the specific heat capacity values of LiCl and $CaCl_2$. The Cp of LiBr and $MgCl_2$ is calculated by the correlation of Zaytsev and Aseyev (1992).

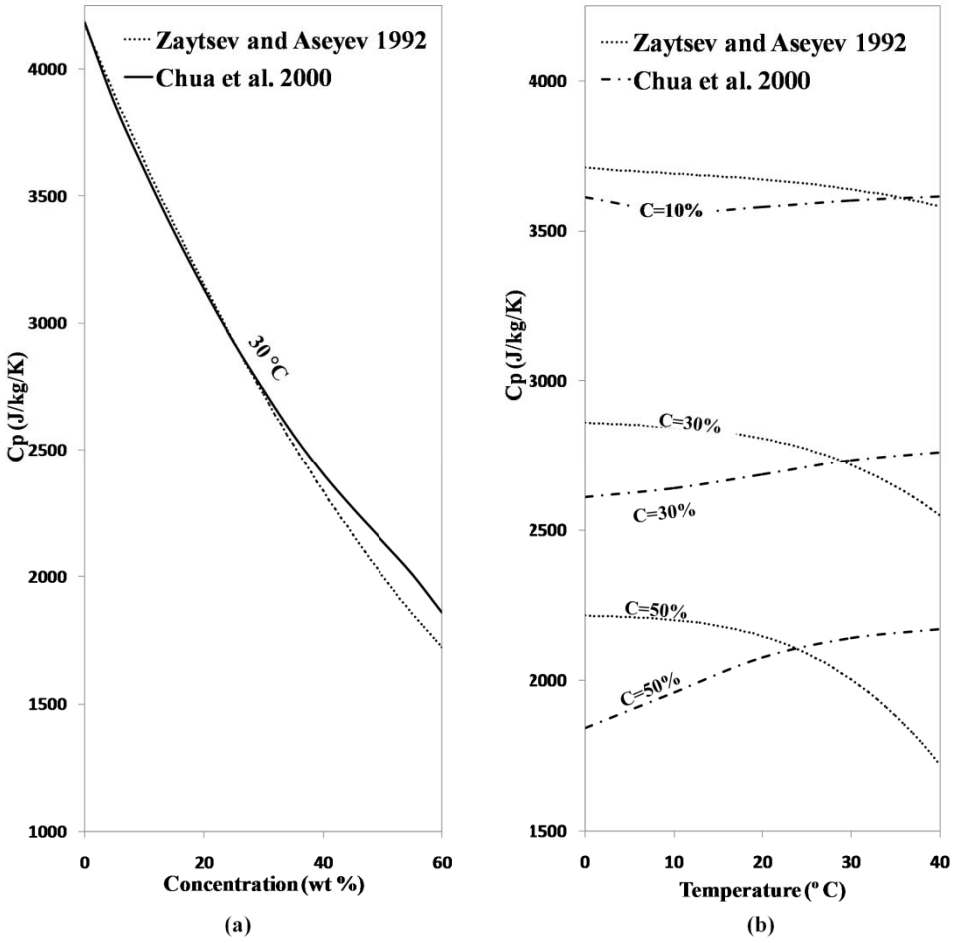

Figure 3.16: Specific heat capacity of a LiBr solution calculated by the correlations of Zaytsev and Aseyev (1992) and Chua et al. (2000) versus (a) concentration, and (b) temperature.

The difference between the specific heat capacity values, calculated by different correlations, increases as the concentration of the salt solution increases. The maximum difference between the correlations of Conde (2004) and Zaytsev and Aseyev (1992) is about 18% and 16.7% for LiCl and $CaCl_2$ solutions respectively. The difference between the Cp values for LiBr as predicted by the correlations of Chua (2000) and Zaytsev and Aseyev (1992) is 25%.

The specific heat capacity of the salt solution is included in the formula to calculate the Cr* of the RAMEE (see section 2.2.5). When the flow rate of the salt

solution is an input for the program (e.g. to compare numerical data with experimental results), different correlations may give different Cr* values. For example in summer operating conditions, the Cr* value of a RAMEE with LiCl as an operating liquid desiccant would be 12% less if calculated with correlation of Conde (2004) rather than Zaytsev and Aseyev (1992). If the value of Cr* is calculated to be 3 with the correlation of Zaytsev and Aseyev (1992), the correlation of Conde (2004) will result in a value of 2.64 for the same operating and design conditions. Therefore the total effectiveness of a RAMEE with NTU=10 would be 0.5% lower if the Cr* is calculated by correlation of Conde (2004) compared to the case when the Cr* is calculated by the correlation of Zaytsev and Aseyev (1992) for the same solution flow rate.

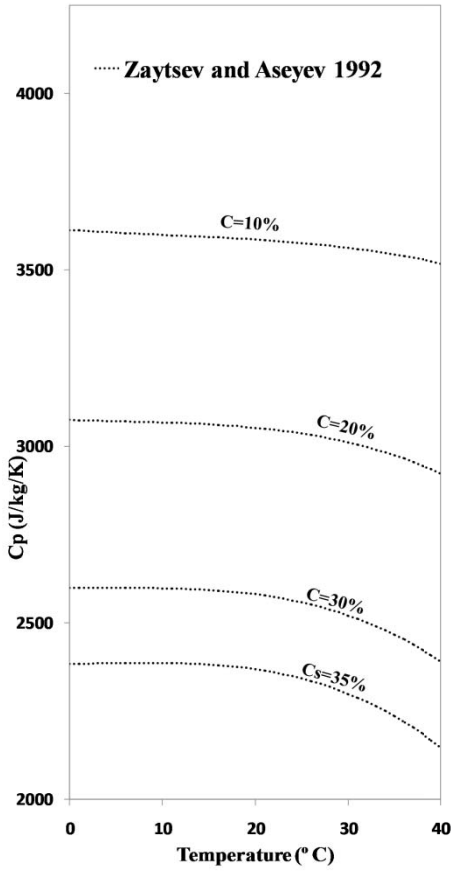

Figure 3.17: Specific heat capacity of a $MgCl_2$ solution versus temperature.

As mentioned previously, different values for specific heat capacity of the salt solution may result in different temperatures or humidities distributions in the liquid channels. However, the simulations show that the maximum change in the temperature of the liquid stream is less than 0.2˚C if different correlations are used. Using different correlations also only causes less than 0.01% difference in the total effectiveness of the RAMEE system with specified design and operating conditions (i.e., NTU=10 and Cr*=3).

3.3.5 Thermal Conductivity

The thermal conductivity of the aqueous salt solution, flowing in the LAMEEs, is another important parameter which can affect the performance of a RAMEE system.

A liquid desiccant with a higher thermal conductivity would result in higher energy transfer rate between the air and liquid streams which enhances the performance of the system.

Thermal conductivities of a large number of salt solutions have been experimentally measured and are available in the literature. Several researchers have used these experimental data to generate correlations. Thermal conductivities of the selected salt solutions (LiCl, $CaCl_2$, LiBr and $MgCl_2$) are shown in Figures 3.18 and 3.19. These values are calculated using correlations of Zaytsev and Aseyev (1992) and Conde (2004). The equations to calculate the thermal conductivity of these salt solutions are given in Appendix A.

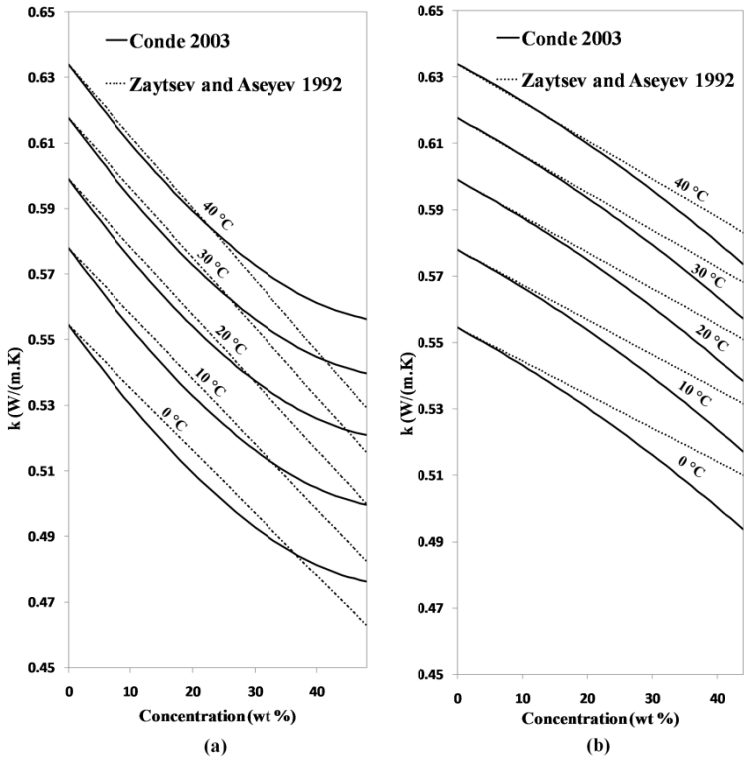

Figure 3.18: Thermal conductivity of aqueous (a) LiCl, and (b) $CaCl_2$ solutions.

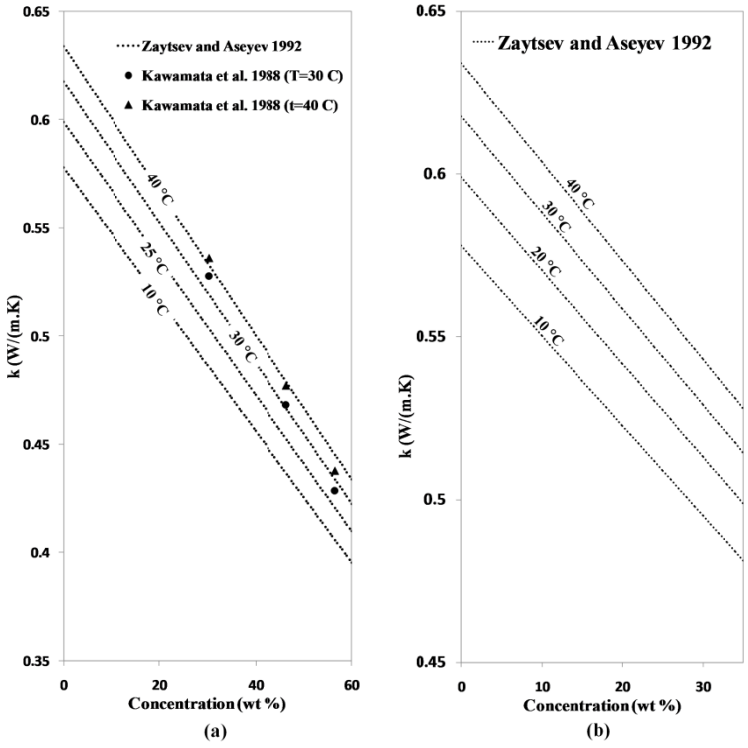

Figure 3.19: Thermal conductivity of aqueous (a) LiBr solution, and (b) $MgCl_2$ solutions at different temperatures and concentrations.

The correlation of Zaytsev and Aseyev (1992) predicts that the thermal conductivity of the salt solutions will decrease almost linearly with concentration. However, the correlation of Conde (2004) shows a non-linear behavior for LiCl and $CaCl_2$ solutions. The difference between the thermal conductivities, calculated with the correlations of Zaytsev and Aseyev (1992) and Conde (2004), increases as the concentration of salt increases. At 40˚C, the difference between the two correlations for a saturated LiCl and $CaCl_2$ becomes 5% and 1% respectively. Thermal conductivity of LiBr and $MgCl_2$ are shown in Figure 3.19. The correlation of Zaytsev and Aseyev (1992) is the only correlation found in the literature to predict the thermal conductivity of these two salt solutions (LiBr and $MgCl_2$). The correlation of Zaytsev and Aseyev (1992) for a LiBr solution is compared to experimental measurements of Kawamata (1988) in Figure 3.19. The experimental values also show a slightly non-linear relationship between thermal conductivity and concentration.

In order to investigate the impact of using different correlations on the effectiveness, predicted by the numerical model, a RAMEE system with a LiCl solution used as the liquid desiccant is simulated with the two different correlations. At NTU=10 and Cr*=3, the effectiveness is only decreased by 0.1% if the correlation of Conde (2004) is used instead of Zaytsev and Aseyev's (1992).

The thermal conductivity of the salt solution also affects the calculated NTU value of the system (see chapter 2, section 2.2.5). During summer operating conditions, when the maximum difference between the calculated thermal conductivities of Conde (2004) and Zaytsev and Aseyev (1992) occur, the difference between the two calculated

NTU values is less than 0.05%. Therefore the change in the effectiveness of the system due to the difference in the calculated NTU vales will be negligible.

3.3.6 Diffusion Coefficient

Mass transfer from the airstream to the liquid desiccant depends on the binary diffusion coefficient of water into the salt solution. The diffusion coefficient appears in the Lewis number (in Equation (2-13)) and is required to calculate the convective mass transfer coefficient of the salt solution. Figure 3.20 shows the diffusion coefficients of LiCl and $CaCl_2$ solutions at different concentrations and temperatures. The equations to calculate the diffusion coefficients of LiCl and $CaCl_2$ solutions are given in Appendix A. As expected, the diffusion coefficient decreases as the concentration of salt in the solution increases. This means that the diffusion of water is lower in highly concentrated salt solutions compared to dilute solutions. As expected from kinetic theory, Figure 3.20 shows that increasing temperature increases the diffusion coefficient of water in the salt solution.

Some experimental measurements of diffusion coefficients of LiBr and $MgCl_2$ solutions at 23˚C are shown in Figure 3.21. Unfortunately no correlated or experimental data were found for these salt solutions at other temperatures.

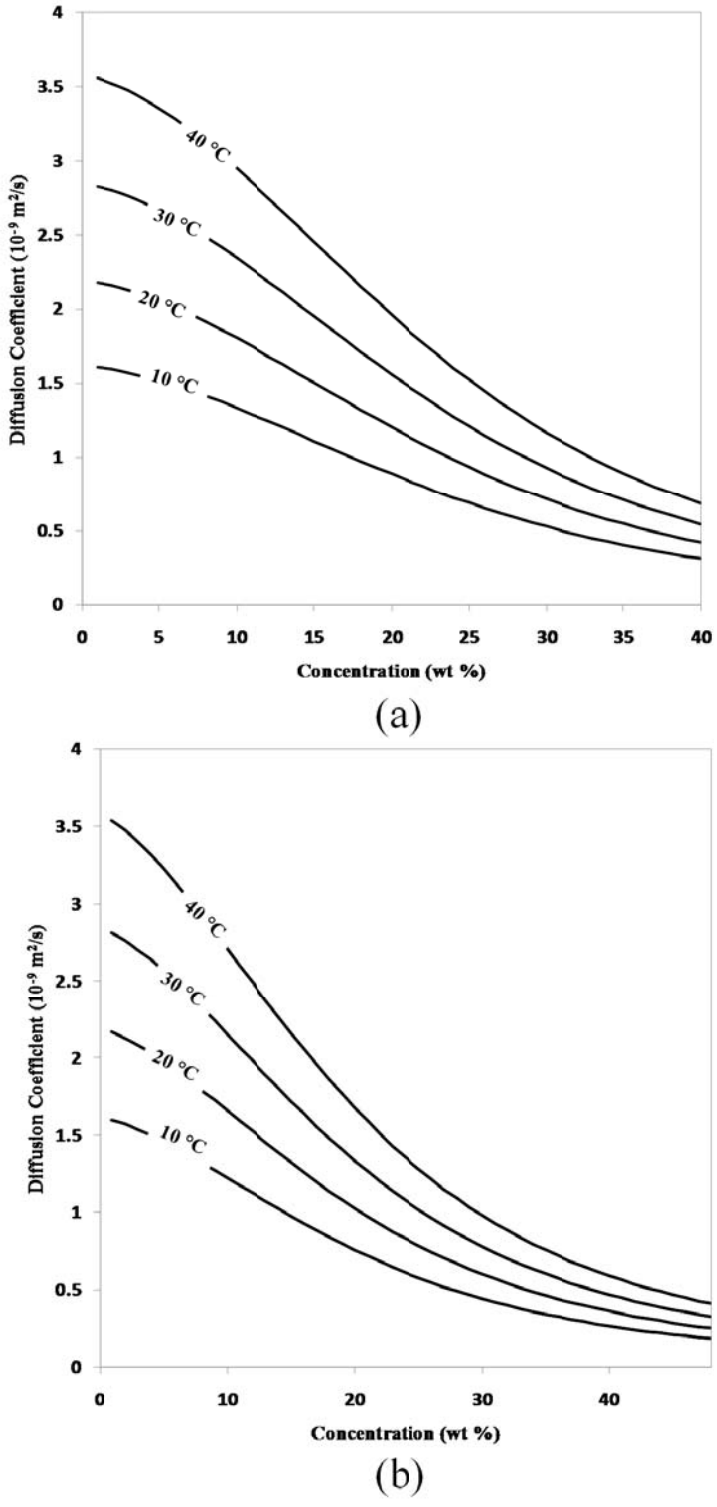

Figure 3.20: Binary diffusion coefficient of water in (a) LiCl, and (b) $CaCl_2$ solutions at different concentrations and temperatures (Conde 2003).

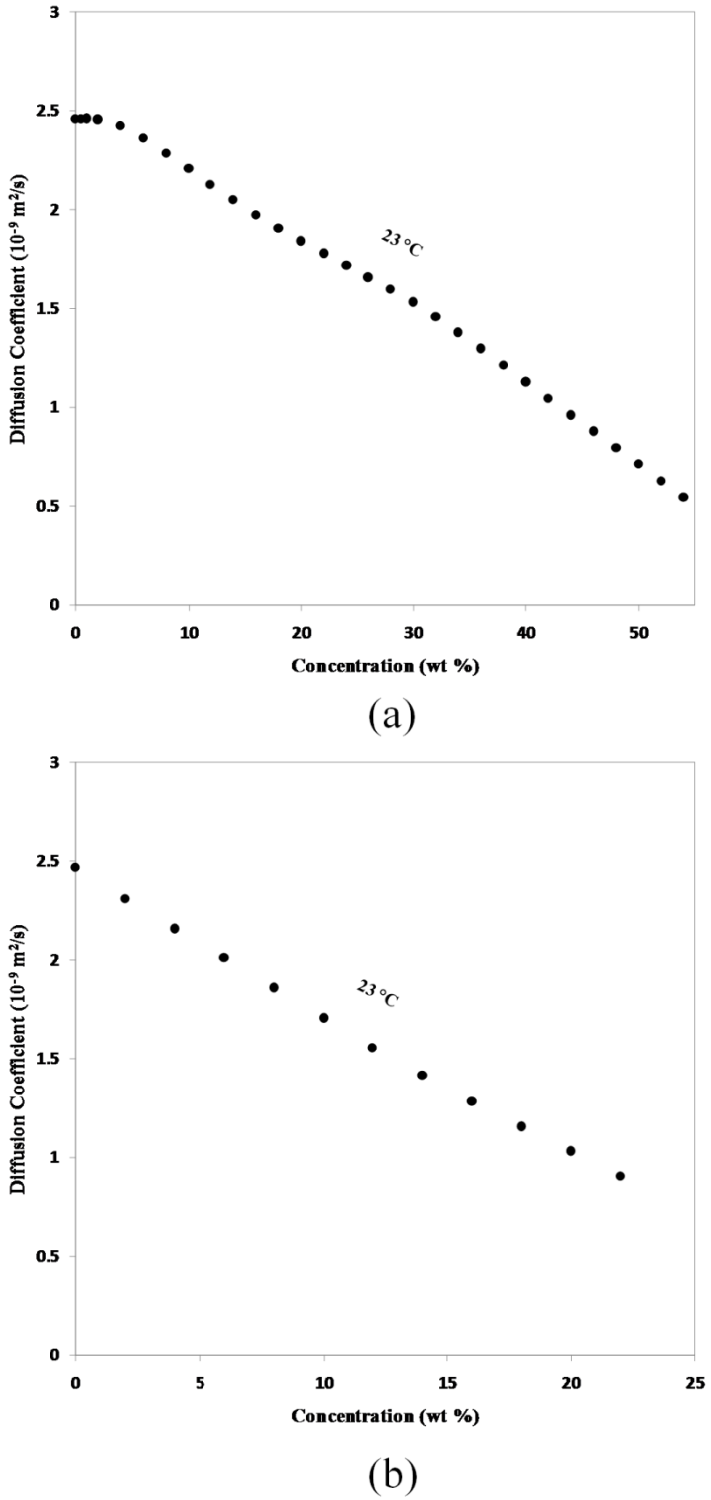

Figure 3.21: Binary diffusion coefficient of water in (a) LiBr, and (b) $MgCl_2$ solutions at T=23 ˚C and different concentrations (Zaytsev and Aseyev 1992).

Vali (2009) and Fan (2005) used a constant value for the diffusion coefficient of the liquid desiccant in their numerical model. They chose an available experimental value of diffusivity at 25˚C and the steady state concentration of the salt solution operating in the RAMEE system (e.g. D=0.803e-9 m^2/s for LiCl). The impact of using temperature and concentration dependent correlations to calculate the diffusion coefficient has only a slight effect on the calculated effectiveness. For example, the effectiveness of a RAMEE system with NTU=10 and Cr^*=3 only increases 0.5% if different coefficient correlations are used instead of a constant value.

3.4 Additional Properties

The thermo-physical properties discussed in the previous sections may directly affect the performance of the RAMEE system. In addition to these properties, some other features of the liquid desiccants are important in the selection of the proper salt solution for the RAMEE system. These properties include safety and cost of the salt solutions.

3.4.1 Safety

Major potential markets for the RAMEE system are residential and commercial buildings. Therefore, all the components of the system must be safe to operate in these facilities. The liquid desiccant has to be selected carefully according to its safety features because in some cases, the desiccant may leak through the membrane and into the air channels or the surroundings. Therefore, the salt solution should not be hazardous to health, be flammable or have other special hazards (e.g. be reactive).

Inorganic salts have different safety characteristics in the liquid form than in the solid form. Since salts are used in solution form in the RAMEE system, the material

safety characteristics of these salts need to be investigated as aqueous solutions. The material safety data of these salt solutions are summarized in Table 3.1. The numbers shown in parentheses in the health hazard column of Table 3.1 show the National Fire Protection Agency (NFPA) rating of each specific salt solution (MSDS 2005 and 1993). According to this rating system, a value of 0 means no specific hazard and a value of 1 means slightly hazardous. As seen in Table 3.1, the salt solutions investigated in this thesis are safe if stored far from incompatible materials (i.e., strong acids such as nitric and sulfuric acids) and if not swallowed.

Table 3.1: Summary of the material safety data of some selected salt solutions.

Salt solution	Health hazard	Flammable	Stability	Incompatible with other materials
LiCl	Harmful if swallowed (1)	No	Stable	Yes (Acids)
$CaCl_2$	Safe (0)	No	Stable	No
LiBr	Harmful if swallowed (1)	No	Stable	No
$MgCl_2$	Safe (0)	No	Stable	Yes (Strong acids)

Handling and storage of the salt solutions is also important if the solutions are purchased in volumes and stored in the factory. All of the selected salt solutions (listed in Table 3.1) are harmful in solid form and may cause eye or skin irritation. Therefore, salts in powder form have to be stored in tightly sealed packages and kept in well ventilated areas. LiCl and $MgCl_2$ solutions have to be stored away from sulfuric and nitric acids, caustics, ammonia, and cyanides.

$CaCl_2$ and $MgCl_2$ may be drained in the public sewer system if diluted by large amount of water while the contact of LiCl and LiBr solutions with soil, sewers, waterways and drains should be avoided.

3.4.2 Cost

More than 35 L of salt solution were required to fill the exchangers and storage tanks of the latest prototype of the RAMEE system (Mahmud 2009). This amount of required salt solution will be even higher in most commercial RAMEE systems. Therefore, considering the volume of the liquid desiccant in the system, desiccant price may create a large portion of the initial cost of the RAMEE system. There is a significant difference between the prices of the solutions of halides of Lithium compared to other inorganic salt solutions. The reason is an increase in the demand for Lithium products since the creation of the Lithium ion batteries. Table 3.8 shows the prices of the salt solutions (LiCl, $CaCl_2$, LiBr and $MgCl_2$), obtained from Asian suppliers in January 2009. The prices shown in Table 3.2 are for the salts in solid form and do not include shipping expenses.

Table 3.2: Prices of selected salts in solid form as obtained from Asian suppliers in January 2009.

Salt	Price per metric ton (USD)
LiCl-anhydrous	7400
$CaCl_2$-dihydrate	284
LiBr-anhydrous	3660
$MgCl_2$-hexahydrous	155

As seen in Table 3.2, the price of LiCl is almost twice the price of LiBr and 47 times more than the price $MgCl_2$. However, the prices listed in Table 3.8 do not exactly show the cost of liquid desiccant in a RAMEE since the concentration of each specific salt solution is different in the system. For example during AHRI summer conditions, the RAMEE system operates with a 32% wt concentration $MgCl_2$ at steady state while the concentration of LiCl is 28% under the same conditions. Also the number of water

molecules bonded with the salt molecules affects the mass of salt that must be purchased. For example at room temperature, $MgCl_2$ exists in hexahydrate form, which means that each molecule of $MgCl_2$ contains six molecules of water. Therefore, a large part of the purchased $MgCl_2$ is water and this amount of water has to be accounted for when calculating the mass of the salt in the liquid desiccant. Table 3.3 shows the actual mass of each specific salt that must be purchased for the RAMEE prototype of Mahmud (2009) (i.e., to create 35 L of salt solution at AHRI summer equilibrium concentration).

Table 3.3: Price for 35 L of the liquid desiccant in the RAMEE prototype.

salt	Unit price per ton (USD)	Steady-state concentration for AHRI summer conditions	Salt mass in solution (kg)	Price of the desiccant in the prototype (USD)	Price of the desiccant per CFM (USD)	Relative price
LiCl	7400	28%	12.16	89.98	1.21	20
$CaCl_2$	284	37%	32.8	9.30	0.12	2
LiBr	3660	41%	21.73	79.53	1.12	19
$MgCl_2$	155	32%	26.5	4.10	0.06	1

The most right column in Table 3.3 shows the price of the liquid desiccant per unit flow rate (CFM) of the RAMEE prototype of Mahmud (2009). The characteristics of this prototype are given in Table 2.1 (chapter 2) and the price per CFM is based on the maximum tested air flow rate in this prototype of 77 CFM. As seen in Table 3.3, the prices of the Lithium salts are still higher than other salt solutions. $MgCl_2$-water solution is the least expensive among the studied salt solutions and is 20 times less expensive than LiCl solution.

3.5 RAMEE Properties

The thermo-physical properties of the salt solutions will impact the characteristics of some component of the RAMEE (i.e., liquid pumps and storage tanks). The effect of the solution properties are discussed in the following sections.

3.5.1 Pumping Cost

In addition to the initial cost of the liquid desiccant, the operating cost of a RAMEE system may also be dependent on the liquid desiccant used. Electric power used by the pump motors to circulate the salt solution is one of the operating expenses of the RAMEE system. Pumping power is a function of pressure drop of the salt solution in the connecting pipes and the LAMEEs.

Pressure drop in a laminar, fully developed flow in a pipe may be calculated using the following equation (Fox and McDonald 1994):

$$\Delta p = \frac{128 \mu L_p \dot{m}}{\pi \rho D_p^{\ 4} \cdot 1000} \tag{2-3}$$

where

L_p is the length of the pipe [m]

D_p is the diameter of the pipe [m]

$\dot{m}$ is the mass flow rate of the salt solution [kg/m^3]

Δp is the pressure drop [kPa]

Similarly pressure drop in liquid flow between two parallel plates (liquid channels of a LAMEE) may be calculated by (Fox and McDonald 1994):

$$\Delta p = \frac{12 \mu y_0 \dot{m}}{\rho x_0 \delta^3 \cdot 1000} \tag{2-4}$$

where

δ is the liquid channel spacing [m]

y_0 is the length of the liquid channel [m]

x_0 is the width of a liquid channel [m]

Equations (2-3) and (2-4) show that the pressure drop depends on, among other things, the viscosity and density of the salt solution, which vary among salt solutions as described in sections 2.3.2 and 2.3.3.

Figure 3.22(a) shows the pressure drop in the piping and exchangers of a RAMEE. Characteristics of the LAMEEs simulated in this section are given in Table 2.1 (chapter 2). The pipes in the RAMEE prototype are ¾" (19.05 mm) diameter and are assumed to be straight in this example. Figure 3.22 (b) shows the electric energy consumption of the pump and its cost per unit flow rate of air of a RAMEE system operating with Cr*=3 (based on 12 hours a day operation of the system throughout a year). The pump in this example is assumed to have 60% mechanical efficiency and the electricity price is assumed to be 10 ¢/(kW·h) as indicated by the Canadian National Board of Energy for Saskatchewan (NBE 2010). As mentioned earlier in chapter 2, the value of Cr* of a RAMEE is the ratio of the solution flow rate to the air flow rate. Therefore at a constant Cr*, the flow rate of the salt solution and consequently its pressure drop depends on the flow rate of air. As seen in Figure 3.22, $MgCl_2$ has the maximum pressure drop when flowing through the pipes and the exchangers. The pressure drop of a $MgCl_2$ solution in the exchangers is almost twice the value of pressure drop of a LiCl solution and is more than 3 times that of a LiBr solution.

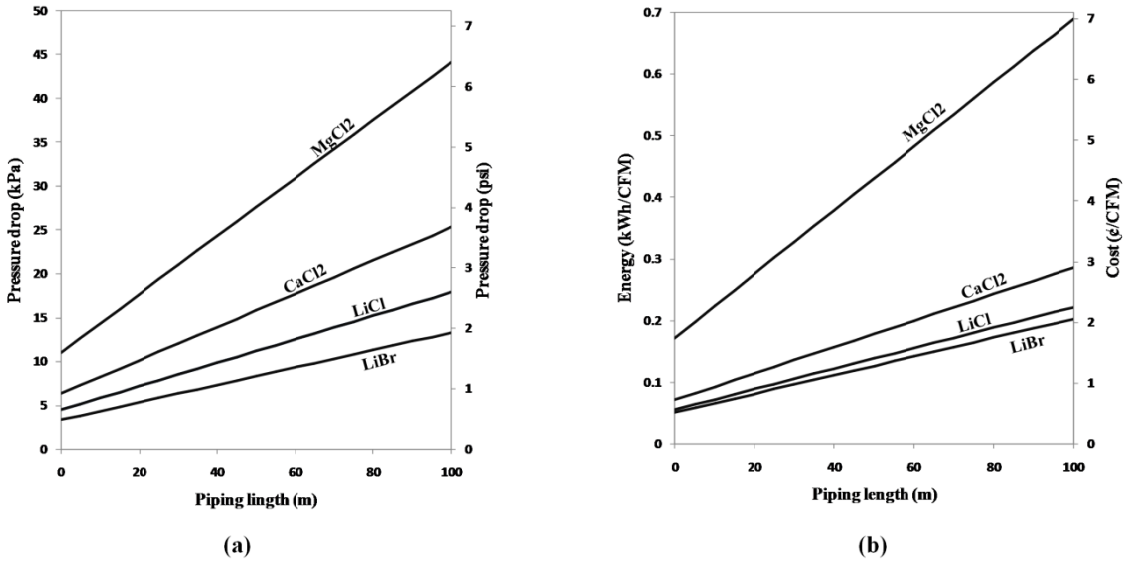

Figure 3.22: (a) Total pressure drop of different salt solutions in a RAMEE with different pipe lengths and (b) annual pump energy consumption and cost per unit flow rate of air.

The higher pressure drop of $MgCl_2$ solution compared to other liquid desiccants is a result of its high viscosity at the steady state operating condition of the RAMEE system. Viscosity of the salt solutions is highly dependent on concentration. The increase in the viscosity becomes very dramatic close to the saturation concentration (see Figures 3.11 and 3.12). As mentioned previously, the saturation concentration of $MgCl_2$ solution at 25 ˚C is 35.5% (by weight). $MgCl_2$ solution in a RAMEE system working during summer AHRI operating conditions circulates with a concentration (32%) that is very close to its saturation concentration. This causes $MgCl_2$ solution to have a higher pressure drop through the pipelines and exchanger flow channels than other salt solutions.

The power required to pump the liquid desiccant is directly proportional to the pressure drop of the liquid in the pipes and exchangers. Therefore, the pumping power required for a RAMEE system operating with $MgCl_2$ solution is almost 2.6 and 3.4

times larger than that required in systems working with LiCl and LiBr solutions respectively.

Figure 3.23 shows the total cost of the different salt solutions (initial and pumping cost) per CFM of the air flow rate in the RAMEE after 15 years of the operation of the system for different pipe lengths. The total volume of the salt solution is assumed to be 35 L without considering the pipes.

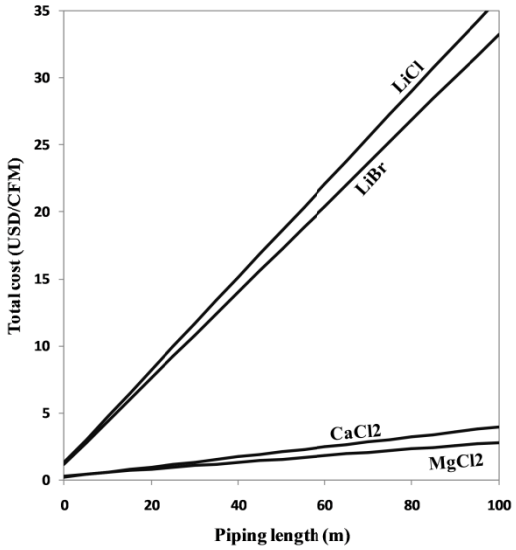

Figure 3.23: Total price of the selected salt solutions (initial and pumping cost) per unit CFM.

As seen in Figure 3.23, the initial cost of the salt solution dominates the pumping cost in the RAMEE. Large increase in the price of the LiCl and LiBr solutions after increasing the pipe length is due to an increase in the volume of the solution in the system. It should also be noted that the difference between the pressure drops of different salt solution is not high enough to affect the pump size or pipes diameter, therefore it is assumed that changing the liquid desiccant would not impose extra costs on the initial RAMEE price.

3.5.2 Storage Tank Size

The liquid desiccant in the RAMEE system is stored in two storage tanks located before each LAMEE. These storage tanks prevent possible damages to the RAMEE system in case of a change in the volume of the salt solution due to temperature change or moisture transfer to/from the desiccant solution. To make the RAMEE system smaller and reduce the transient delay of the system, it is required to minimize the change in the volume of the salt solution and consequently the storage tank size during the normal operation.

The concentration (and therefore total volume) of the salt solution in a RAMEE system depends on the outdoor and indoor operating conditions. The salt solution in RAMEE systems operating in very humid outdoor conditions has a lower concentration (and higher moisture content and volume) than systems operating in dry conditions. Since the mass of salt in the solution stays constant throughout the year, the volume of the salt solution increases in more humid operating conditions. The volume of the salt solution is also higher during winter than summer operating conditions. The reason is that the steady state concentration of the salt solution is normally lower during winter conditions than during summer conditions. Figure 3.24 shows the change in the volume of the salt solution from summer to winter operating conditions for different salt solutions in a system with an initial salt solution volume of 35 L (prototype of Mahmud 2009).

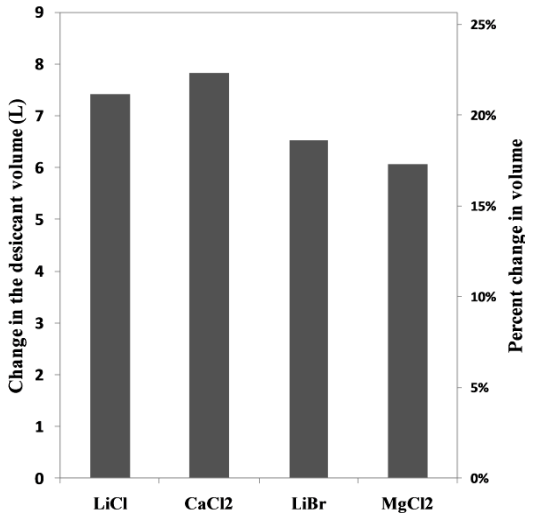

Figure 3.24: Change in the volume of the salt solution from AHRI summer to winter operating conditions.

Table 3.4 shows the bulk concentration and density of the different salt solutions in a RAMEE system during AHRI summer and winter operating conditions as well as the change in the volume of the salt solution.

Table 3.4: Change in the density, concentration and volume of the salt solution from AHRI winter to AHRI summer operating conditions.

	AHRI Winter Operating Condition		AHRI Summer Operating Condition		
Salt solution	**Concentration**	**Density (kg/m^3)**	**Concentration**	**Density (kg/m^3)**	**Change in the Solution Volume (L)***
LiCl	22.5%	1133	26.7%	1157	7.4
$CaCl_2$	30.5%	1288	35.8%	1342	7.8
LiBr	35.50%	1287	40.5%	1339.5	6.5
$MgCl_2$	29%	1267	33.0%	1306.2	6.0

* For 35 L initial volume of liquid

As seen in Table 3.4, the concentration decreases by almost 5% for all the salt solutions as the operating condition changes from AHRI summer to AHRI winter conditions. The change in the volume of the salt solution will be larger if the outdoor air humidity varies more throughout the year. Figure 3.25 shows the change in the volume of a LiCl solution in a RAMEE system operating in some selected cities (Saskatoon, Chicago, Miami and Phoenix) throughout a year.

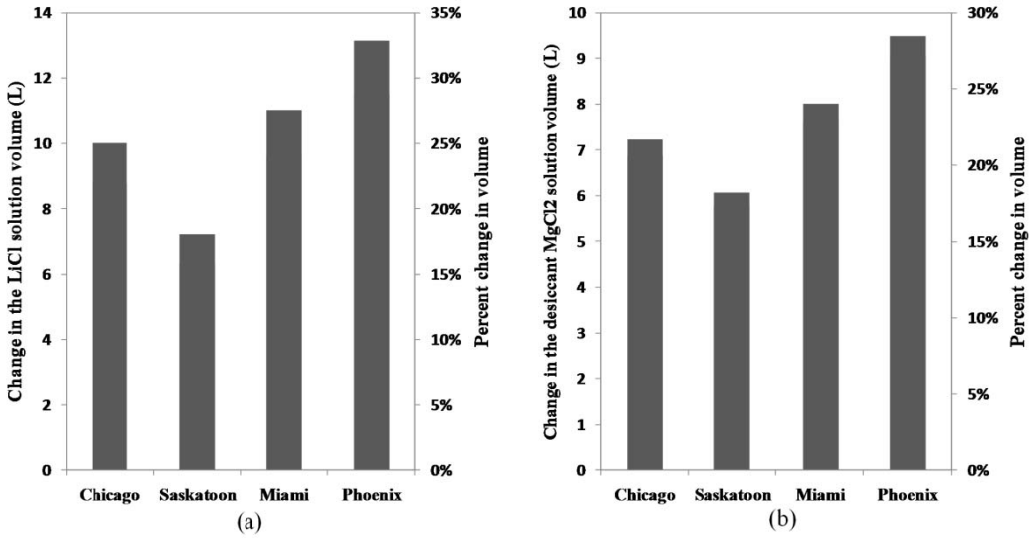

Figure 3.25: Maximum change in volume of a (a) LiCl and (b) $MgCl_2$ solutions during a yearly simulation in some selected cities (NTU=10, Cr*=3).

The volume of the liquid desiccant changes the most in the cities of Phoenix and Miami where humidity varies the most throughout the year. The concentration of LiCl decreases 10% from the driest day in the year to the most humid day in the year (i.e., from 25.5% wt to 35.5% wt) in Phoenix while the concentration changes only 4% in Saskatoon during a year (i.e., from 20.5% to 24.5%). The change in volume of the $MgCl_2$ solution is on average 20% less than that of a LiCl solution in different cities.

3.6 Effectiveness of the RAMEE Systems with Different Salt Solutions

Different salt solutions have diverse thermophysical properties which may impact the effectiveness of the RAMEE systems operating with different salt solutions. Figure 3.26 shows the effectiveness of a RAMEE operating with four different salt solutions (LiCl, $CaCl_2$, LiBr and $MgCl_2$) with AHRI summer operating conditions (NTU=10).

As seen in Figure 3.26, the difference in the effectiveness of the RAMEE systems operating with different salt solutions is very small. For example, the

maximum total effectiveness of the RAMEE systems operating with $CaCl_2$ is 53.5% while this value for the systems operating with $MgCl_2$ is 53.1%. The difference between the latent effectiveness of the systems with various salt solutions is also very small (less than 0.5%). Systems with LiBr as the operating liquid desiccant have the highest effectiveness among the investigated salt solutions but the difference is very minor (less than 0.5%).

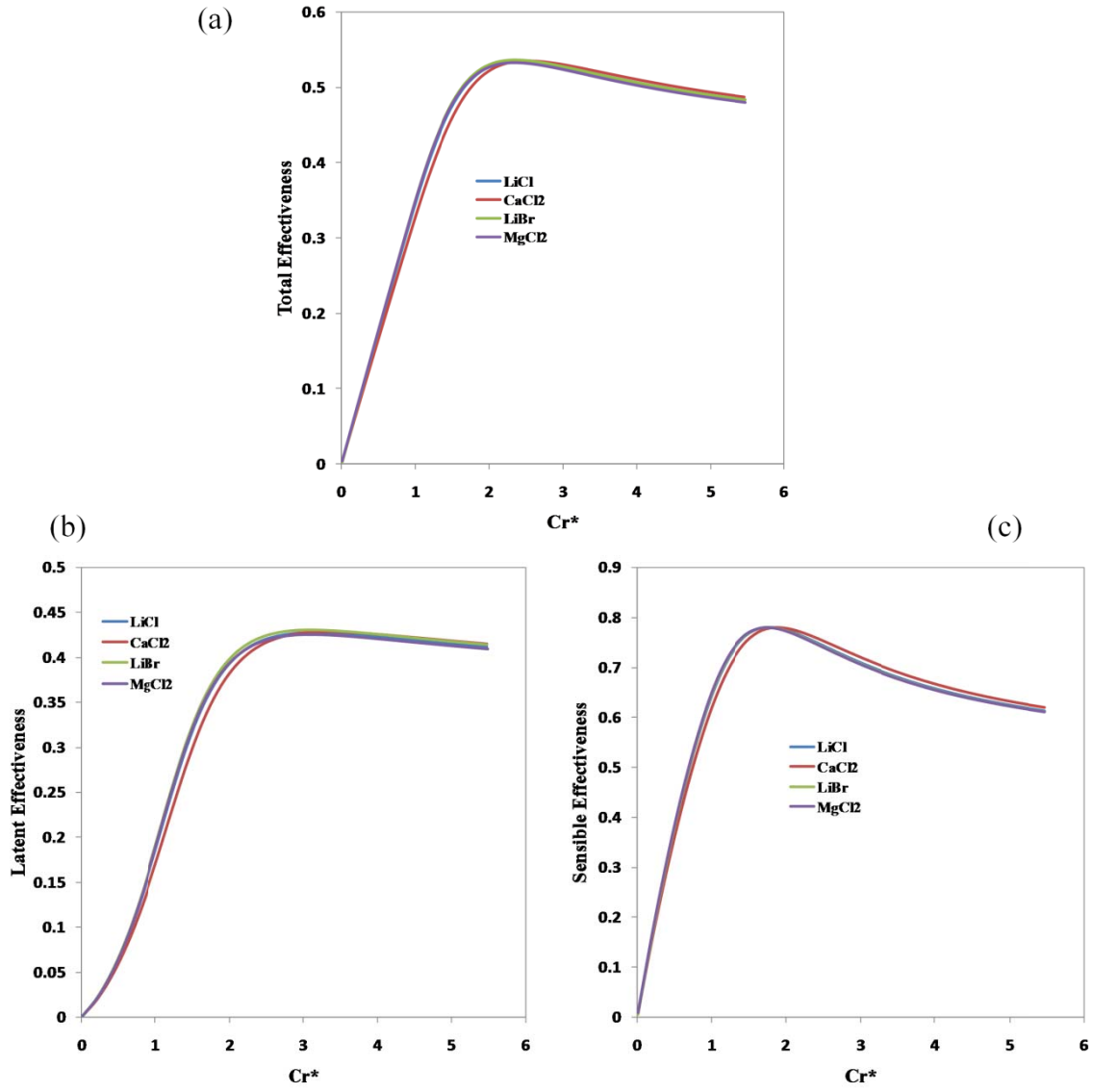

Figure 3.26: (a) Total, (b) latent, and (c) sensible effectiveness of the RAMEE system operating during AHRI summer conditions with different salt solutions (NTU=10).

Minor differences between the effectiveness of the system with different operating salt solutions show that the thermal and physical properties of the salt solution do not significantly affect the performance of the RAMEE provided NTU and Cr* are fixed.

3.7 Summary

This chapter mainly discusses the different properties of some selected salt solutions to be used in the RAMEE system. Thermo-physical properties of the selected salt solutions (including density, viscosity, specific heat capacity, thermal conductivity and diffusion coefficient) are investigated at the beginning of this chapter. Various correlations from different researchers are applied to calculate these properties. Some of these correlations are compared to available experimental measurements and the most accurate correlations are selected for use in the numerical model. Safety features of the salt solutions are also investigated in this chapter and it is shown that the selected salt solutions (in liquid form) may all be safely used for residential and commercial HVAC applications.

Numerical simulations show that the performance of the RAMEE system is not significantly affected by changing the salt solution (maximum variation of 0.5% in total effectiveness). However some properties such as dynamic viscosity and density of the salt solution affect the operational expenses of the RAMEE system (e.g. pumping power and storage tank size).

Table 3.5 summarizes the initial and operational costs of the selected salt solutions. This table ranks different selected salt solutions with relative numbers where a value of 1 is assigned to the salt solution with the lowest cost/smallest size and other numbers are relative to this number. Table 3.5 shows that $MgCl_2$ has the lowest initial cost and required storage tank size, but has the highest pumping cost. The LiCl has a 20 times higher initial cost and requires a 20% larger storage tank than $MgCl_2$.

Table 3.5: Summary of the initial and operating cost an storage tank size of each selected salt solution in the RAMEE system. Value of 1 is assigned to the smallest size/lowest cost and other values are relative to this number.

Salt solution	Initial cost	Pumping cost	Storage tank size
LiCl	20	1.3	1.2
$CaCl_2$	2	1.9	1.3
LiBr	19	1	1.1
$MgCl_2$	1	3.3	1

CHAPTER 4

CRYSTALLIZATION LIMITS

4.1 Introduction

It is important to avoid salt crystallization during the operation of a RAMEE system since salt crystals will negatively impact the performance of the system (i.e., decrease effectiveness and increase the pumping cost). In this chapter, the crystallization risk of four binary salt solutions (LiCl, $MgCl_2$, $CaCl_2$ and LiBr) in the steady-state operation of the RAMEE system is investigated. The effect of climate and RAMEE design parameters (NTU and Cr*) and flow configuration (cross and counter-cross flow) on the risk of crystallization of these salt solutions are also studied in detail.

4.2 Design and Operating Conditions

In this chapter, the RAMEE system is initially simulated with the NTU=10 and Cr^*=3 to investigate the behavior of the liquid desiccant in the system. The simulations are then repeated for the systems with NTUs up to 20 and Cr* values up to 15 to show the effect of changing the design characteristics of the system on the risk of crystallization of the salt solution. Total effectiveness of the system varies between 40 to 70% depending on design and operating conditions.

The operating conditions in which the RAMEE system works are other key factors that may affect the risk of crystallization of the salt solution in the LAMEEs. The system is primarily simulated for outdoor and indoor operating conditions as

specified by AHRI Standard 1060 (AHRI 2005). In order to investigate the effect of changing indoor and outdoor conditions on the crystallization risk additional operating points are simulated as well. Table 4.1 lists the AHRI and additional design operating conditions in summer and winter used in this chapter. Summer operating condition in this thesis means that the outdoor temperature is higher than the indoor temperature and winter operating condition is defined as outdoor temperature is lower than indoor temperature.

Table 4.1: Selected indoor and outdoor operating conditions.

		Indoor			Outdoor		
		T	**Humidity Ratio**	**Relative Humidity**	**T**	**Humidity Ratio**	**Relative Humidity**
Summer	**AHRI Condition (Case A)**	24 °C	9.3 g/kg	50%	35° C	17.5 g/kg	50%
					35° C	11.5 g/kg	33%
	(Case B)	24 °C	5.5 g/kg	30%	35° C	10.5 g/kg	30%
	(Case C)	24 °C	1.8 g/kg	10%	35° C	7.4 g/kg	21.2%
Winter	**AHRI Condition**	21 ° C	7.1 g/kg	46%	1.7° C	3.5 g/kg	82%
		21 ° C	4.6 g/kg	30%	-	-	-

4.3 Humidity Ratio and Relative Humidity at the Solution-Membrane Interface

The concentration of a liquid desiccant is directly proportional to the equilibrium relative humidity at the solution-air interface and temperature. In a RAMEE system, the concentration of the salt solution would depend on the humidity and temperature at the solution-membrane interface which itself is a function of the humidity and temperature conditions of the airstream flowing in the exchangers. As the airstream becomes dryer, the humidity at the solution-membrane interface reduces. The steady state concentration of the salt solution increases when the air relative humidity at the solution-membrane interface is reduced. When the concentration of the salt solution reaches the saturation

concentration value of the salt solution, salt crystals would begin to form in the LAMEEs.

The numerical model, described in chapter 2, may be applied to evaluate the temperature and humidity at the solution-membrane interface. The conditions at the solution-membrane interface may then be compared to that of the saturated solution (evaluated from the VP correlations introduced in chapter 3) to predict the occurrence of crystallization in the LAMEEs.

Figure 4.1 shows contours of humidity ratio at the solution-membrane interface in the supply and exhaust exchangers (with cross flow configuration) of a RAMEE, operating with AHRI summer conditions (NTU=10 and Cr*=3). As seen in Figure 4.1(a), the humidity ratio at the solution-membrane interface increases in the direction of liquid flow in the supply exchanger. This means that the liquid desiccant gains moisture in the supply exchanger while the air loses moisture. The dilute liquid desiccant leaving the supply exchanger is pumped to the exhaust exchanger where it loses its moisture to relatively dry air coming from the building. As a result, the humidity ratio at the solution-membrane interface decreases in the direction of the liquid flow in the exhaust LAMEE (see Figure 4.1(b)). As seen in Figure 4.1(b), the minimum value of humidity ratio in the RAMEE occurs in the upper right corner of the exhaust LAMEE where the liquid leaves and the air enters the exhaust LAMEE.

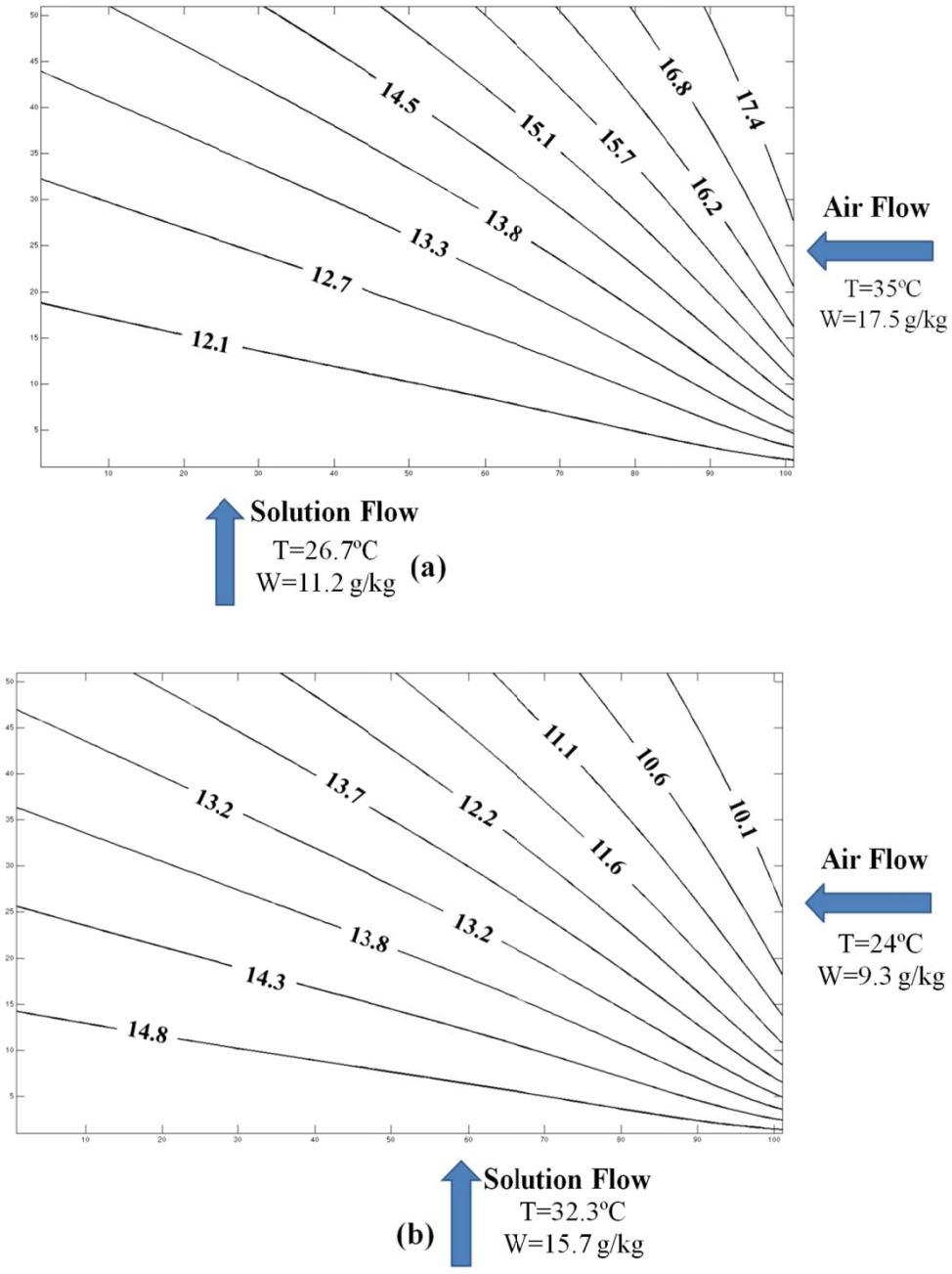

Figure 4.1: Humidity ratio (g/kg dry air) at the solution-membrane interface of the (a) supply and (b) exhaust LAMEEs (NTU=10 and Cr*=3, AHRI summer operating conditions).

The temperature and humidity ratio at the interface of solution and membrane are used in the numerical code to determine the air relative humidity (Figure 4.2) at the solution-membrane interface and the bulk salt concentration (Figure 4.3).

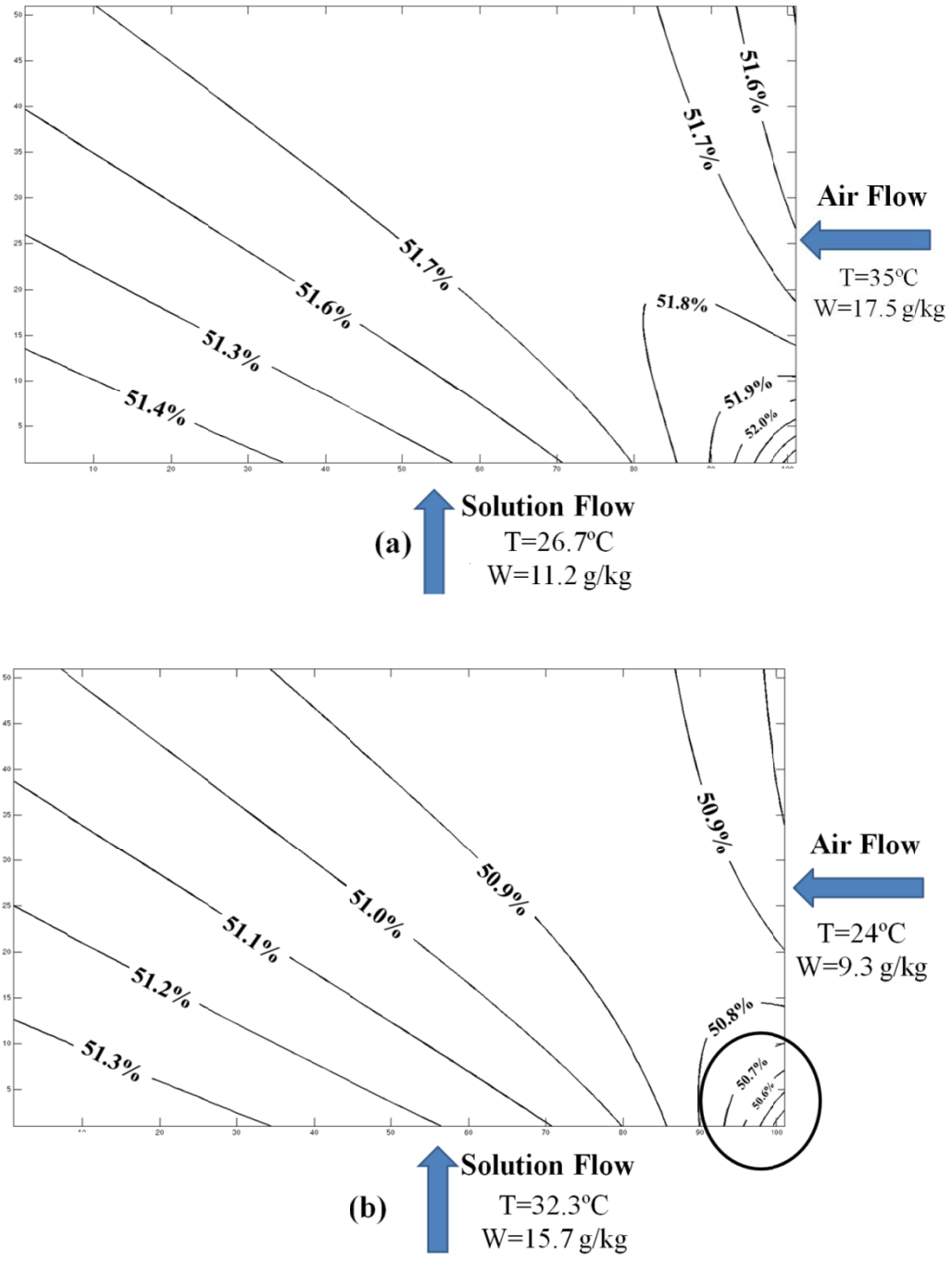

Figure 4.2: Relative humidity at the solution-membrane interface of (a) supply and (b) exhaust LAMEEs (NTU=10 and Cr*=3, AHRI summer operating conditions).

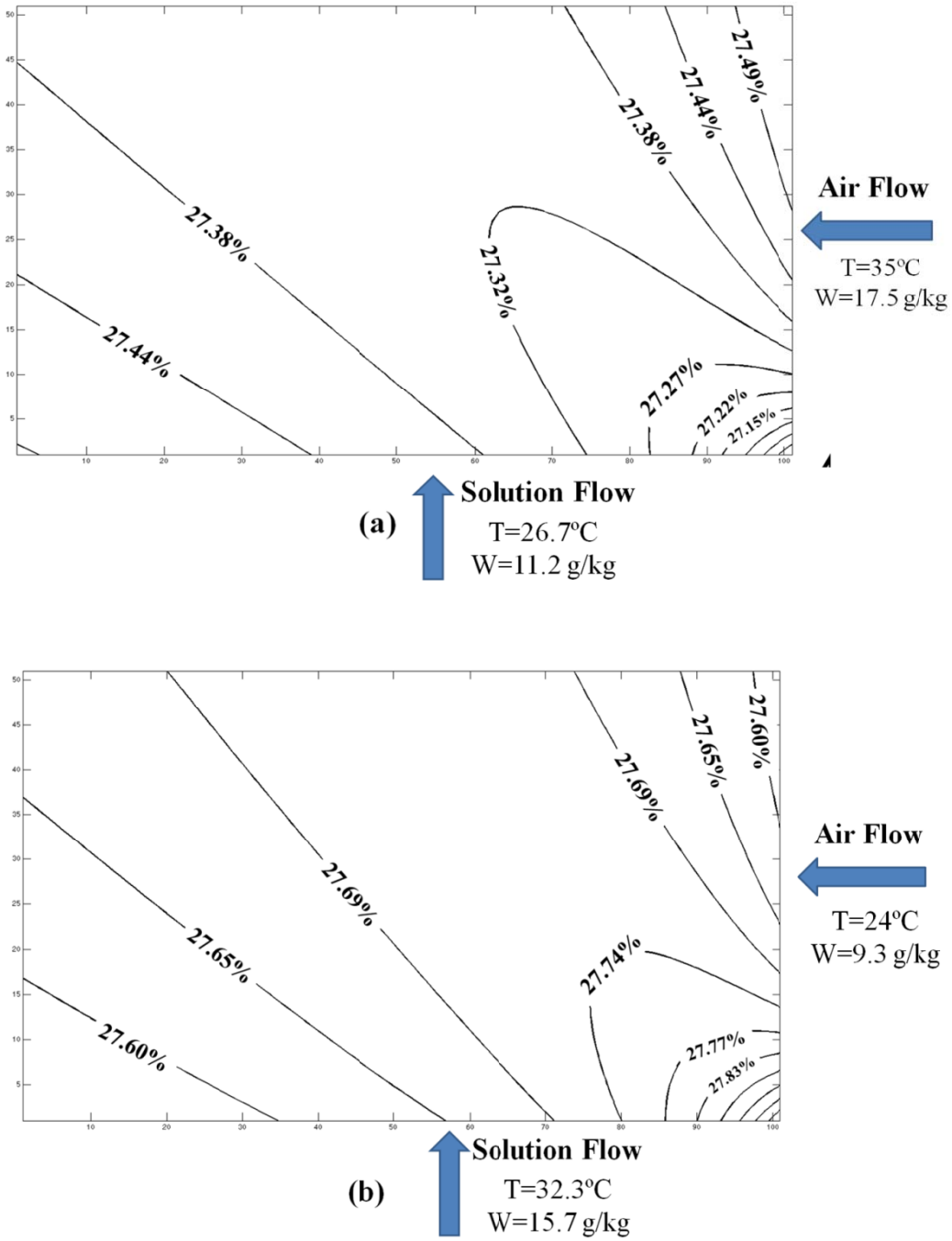

Figure 4.3: Concentration of LiCl solution in a liquid channel of (a) supply and (b) exhaust LAMEEs (NTU=10 and Cr*=3, AHRI summer operating conditions).

As seen in Figure 4.3, the steady state humidity ratio and temperature at the solution-membrane interface change in such a way that the concentration remains

almost constant in the LAMEEs (changes less than 1%). In other words, evaporation of water from the liquid does not significantly affect the concentration of the salt solution. Constant concentration of the salt solution in the LAMEEs would then result in a very small change in the air relative humidity at the solution-membrane interface (see Figure 4.2). Figure 4.2 shows the air relative humidity contours in a RAMEE operating with a specific solution mass flow rate (Cr*=3). The area with the lowest relative humidity value (highest risk of crystallization) is also shown with a circle in Figure 4.2. The change in the concentration of the salt solution may be affected by the mass flow rate of the salt solution. Lower solution flow rates increase the amount of time that the solution stays in the LAMEEs and therefore may increase the concentration change of the salt solution. Figure 4.4 shows the concentration contours in the supply and exhaust LAMEEs of a RAMEE operating with Cr*=0.5 and AHRI summer conditions. As seen in this figure, the change in the concentration of the salt solution is even smaller when Cr* is reduced to 0.5 however, the concentration is higher at lower solution flow rates (i.e., lower Cr*) compared to higher solution flow rates. For example, the highest concentration of LiCl at Cr*=3 is equal to 28.1% while the highest concentration at Cr*=0.5 becomes 28.7%. This shows that the most important factor affecting the concentration of the salt solution is the bulk relative humidity of the inlet air to the exchangers (i.e. that of outdoor air in the supply exchanger and indoor air in the exhaust exchanger).

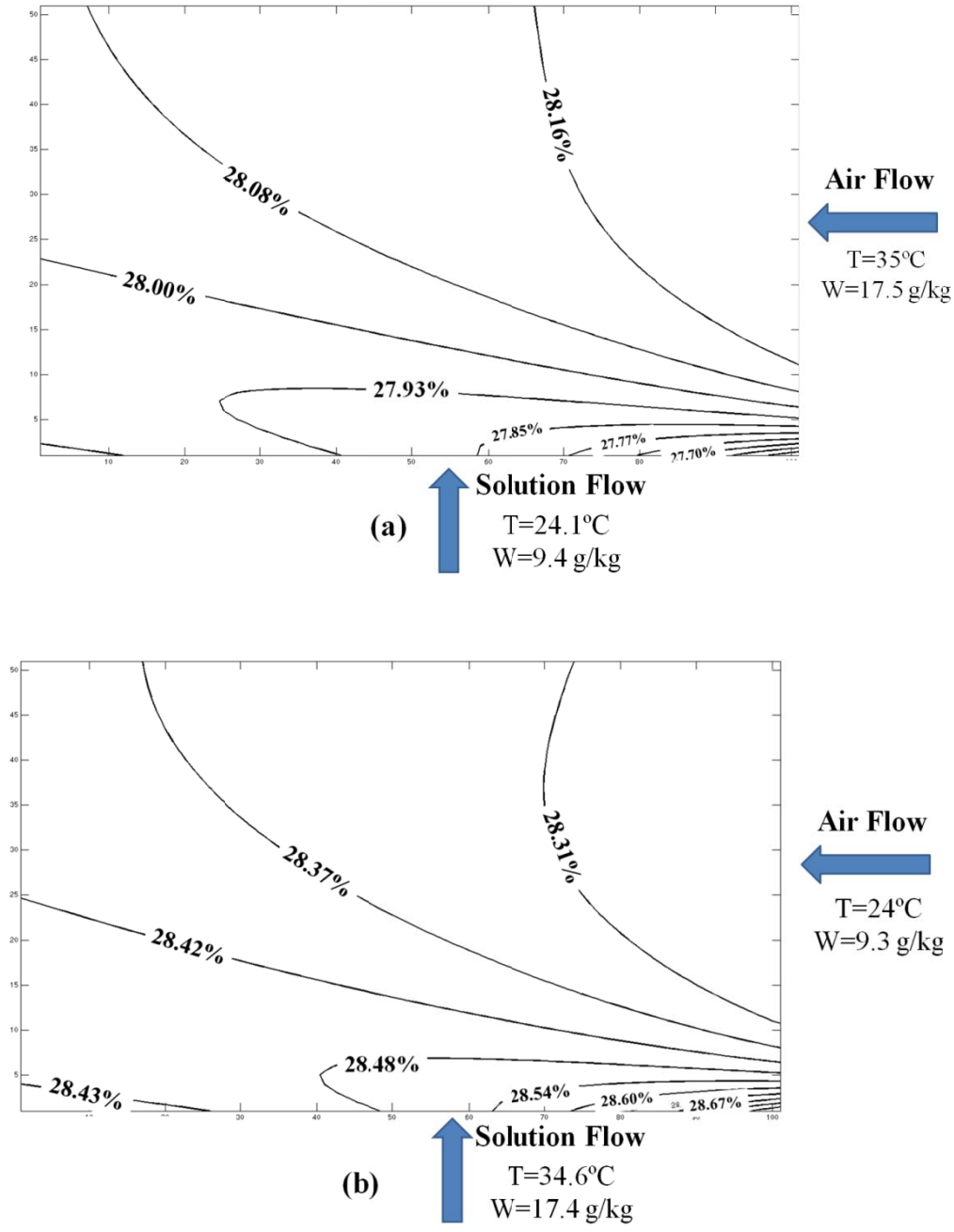

Figure 4.4: LiCl concentration in a liquid channel of (a) supply and (b) exhaust LAMEEs (NTU=10 and Cr*=0.5, AHRI summer operating conditions).

The temperatures and humidity ratios at the solution-membrane interface at all points in the exhaust and supply LAMEEs (shown in Figure 4.1) are superimposed on a

psychrometric chart in Figure 4.4. Since the change of relative humidity is small within each LAMEE, the humidity points at the solution-membrane interface in each LAMEE form a narrow strip on the psychrometric chart located between the indoor and outdoor operating conditions.

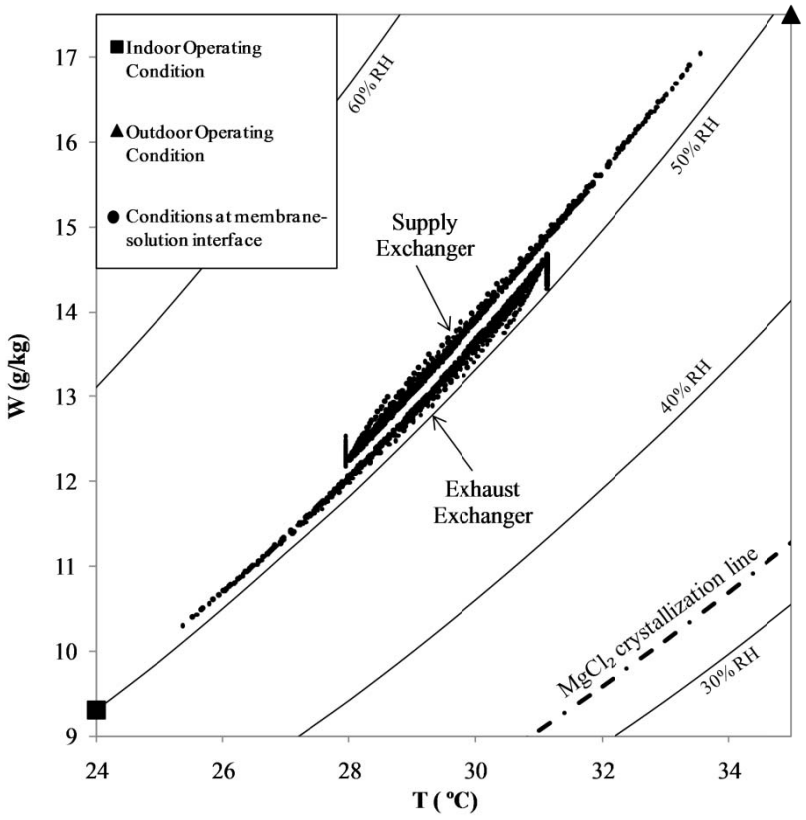

Figure 4.5: Conditions at the membrane-solution interface at all points in the supply and exhaust LAMEEs (AHRI summer operating conditions).

Figure 4.3 shows that the critical concentration values (i.e., maximum concentration) occur at the borders of the liquid channels in the LAMEEs. Figure 4.6 shows the humidity ratio and temperature at the solution-membrane interface on the borders of a liquid channel. Points shown by numbers in Figure 4.6 refer to the corners of the liquid channel. As seen in this figure, the minimum relative humidity (and consequently maximum concentration) occurs in the lower right corner (point 2) of the

liquid channel in the exhaust exchanger in RAMEE operating during AHRI summer conditions with NTU=10 and Cr*=3. This is consistent with the concentration contours (Figure 4.3) in the liquid channel. Figure 4.6 also shows the crystallization line of a $MgCl_2$ solution (approximately 33% RH). The salt may crystallize in the LAMEEs if the humidity-temperature conditions at the solution membrane interface are lower than the salt crystallization line.

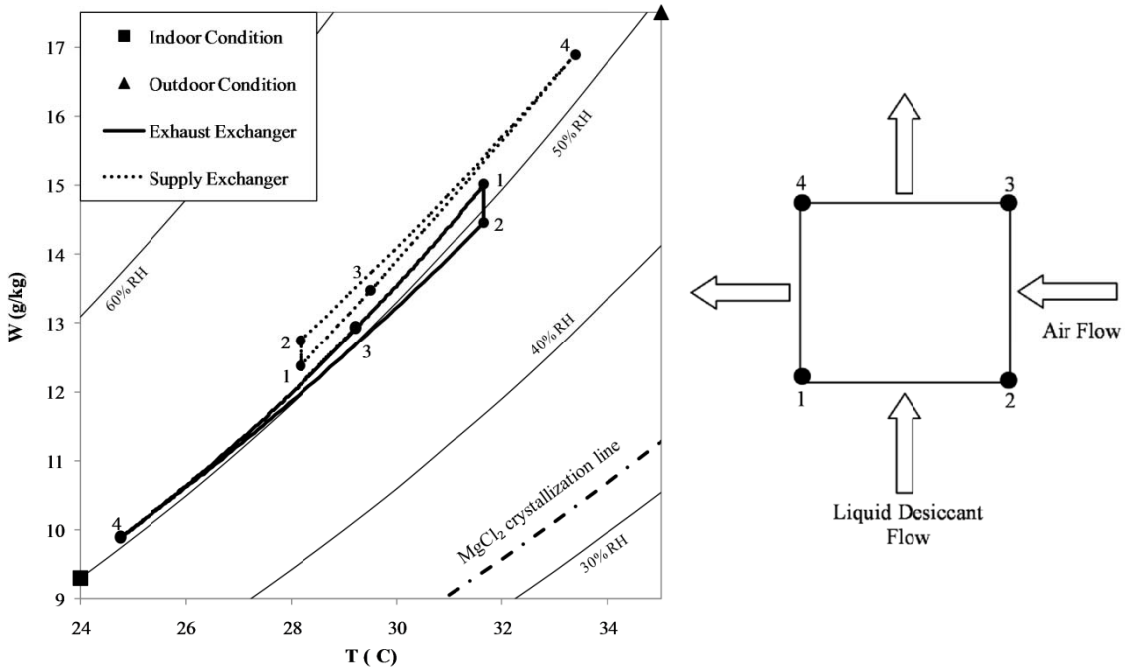

Figure 4.6: Conditions at the membrane-solution interface on the corners of liquid panels in the LAMEEs superimposed on a psychrometric chart (summer operating conditions, NTU=10 and Cr*=3).

As seen in Figures 4.5 and 4.6, the relative humidity at the solution-membrane interface in the exhaust LAMEE is lower than that in the supply LAMEE during summer operating conditions. Therefore, the salt solution has a higher risk of crystallization in exhaust LAMEE during summer operating conditions since the

humidity ratio is closer to crystallization line of the salt solution. Similarly it can be shown that during winter operating conditions, the supply exchanger has lower surface humidities and has a greater risk of crystallization. Figure 4.7 shows the conditions at the solution-membrane interface of a liquid channel in a RAMEE operating during AHRI winter conditions.

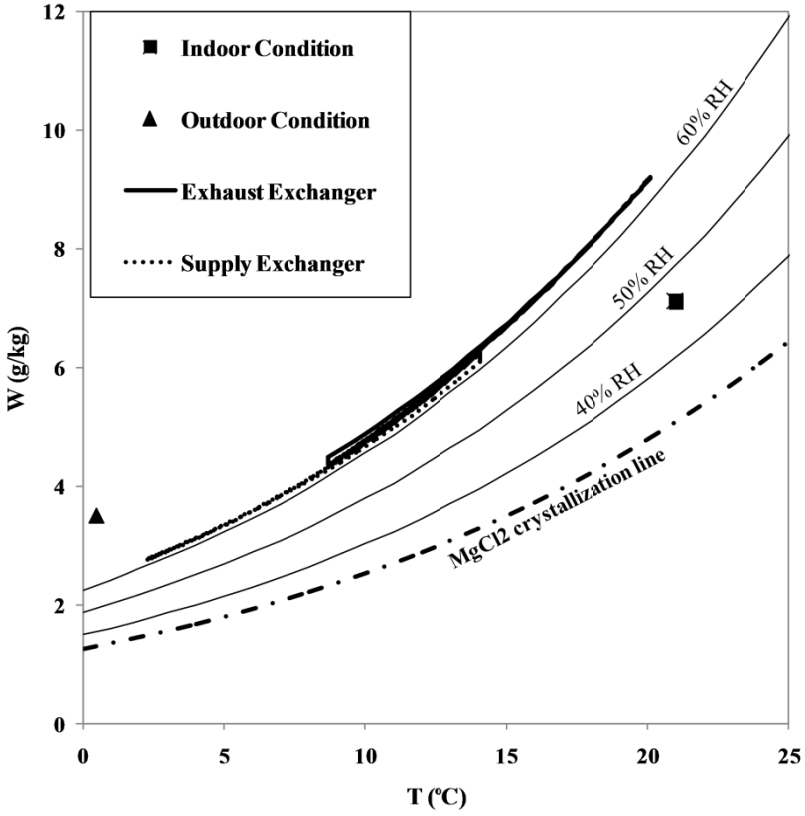

Figure 4.7: Conditions at the membrane-solution interface on the corners of a liquid channel in the LAMEEs, superimposed on a psychrometric chart (winter operating conditions, NTU=10 and Cr*=3).

4.4 Effect of Supply and Exhaust Air Conditions on the Risk of Crystallization

As shown in the previous section, no crystallization is expected during AHRI summer and winter test conditions, however, the risk of crystallization depends on the supply and exhaust air inlet conditions. When the system operates in dryer conditions, the relative humidity at the solution-membrane interface in the LAMEEs reduces and

the risk of crystallization increases. Figure 4.8 shows the conditions at the solution-membrane interface at the corners of a liquid channel in the exhaust LAMEE superimposed on a psychrometric chart for three different outdoor relative humidities (listed in Table 4.1). The indoor conditions are kept constant at the AHRI Standard summer test condition for all three cases.

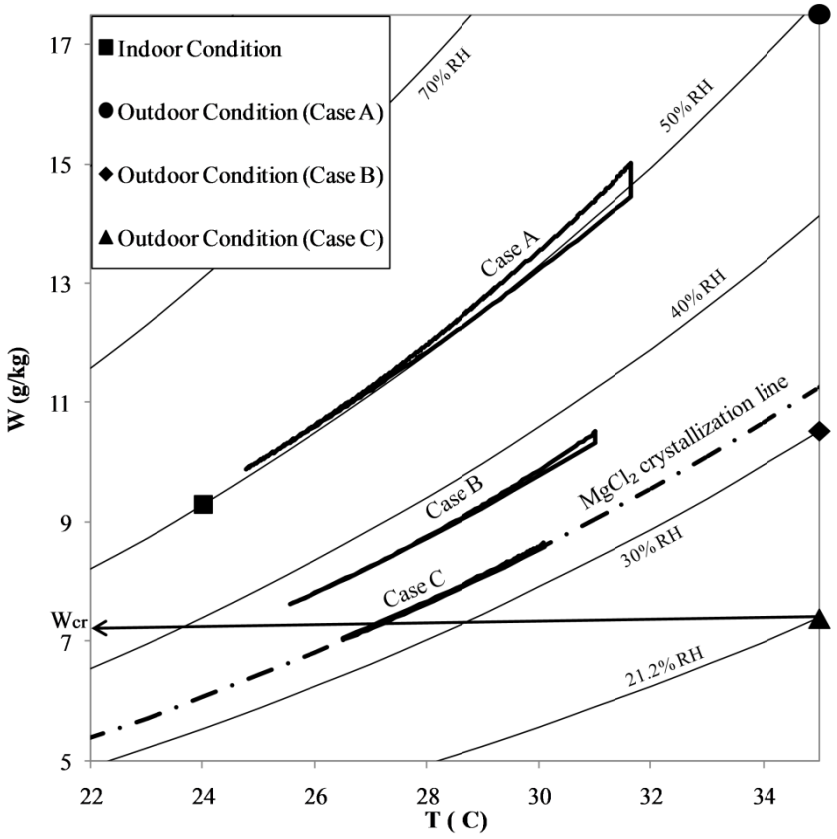

Figure 4.8: Conditions at the membrane-solution interface in the liquid flow path for different outdoor operating conditions (summer operating conditions, NTU=10 and Cr*=3).

The minimum equilibrium air relative humidity at the solution-membrane interface in the exhaust LAMEE decreases as the outdoor relative humidity is reduced. The minimum equilibrium relative humidity at the solution-membrane interface changes from 49.4% RH for a supply inlet relative humidity of 50% (shown as Case A in Figure 4.8) to 36.9% RH for outdoor relative humidity of 30% (Case B). The average

concentration of a $MgCl_2$ solution in case A is C=30% wt which will be increased to 34% wt if the outdoor relative humidity is reduced to 30%. In the third case, at a critical outdoor humidity ratio (W_{cr}) of 7.4 g/kg at 35°C, the minimum relative humidity at the solution-membrane interface in the exhaust exchanger becomes 32.5%. The concentration of the $MgCl_2$ solution during this operating condition is equal to 35.9% wt which is equal to the saturation concentration of $MgCl_2$. At this critical outdoor humidity ratio the exhaust LAMEE is on the verge of crystallization.

W_{cr} is almost 2.9 g/kg lower than the equilibrium humidity ratio of a saturated $MgCl_2$ solution at 35°C (11.3 g/kg). This shows that the salt solution in the RAMEE system does not necessarily crystallize when the outdoor relative humidity is lower than the saturation relative humidity of the liquid desiccant and points to the need for a detailed numerical model to properly assess the risk of crystallization in the RAMEE system.

The model can also be applied to simulate the risk of crystallization when the RAMEE system is operating during different indoor operating conditions. Figure 4.9 shows the humidity ratio at the solution-membrane interface at the corners of a liquid channel in the exhaust exchanger of a RAMEE system while the indoor operating condition is 30% RH and 24°C. The critical outdoor humidity increases from W=7.4 g/kg at an outdoor humidity of 50% RH to 11.5g/kg at an indoor humidity of 30% RH. Figure 4.9 shows that with an indoor RH below the crystallization line (saturation line) the critical outdoor humidity is in fact higher (3.1 g/kg and 12% RH) than the saturation condition at 35°C. In other words reducing indoor relative humidity increases the risk of crystallization in the RAMEE system. There is no simple rule, based on the indoor

and outdoor conditions, to determine when crystallization happens in the LAMEEs. The conditions at the solution-membrane interface have to be evaluated by the numerical model to predict the occurrence of crystallization for a particular salt in a RAMEE system.

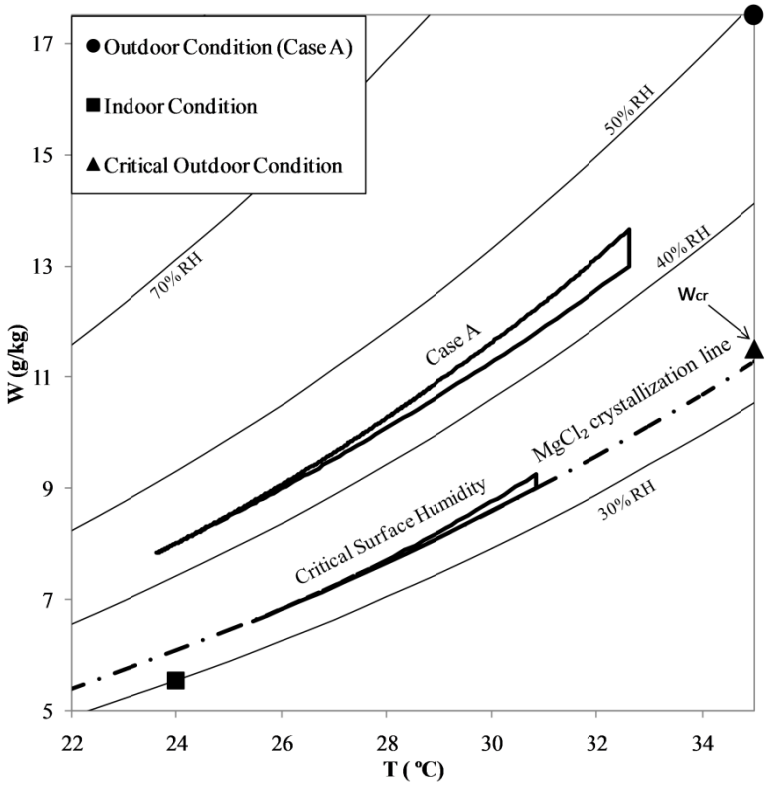

Figure 4.9: Conditions at the membrane-solution interface in the liquid flow path for different indoor operating conditions (summer operating conditions, NTU=10 and Cr*=3).

4.5 Outdoor Humidity Ratio Limitations

By simulating the RAMEE system with different outdoor temperatures and a fixed indoor operating condition, W_{cr} can be determined for different salt solutions over a range of temperatures. If the humidity ratio of the inlet supply air at any given temperature falls below W_{cr} for that specific salt solution, it may supersaturate and will be in risk of crystallization. In the following sections the W_{cr} line of $MgCl_2$, $CaCl_2$, LiBr and LiCl solutions are determined for RAMEE systems with NTU=10 and Cr*=3.

It should also be noted that the results in the following sections are determined for LAMEEs with a cross flow configuration. The effect of changing the flow configuration to counter-cross flow is investigated in section 4.7.

4.5.1 $MgCl_2$-Water Solution

Critical humidity ratio lines during summer and winter operating conditions are illustrated in Figure 4.10 for a RAMEE system using a $MgCl_2$ solution. The W_{cr} lines are shown for two indoor relative humidities of 50 and 30%.

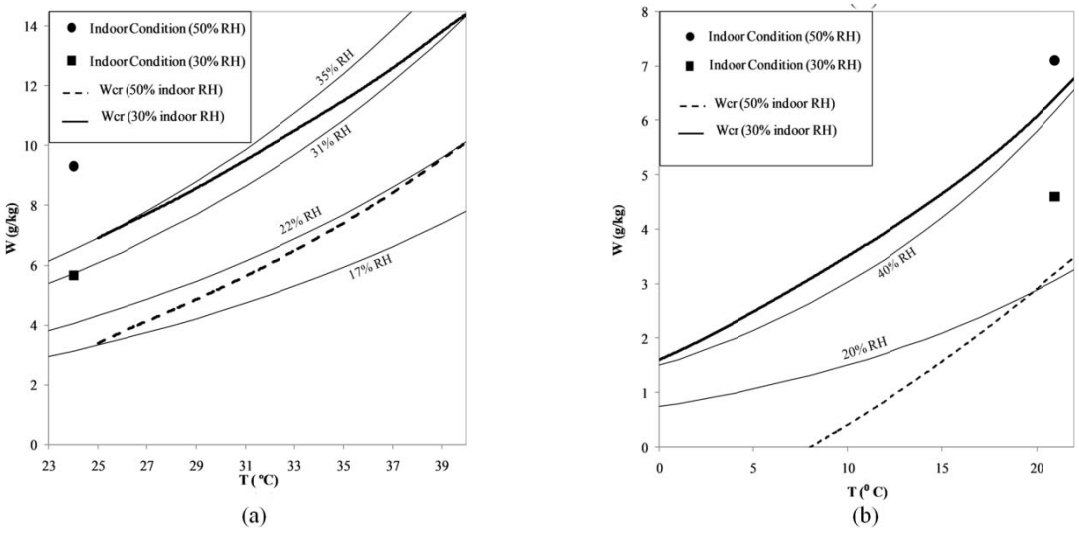

Figure 4.10: Minimum allowable supply air relative humidity for the $MgCl_2$ solution in (a) summer and (b) winter operating conditions for two different indoor conditions (NTU=10 and Cr*=3).

For the 50% indoor relative humidity operating condition during summer, the critical humidity ratio of $MgCl_2$ solution varies from 7.7 g/kg at 40°C (22% RH) to 3.3 g/kg at 25°C (17% RH). Reducing indoor relative humidity increases W_{cr}. At an indoor relative humidity of 30%, W_{cr} becomes 14.2 g/kg at 40°C (31% RH) and 6.9 g/kg at 25°C (35% RH).

Figure 4.10(b) shows the critical humidity ratio lines of a RAMEE system with $MgCl_2$ solution as the coupling fluid during winter conditions. W_{cr} lines are illustrated

for two indoor relative humidities of 50% and 30%. As seen in Figure 4.10(b) for the case of 50% indoor relative humidity, crystallization will not occur for supply air temperatures lower than 8ºC; and for higher temperatures the critical humidity is less than 22% RH. In other words, crystallization is not a concern for most of the winter unless the system is supplied by a preheated air stream. Reducing the indoor relative humidity increases the critical humidity ratio during winter. W_{cr} for 30% indoor relative humidity closely follows the 42% RH line on the psychrometric chart. Since outdoor relative humidity nearly always exceeds 80% RH for temperatures below 5ºC, crystallization is very unlikely during winter operation unless cold outdoor is preheated prior to entering the supply LAMEE.

4.5.2 $CaCl_2$-Water Solution

Critical humidity ratio lines for a RAMEE systems operating with $CaCl_2$ solution are illustrated in Figure 4.11 for summer and winter operating conditions. The W_{cr} lines for the $CaCl_2$ solution are slightly lower than those for $MgCl_2$ solution. On average, the critical outdoor relative humidities are 2% lower when $CaCl_2$ is used rather than $MgCl_2$. The $CaCl_2$ solution has a lower critical humidity than a $MgCl_2$ solution because a solution of $CaCl_2$ has a lower saturation relative humidity than a $MgCl_2$ solution.

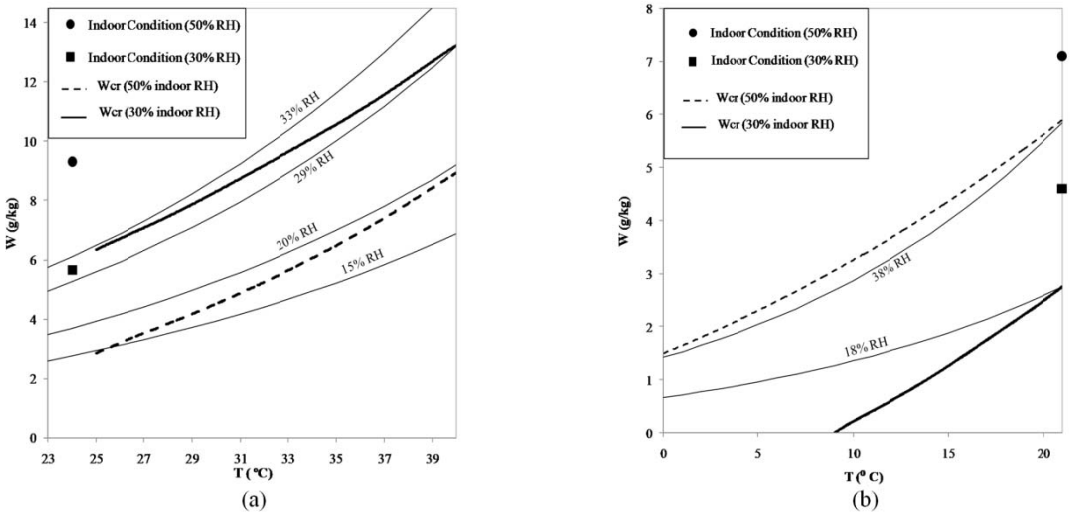

Figure 4.11: Minimum allowable supply air relative humidity for the $CaCl_2$ solution in (a) summer and (b) winter operating conditions for two different indoor conditions (NTU=10 and Cr*=3).

4.5.3 LiCl-Water and LiBr-Water Solutions

Crystallization limit lines can be illustrated for the LiCl and LiBr solutions as was done for $MgCl_2$ and $CaCl_2$ solutions in the previous sections. As mentioned previously, the equilibrium humidity of air at solution-membrane interface of a saturated LiCl solution is 11% RH (i.e. about 22% RH lower than that of a saturated $MgCl_2$) and the equilibrium humidity at the surface of a saturated LiBr solution is less than 9% RH. Figure 4.12 show the critical humidity lines of LiCl and LiBr solutions in a RAMEE system operating during summer conditions.

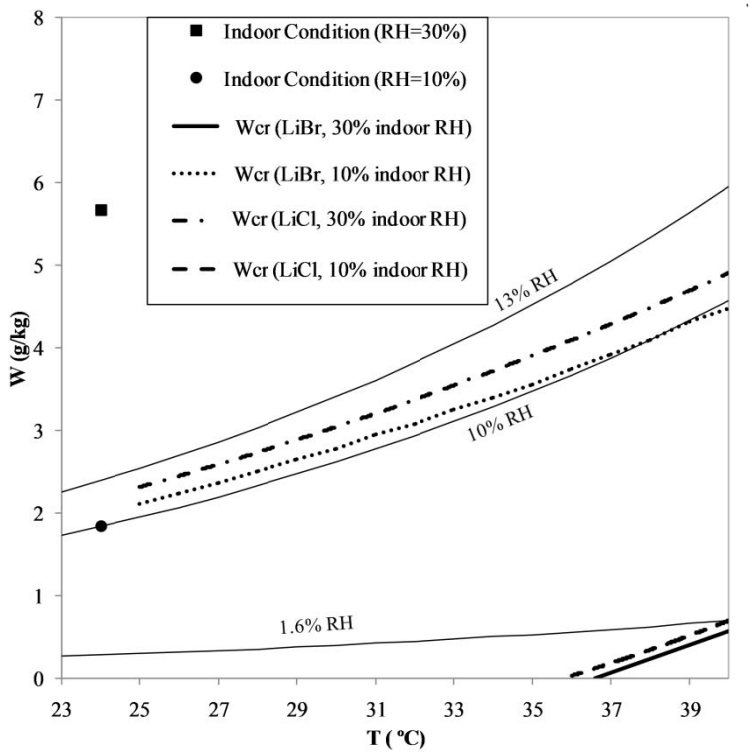

Figure 4.12: Minimum allowable supply air relative humidity for LiCl solution in summer operating conditions for two different indoor conditions (NTU=10 and Cr*=3).

As expected, Figure 4.12 shows that LiCl and LiBr solutions may operate without crystallization in nearly all climates because of their low critical humidity. During summer, for the AHRI indoor operating condition (50% RH), crystallization will not occur if LiCl or LiBr solutions are used for the temperature range shown in Figure 4.12 and, therefore, the W_{cr} lines for outdoor RH of 50% are not shown in Figure 4.12. When indoor relative humidity is reduced to 30% RH, only very dry operating conditions less than 2% RH may cause crystallization of LiCl or LiBr solutions in the RAMEE system. Figure 4.9 also illustrates the critical outdoor humidity (~ 11% RH) when the indoor humidity is 10% RH. These results confirm that crystallization risk is very minimal with LiCl and LiBr solutions.

Simulations also show that the LiCl and LiBr solutions work properly without any risk of crystallization during winter operating conditions for indoor relative humidities higher than 20%.

4.6 Practical Examples of Different Climatic Conditions

In order to investigate the crystallization risk of the selected salt solutions ($MgCl_2$, $CaCl_2$, LiBr and LiCl) in different climatic conditions, the RAMEE system is simulated in several cities in North America. The cities were chosen in different climate zones as specified by ASHRAE Standard 90.1 (2004) to cover the climatic diversity of North America. Figure 4.13 illustrates the climate classification of the US in the form of a map and Table 4.1 provides an example city for each zone. ASHRAE has divided the US into eight thermal climate zones (shown by numbers in Figure 4.10) and three divisions based on atmospheric moisture (shown by letters in Figure 4.10). Each zone may be represented by a combination of a digit and a letter, for instance, zone 2B refers to a location in thermal zone 2 and dry region (B).

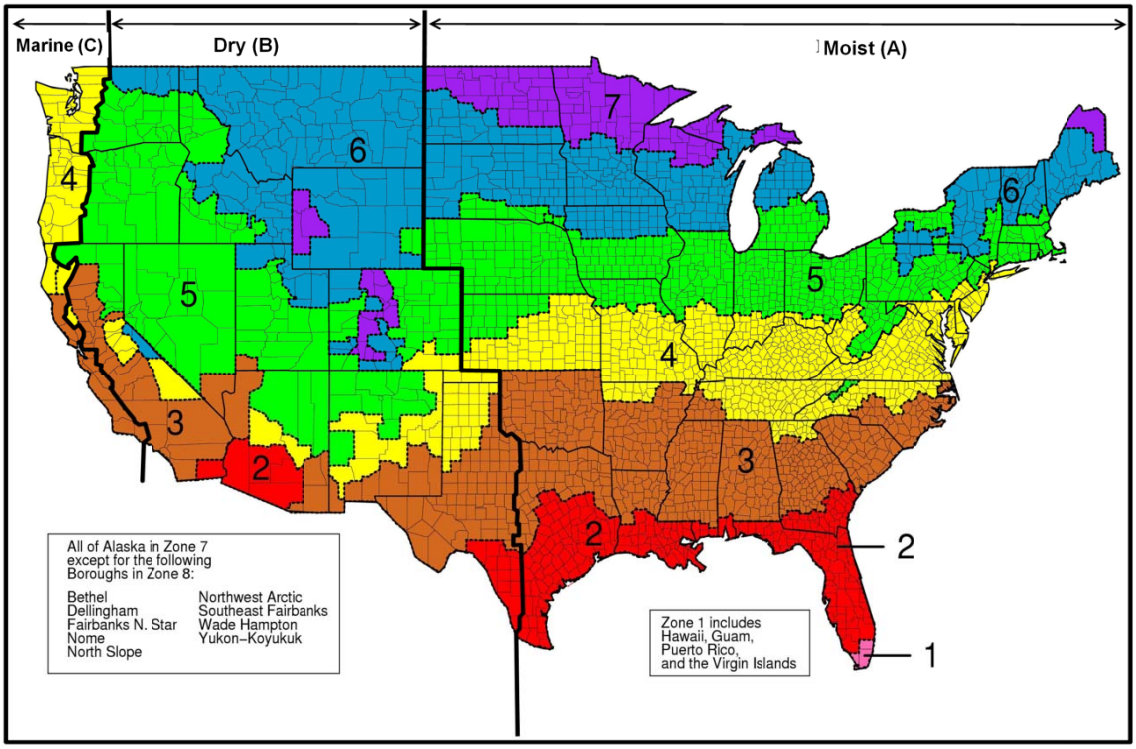

Figure 4.13: Map of the US showing the ASHRAE 90.1 climate zones (Briggs et al. 2002).

Table 4.2: List of the selected cities and their climate zones.

City	Zone No.	Climate Zone Description
Miami, FL	1A	Very Hot - Humid
Houston, TX	2A	Hot - Humid
Phoenix, AZ	2B	Hot - Dry
Memphis, TN	3A	Warm - Humid
EL Paso, TX	3B	Warm - Dry
San Francisco, CA	3C	Warm - Marine
Baltimore, MD	4A	Mixed - Humid
Albuquerque, NM	4B	Mixed - Dry
Salem, OR	4C	Mixed - Marine
Seattle, WA	4C	Mixed - Marine
Chicago, IL	5A	Cool - Humid
Madison, WI	6A	Cold - Humid
Boise, ID	5B	Cool - Dry
Burlington, VT	6A	Cold - Humid
Helena, MT	6B	Cold - Dry
Saskatoon, SK	6B	Cold - Dry

TMY 2 hourly weather data are used for each city to find the number of hours in which each of the salt solutions may crystallize in the RAMEE system (NREL 2009). For an example, hourly weather data are shown in Figure 4.14 for Phoenix (AZ) superimposed on a psychrometric chart. The critical humidity ratio lines for the $MgCl_2$ solution are also shown in Figure 4.14 for different indoor RH cases. All the points located below the W_{cr} lines in the psychrometric chart represent the hours in which $MgCl_2$ crystallization will occur in one or both of the LAMEEs. For Phoenix, crystallization is expected to occur in 1368 hours (15.6%) and 4975 hours (57%) of the year when the indoor humidity is normal (50% RH) and lower (30% RH) respectively.

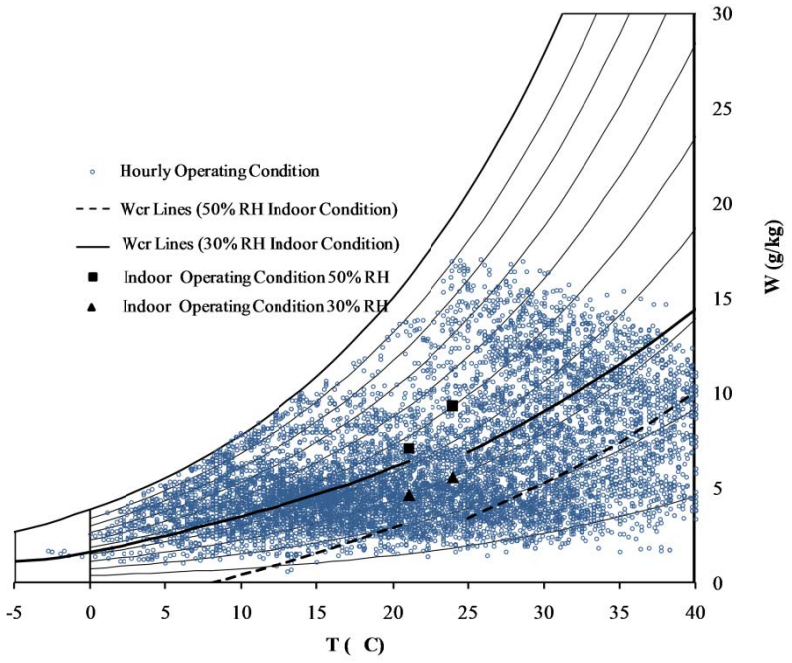

Figure 4.14: Hourly climate condition of Phoenix (AZ) superimposed on psychrometric chart as well as critical humidity ratio lines for 50% and 30% indoor relative humidities.

Figure 4.15 shows the percentage of the year in which $MgCl_2$ and $CaCl_2$ solutions have a risk of crystallization for all cities listed in Table 4.1. As seen in Figure

4.15, the risk of crystallization is very small (less than 1% of the year) for indoor operating condition of 50% RH for all cities except Phoenix (2B), Abuquerque (4B) and El Paso (3B) (i.e., cities in the mixed-hot and dry regions). The risk of crystallization increases as indoor relative humidity is reduced to 30%, yet crystallization will occur for less than 10% of the year in all the cities located in marine (C) and humid (A) zones. As expected, the percentage of the year that $CaCl_2$ has a risk of crystallization is slightly lower than that of $MgCl_2$ solution. LiCl and LiBr solutions have no risk of crystallization when the RAMEE system operates with 50% and 30% indoor conditions in any of the cities listed in Table 4.1. However as mentioned in chapter 3, the price of LiBr and LiCl solutions is considerably higher than that of $CaCl_2$ and $MgCl_2$ solutions. Therefore the results from this investigation leads to a study of mixtures of salt solutions in the next chapter as an alternative for the highly-priced LiCl and LiBr solutions to be used in dry climates.

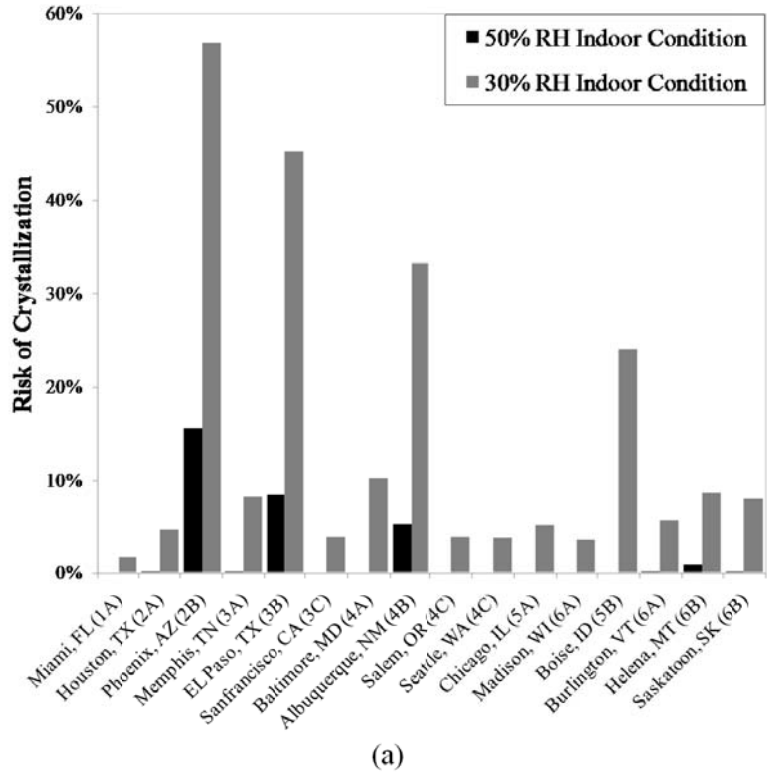

(a)

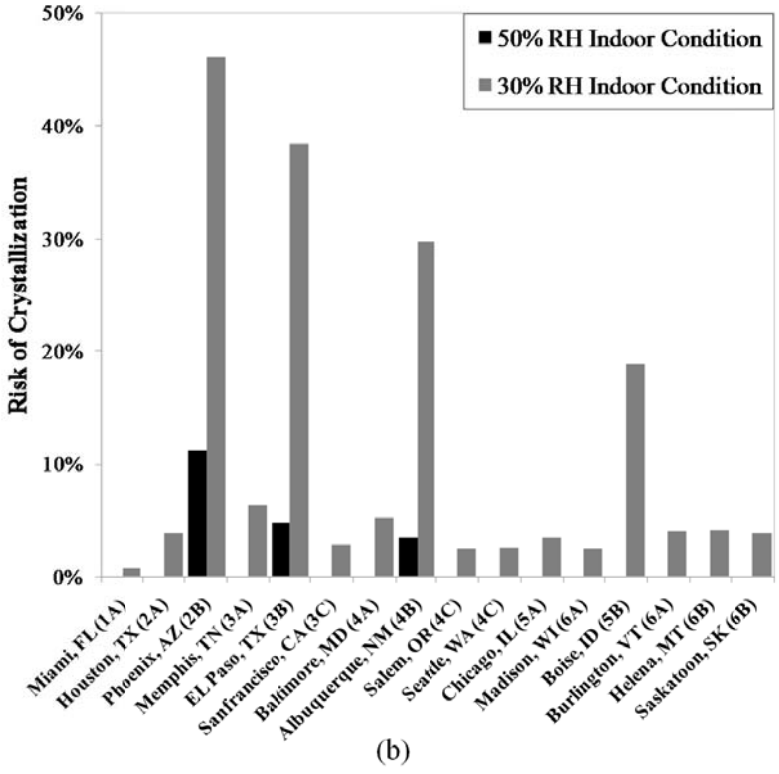

(b)

Figure 4.15: Percentage of the year in which (a) $MgCl_2$ and (b) $CaCl_2$ solutions have a risk of crystallization for systems operating with 30% and 50% indoor RH for ASHRAE 90.1 climate zone example cities.

4.7 Impact of System Design Parameters on the Risk of Crystallization

The moisture and heat transfer rates between the air and liquid streams is affected by the design and operational characteristics (NTU, Cr* and ε) of the RAMEE. As the moisture transfer rate increases in a dry climate, the risk of the solution reaching saturation increases. Therefore, the RAMEE design and operational characteristics may be modified to reduce the risk of crystallization during specific outdoor weather conditions. The design of the system may not be changed when the system is in operation but NTU and Cr* values may be changed by changing the solution and air flow rates. Figure 4.16 shows the percentage of number of hours during summer operating conditions in which a $MgCl_2$ solution has a risk of crystallization in Phoenix (2B), El Paso (3B) and Helena (6B) for different values of Cr* and NTU=10. As seen in Figure 4.16, the number of hours in risk decreases by 6% as Cr* is increased from 1 to 10 in the selected cities. In other words, increasing Cr* of the system (i.e. increasing mass flow rate of the salt solution or reducing the mass flow rate of air stream) decreases the risk of crystallization in the LAMEEs.

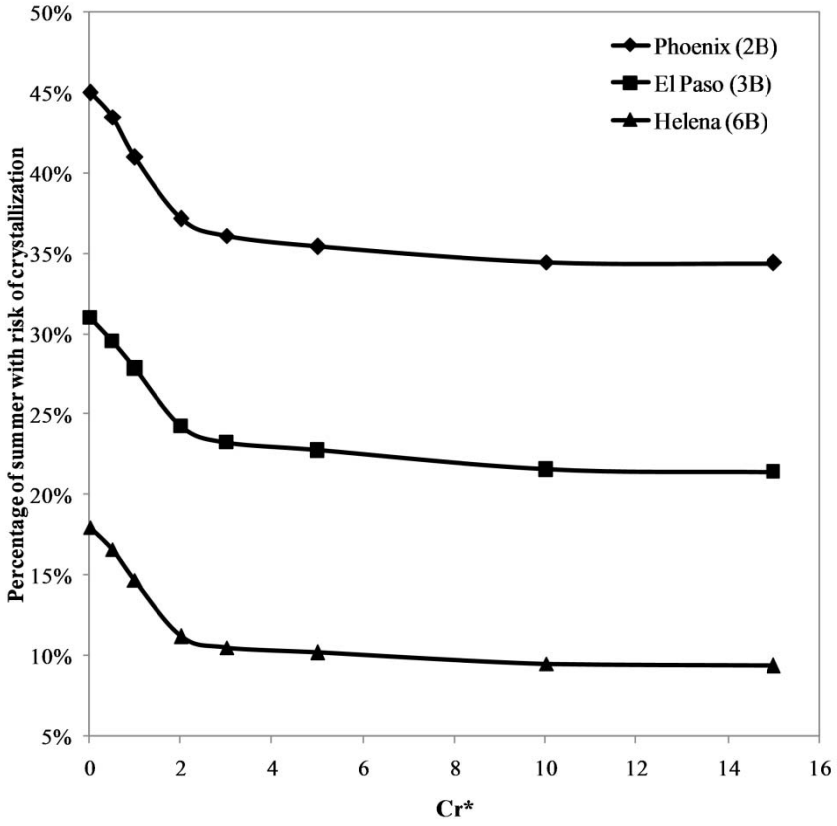

Figure 4.16: Percentage of summer time in which a $MgCl_2$ solution has risk of crystallization in Phoenix, El Paso and Helena for the RAMEE systems with different Cr* values (NTU=10).

Figure 4.17 shows the percentage of hours during summer that a $MgCl_2$ solution has a risk of crystallization in three cities of Phoenix (2B), El Paso (3B) and Helena (6B) for the RAMEE systems with different average total effectiveness values. The number of hours that the solution has risk of crystallization is higher when the system has higher effectiveness (i.e. when the system transfers more moisture in the LAMEEs). Each point in Figure 4.17 is calculated from counting the number of hours during summer operating conditions located below the W_{cr} line of $MgCl_2$. The total effectiveness of the system varies as outdoor temperature changes, therefore, the effectiveness would not be a single value for the points shown in Figure 4.17. The

values shown in this figure for effectiveness of the system are the effectiveness values of a RAMEE operating with AHRI conditions.

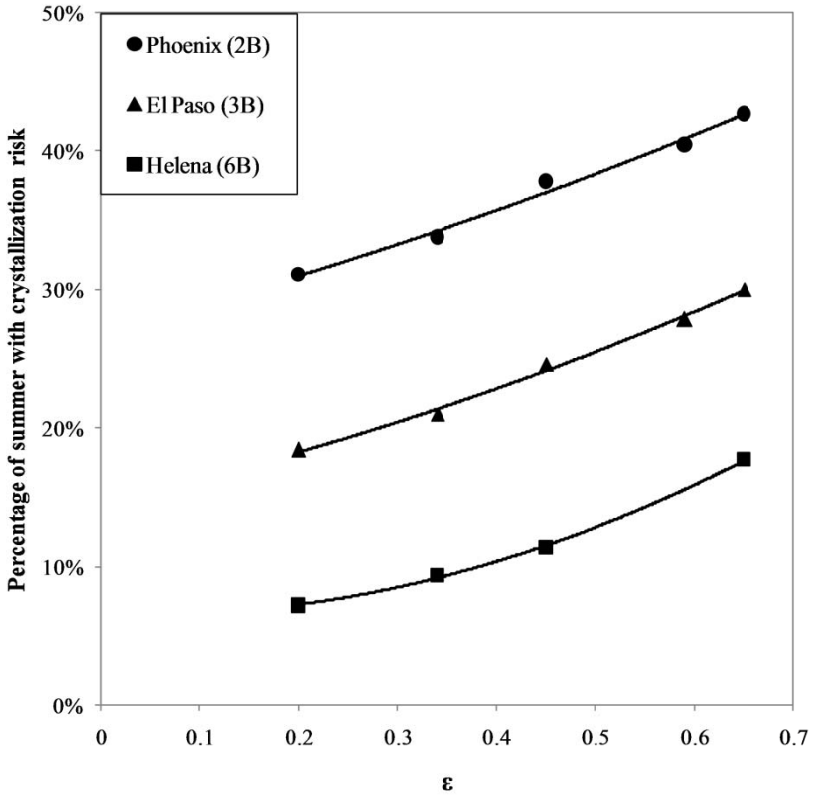

Figure 4.17: Percentage of number of hours in which a $MgCl_2$ solution has risk of crystallization during summer operating conditions in Phoenix, El Paso and Helena for the RAMEE systems with different effectivenesses.

4.8 The Risk of Crystallization on the Membrane Surface Area

In the previous sections, the risk of crystallization of salt was discussed for different outdoor operating conditions. However it is important to know how much of the membrane surface and which locations of the membrane is in risk of crystallization when the outdoor humidity is lower than W_{cr}. Figure 4.18 shows the surface of a membrane in the liquid channel of an exhaust LAMEE in a RAMEE operating with summer AHRI indoor condition and outdoor condition of 40˚C and 22% RH and 40˚C and 20% RH. As seen in Figure 4.18, the crystallized area increases very quickly from

35% of the total surface at 22% outdoor humidity to 100% of the total surface at outdoor humidity of 20% RH.

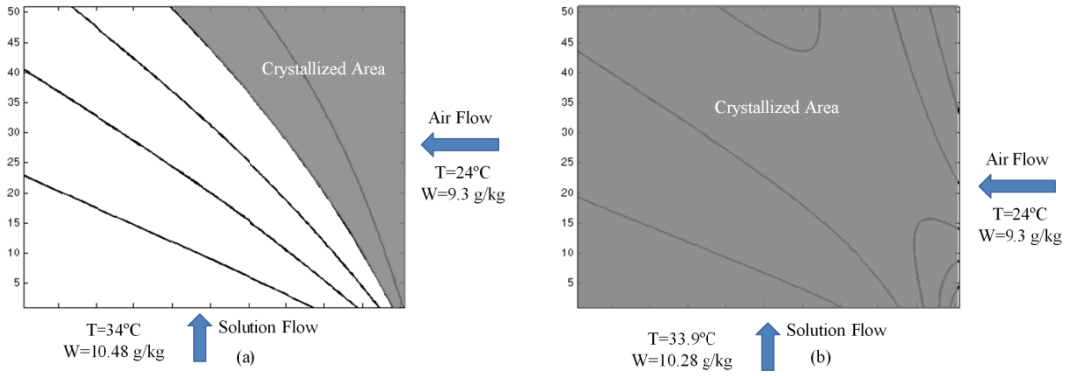

Figure 4.18: Area with risk of crystallization on the membrane of the exhaust exchanger of a RAMEE (NTU=10 and Cr*=3) with outdoor condition of 40˚C and (a) 22% RH (b) 20% RH.

Figure 4.19 shows the percentage of the surface of a liquid channel in a RAMEE system with risk of crystallization. The outdoor operating condition is 40˚C and 22% RH and indoor condition is 24˚C and 50% RH in this simulation. As seen in Figure 4.19, increasing the flow rate of the salt solution (i.e., increasing the Cr*) decreases the area of the liquid channel with risk of crystallization of $MgCl_2$. The area of the liquid channel with risk of crystallization decreases drastically when Cr* is increased from 1 to 4. For example at NTU=10, the area of liquid channel with crystallization risk decreases from 100% at Cr*=0.5 to less than 18% at Cr*=4 and by increasing the Cr* to 7 the area will become less than 10% of the total liquid channel surface. Figure 4.19 also illustrates the effect of changing NTU of system on the risk of crystallization. As seen in this figure, at low Cr* values (Cr* values less than 3) the risk of crystallization decreases as the NTU is decreased. The NTU of a RAMEE may be decreased by reducing the air flow rate. On the other hand at higher Cr* values, decreasing the NTU of the system will result in an increase in the risk of crystallization of $MgCl_2$ in the

LAMEEs. However, changing the solution (or air) flow rate may not decrease the risk of crystallization when the outdoor humidities more than 2% RH lower than the critical humidity of each particular salt solution. For example in a RAMEE with $MgCl_2$ as the liquid desiccant when the outdoor humidity is 15% RH, increasing the solution flow rate will not prevent the crystallization of salt in the system (the critical humidity of $MgCl_2$ is 22% RH). The reason is that the salt solution becomes saturated very quickly as the air relative humidity at the solution-membrane interface drops below the saturation limits (see Figure 4.18).

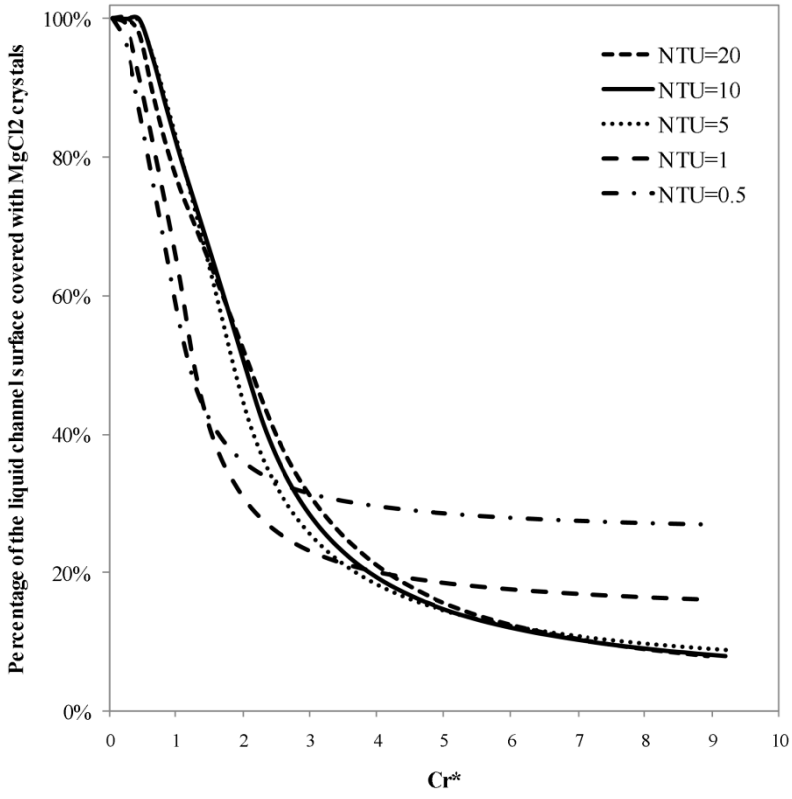

Figure 4.19: Percentage of the surface of a liquid channel where $MgCl_2$ is in risk of crystallization for different Cr* and NTU values.

Increasing the flow rate of the salt solution may only reduce the risk of crystallization when outdoor humidity is close to W_{cr}. At very low humidities, reduction of the solution concentration caused by changing the solution flow rate would not be enough to prevent the crystallization. For example when outdoor humidity is 8 g/kg at 40˚C (2 g/kg less than W_{cr}), the risk of crystallization may not be controlled by increasing Cr*.

Figure 4.20 illustrates the percentage of the membrane surface in a liquid channel at risk of crystallization for different membrane mass transfer resistances (k_m). As seen in Figure 4.20, the risk of crystallization is reduced as the k_m decreases. The reason is that moisture transfer rate reduces as k_m decreases which eventually results in a reduction in the risk of crystallization. More moisture transfer in dry climates will result in more concentration increase in the solution flow rate and consequently more risk of crystallization. The results shown in Figure 4.19 are tabulated in Table 4.3. As seen in Table 4.3, the total effectiveness of the system increases from 53% at $k_m=1.66\times10^{-8}$ to 75% at $k_m=1.66$. It should be noted that the mass transfer resistance of the Propore membrane used in RAMEE prototype III was $k_m=1.66\times10^{-6}$ (Mahmud 2009).

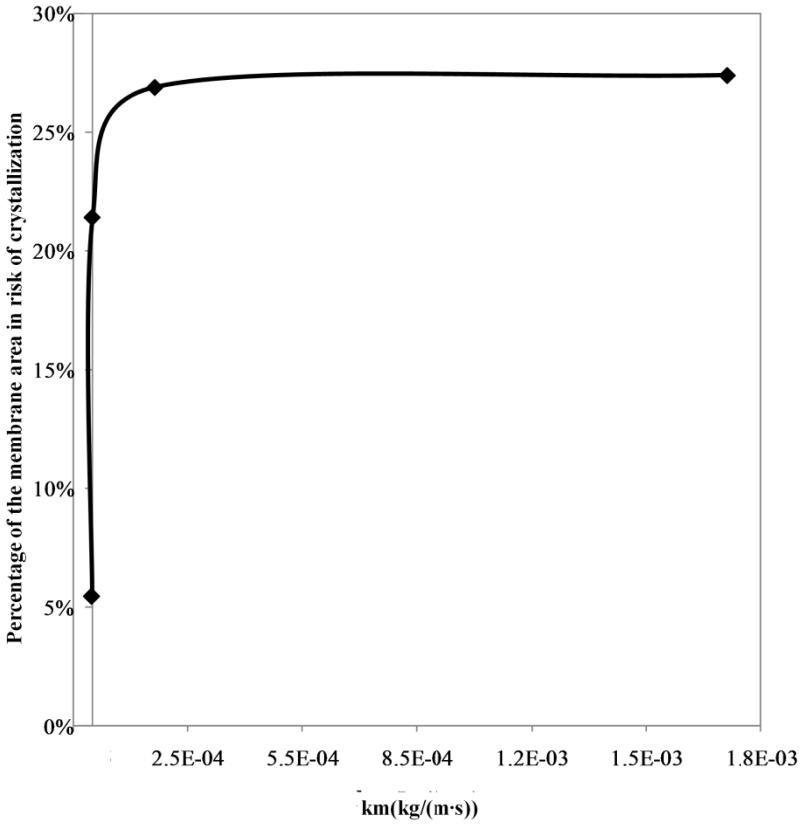

Figure 4.20: Percentage of the membrane surface of a liquid channel in risk of crystallization at different membrane mass transfer resistances (NTU=10 and Cr*=3, AHRI summer indoor condition and 40˚C and 22% RH outdoor condition).

Table 4.3: Percentage of a liquid channel in crystallization risk at different (membrane vapor permeabilities (k_m) and effectiveness values.

k_m [kg/(m·s)]	Total ε	Percentage of a liquid channel in crystallization risk
1.66×10^{-8}	53%	5%
1.66×10^{-7}	54%	5%
1.66×10^{-6}	65%	21%
1.66×10^{-5}	74%	27%
1.66×10^{-3}	74%	27%
1.66×10^{-2}	75%	28%
1.66	75%	28%

4.9 Impact of the Flow Configuration on the Risk of Crystallization

Changing the flow configuration in the LAMEEs affects the latent and sensible effectiveness of the RAMEE system. Heat and moisture transfer is enhanced when counter-cross flow LAMEEs are used instead of cross flow exchangers (Vali 2009). Since the performance of the cross and counter-cross flow exchangers is different, the risk of crystallization may also vary.

Figure 4.21 shows the W_{cr} lines of RAMEE systems operating during summer conditions with a 50% indoor operating condition for two different flow configurations. As expected, the W_{cr} is slightly higher for the counter-cross flow RAMEE. However, the difference in W_{cr} for the two different flow configurations is very small. At 40ºC, W_{cr} for a cross flow system is equal to 10 g/kg while that of a counter-cross flow system is 10.5 g/kg. The difference between W_{cr} for different flow patterns decreases as the outdoor temperature decreases and W_{cr} becomes almost equal at an outdoor temperature of 25 ºC.

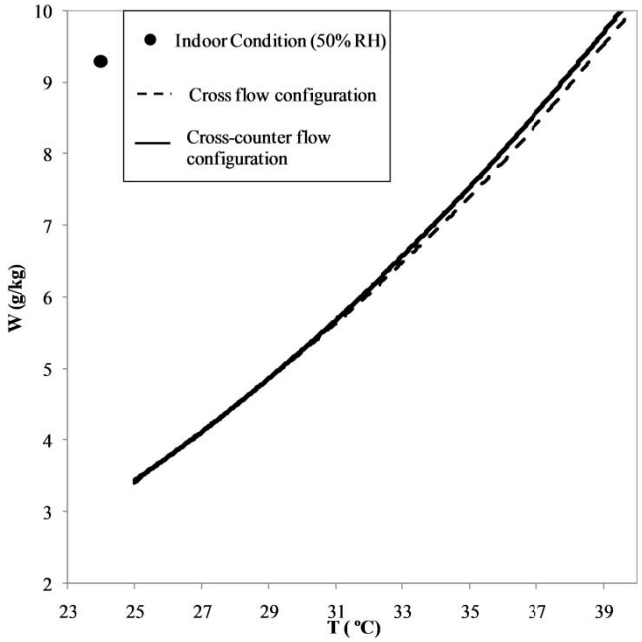

Figure 4.21: Critical humidity ratio lines of RAMEE systems with cross and counter-cross flow configurations operating during summer conditions($MgCl_2$ as liquid desiccant, NTU=10 and Cr*=3).

4.10 Recommendations to Control Crystallization

Results from the previous sections show that the risk of crystallization of salt in a RAMEE strongly depends on the operating conditions. The risk of crystallization increases as the humidity of the supply or exhaust air decreases. Therefore, one way to reduce the risk of crystallization in very dry climates is to use evaporative cooling systems to humidify the outdoor air before it enters the supply exchanger. Humidifying the supply air increases the moisture content of the airstream in the supply exchanger and consequently decreases the moisture transfer rate from the salt solution to the air which eventually would decrease the risk of crystallization in the LAMEEs.

In addition to the outdoor and indoor operating condition, operational characteristics of the RAMEE system also impact the risk of crystallization. The risk of crystallization may be reduced by increasing the mass flow rate of the salt solution.

Increasing the mass flow rate of the salt solution may significantly reduce the area of the membrane in risk of crystallization when the outdoor humidity is close to W_{cr}. Another way to control the crystallization of the salt in the system is to reduce the air flow in the exchanger where the moisture is rejected from the solution while keeping the other exchanger (where the solution is regenerated) in full operation. For example during summer operating conditions, when moisture rejection occurs in the exhaust exchanger reducing the air flow rate in the exhaust LAMEE may increase the concentration of the salt solution and prevent the crystallization.

The techniques mentioned above may prevent crystallization when the operating humidity condition is close to the critical value (i.e., within 2% of critical relative humidity). If the system is designed to operate in very dry climates, salt solutions with lower equilibrium saturation humidity should be selected (i.e., LiCl and LiBr instead of $CaCl_2$ and $MgCl_2$). The next chapter discusses the possibility of using mixtures of salt solutions in the RAMEE system as a cost effective substitute for expensive LiBr and LiCl solutions in dry climates.

4.11 Summary

In this chapter, the numerical model, described in chapter 2, was used to predict the risk of crystallization of four desiccant solutions (LiCl, LiBr, $MgCl_2$ and $CaCl_2$) in a RAMEE system. It was shown that the selected salt solution as well as the indoor and outdoor operating conditions have a significant effect on the risk of crystallization. The risk of crystallization is greater for $MgCl_2$, followed by $CaCl_2$, LiCl and LiBr. The risk increases as the supply or exhaust air streams become dryer. For a cross flow RAMEE with NTU=10 and Cr*=3 operating in a building with indoor RH of 50%, the critical

outdoor humidity below which crystallization will begin to occur is 28% RH for $MgCl_2$, 20% for $CaCl_2$ and 0%RH for LiCl and LiBr.

The effect of changing the indoor air relative humidity was also investigated in this chapter. Salt solutions crystallize at higher outdoor humidities when the relative humidity of the indoor air is decreased. For example, when the relative humidity of the supply air in the RAMEE, described previously (NTU=10 and Cr*=3), is reduced from 50% to 30% RH, the critical outdoor humidity increases from 28% RH to 35% RH. This increase in the critical relative humidity is due to lower ability of dry indoor air to regenerate the salt solution. Risk of crystallization of LiCl and LiBr is still very low even with indoor relative humidities as low as 30%. With a 30% indoor relative humidity, LiCl and LiBr solutions will not crystallize unless the outdoor RH is less than 2%.

$CaCl_2$ and $MgCl_2$ solutions may be used in most North American cities without crystallization risk for indoor operating humidities of 50% RH, while LiCl and LiBr can be used safely without crystallization in the RAMEE system, all over North America, even with indoor relative humidities down to 30%. At 30% RH indoor condition, $MgCl_2$ and $CaCl_2$ may only be used in the moist and marine climate regions (Zones A and C) of North America.

Operational and design characteristics of the RAMEE system also affect the risk of crystallization of the salt in the LAMEEs. It was shown that the crystallization may be prevented by increasing the solution mass flow rate when outdoor air humidity is close to the critical humidity of the particular salt solution. Decreasing the air mass flow rate at low Cr* values may also reduce the risk of crystallization. Another way to

reduce the risk of crystallization in the RAMEE is to use evaporative cooling systems to humidify outdoor air before entering the supply exchanger during very dry outdoor conditions. There is lower risk of crystallization in systems with lower effectiveness values, however, systems with low effectiveness values are not desirable

CHAPTER 5

MIXTURES OF SALT SOLUTIONS

5.1 Introduction

The purpose of this chapter is to investigate the equilibrium humidity at the surface of a solution of mixed $MgCl_2$ and LiCl salts. Results from chapter 3 showed that $MgCl_2$ solution is the most cost-effective among the investigated salt solutions. However, high equilibrium vapor pressure at the surface of $MgCl_2$ solution may cause crystallization of salt in LAMEEs during some typical HVAC application and operating conditions (chapter 4). In this chapter, mixtures of $MgCl_2$ (as a cost effective liquid desiccant) and LiCl (as a desiccant with low crystallization risk) are investigated. The equilibrium relative humidity of air in contact with the $MgCl_2$-LiCl mixture is measured. A certain mixing ratio of $MgCl_2$-LiCl solution is recommended as a cost effective alternative liquid desiccant for pure LiCl solution in climatic conditions where $MgCl_2$ and $CaCl_2$ solutions have a high risk of crystallization.

5.2 Experimental Setup

Figure 5.1 shows a picture of the experimental instruments used to measure the air humidity at the surface of a $MgCl_2$-LiCl mixture. In order to conduct the experiment, $MgCl_2$ and LiCl salts with different mass ratios are mixed with specific amount of water in a small jar. The temperature and humidity sensor is then placed at the top of the solution and the opening of the jar is sealed. The mixture is allowed enough time to

reach equilibrium and then the humidity and temperature values are recorded. The mixture is placed in a water bath with cooling coils in order to repeat the experiment at different temperatures.

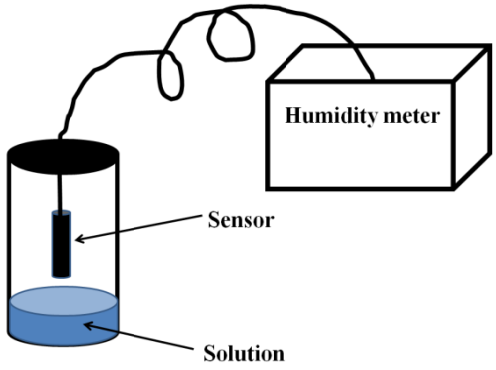

Figure 5. 1: Schematic of the experimental setup.

5.3 Experimental Instrumentation and Uncertainty

The equilibrium vapor pressure of air above a salt solution may be calculated from the relative humidity and temperature. In this study, the air relative humidity and temperature are measured using VAISALA humidity and temperature transmitter (model: HMP230). The humidity measurement range of this device is 0 to 100% RH and the temperature measurement range is -40 to +180 ˚C. Vaisala HMP230 humidity transmitters use HUMICAP® sensor to measure the relative humidity of air. The HUMICAP sensors operate based on the changes in the capacitance of the sensor as its thin polymer film gains water molecules (VAISALA operating manual, 1998).

Prior to measuring the equilibrium humidity at the salt solution surface the humidity transmitter has to be calibrated. The humidity sensor was calibrated with a Mini two-pressure humidity generator (MINI-Series 1200, 2004). A schematic of the Series 1200 humidity generator is shown in Figure 5.2. As shown in Figure 5.2, the humidity generator consists of a saturator, expansion valve and a test chamber. Air or

some other gas, such as nitrogen, is saturated with water vapor at a given temperature and pressure in the humidity generator. Later, the saturated gas flows through the expansion valve where its pressure is reduced to the desired pressure. The humidity generator may generate relative humidities between 10 to 95% in a temperature range of 10 to 60 ˚C. The humidity generator calculates the relative humidity of the chamber with an uncertainty of ± 1% RH.

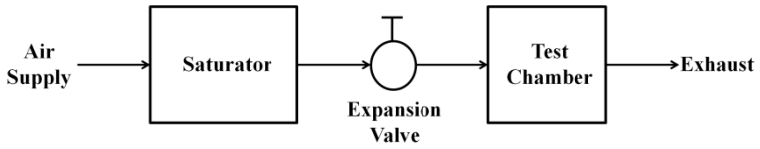

Figure 5.2: Schematic of a Series 1200 Mini Two-Pressure humidity generator (Mini 1200, 2004).

In order to calibrate the humidity transmitter, it was placed in the test chamber of the humidity generator and the humidity generator was set to create a specific humidity and temperature. The readings from the humidity and temperature transmitter were recorded at each humidity setting of the generator. Figure 5.3 shows the calibration curve of the RH sensor as well as the difference between the sensor reading and the calibrator reading. The maximum precision error was found to be 0.3% after the variance analysis of the measured data and the bias error was found to be linear ($y = 1.014x + 0.013$). At worst case scenario the 95% uncertainty was found to be ± 1.2% RH.

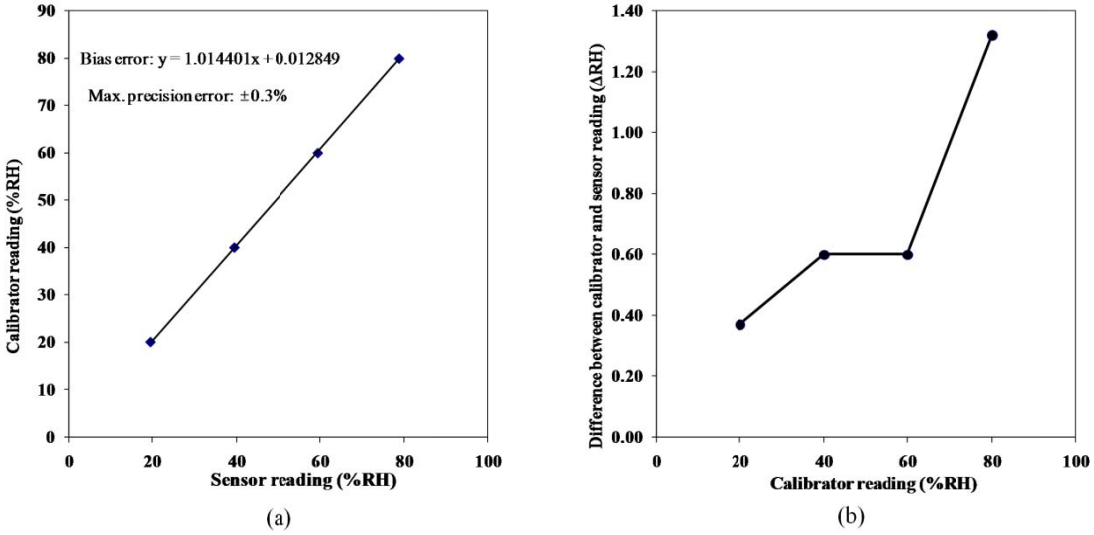

Figure 5.3: (a) Average sensor humidity vs. the humidity generator and (b) difference between the calibrator and sensor readings.

To calibrate the temperature sensor, the temperature and humidity transmitter was placed in a dry block temperature generator (model: 9107). The 95% uncertainty of the temperature sensor was found to be ± 0.2 ˚C.

5.4 Results and Discussion

Initially, the experiments were performed on pure LiCl and $MgCl_2$ solutions and the results were compared to some available data in the literature. Figure 5.4 compares the current experimental measurements with previous works. As seen in Figure 5.4, most of the data from previous research lie in the uncertainty bounds of the measurements of the current study. However, there is a significant difference between the measured humidities of $MgCl_2$ at higher concentrations and the values calculated with the correlation of Cisternas and Lam (1991). This discrepancy is due to the inaccuracy of this correlation at high concentrations (as discussed in chapter 3).

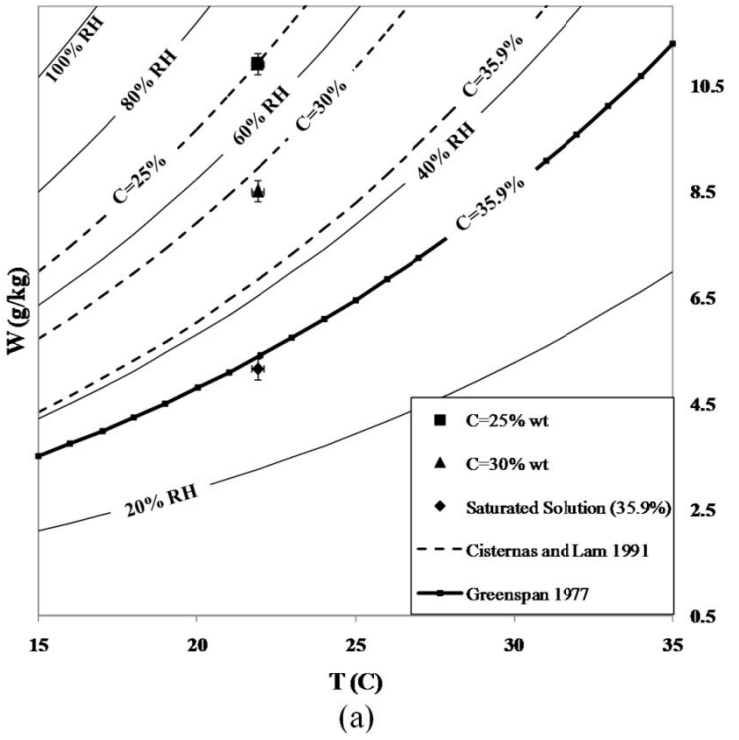

(a)

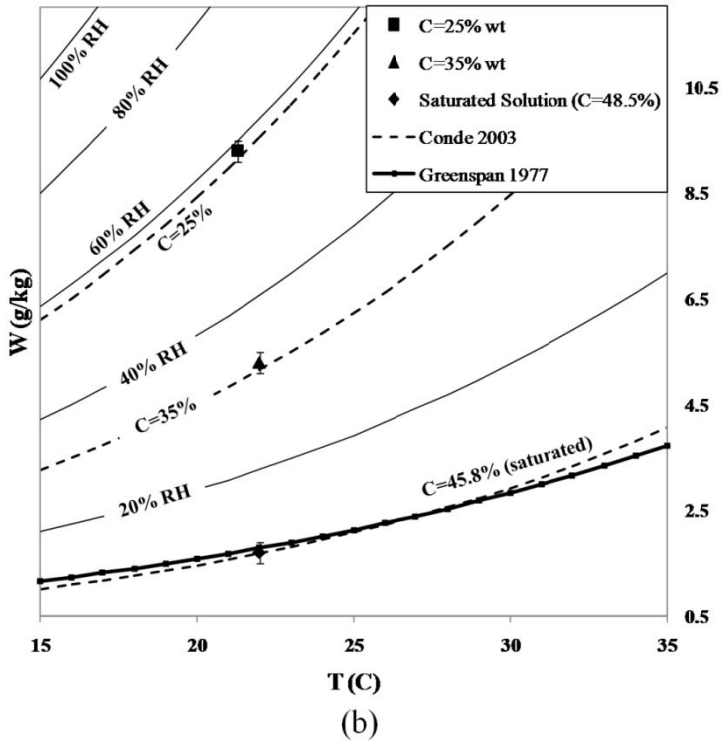

(b)

Figure 5.4: Air humidity ratio at the surface of (a) $MgCl_2$ and (b) LiCl solutions compared with calculated values from available correlations.

Following the experiments on pure salt solutions, several different mixtures of $MgCl_2$ and LiCl were investigated. Four different LiCl/$MgCl_2$ weight combinations were tested in this study. The total concentration of the salt solution was kept very close to the saturation concentration of the mixture at the temperature in which the humidity of the solution was measured. In order to create saturated mixtures of LiCl-$MgCl_2$, the saturation concentration is required for different weight combinations. The saturation concentration of different LiCl-$MgCl_2$ mixtures are shown in Table 5.1 at 25˚ C.

Table 5.1: Saturation concentration of the LiCl-$MgCl_2$-water mixtures at 25˚ C (Stephen and Stephen 1963).

$MgCl_2$ Concentration	LiCl Concentration	Total Saturation Concentration	The Crystallized Salt
14.3%	28.0%	42.3%	$MgCl_2$
18.0%	22.0%	40.0%	$MgCl_2$
20.0%	18.9%	38.9%	$MgCl_2$
28.3%	8.4%	37.1%	$MgCl_2$

The weight concentrations of each salt in the mixture for different mass ratio combinations that were tested in this experiment are presented in Table 5.2. The mass ratio shows that what percentage of the total salt in the solution is made up of each specific salt. For example, a pure saturated $MgCl_2$ (C=35.9%) is made up of 100% $MgCl_2$ and 0% LiCl.

Table 5.2: Humidity ratio and price of LiCl-$MgCl_2$ solution mixture at 23 ˚C for different mass combinations.

Test Number	$MgCl_2$ Concentration	LiCl Concentration	$MgCl_2$ mass ratio	LiCl mass ratio	Equilibrium humidity ratio (g/kg)	Total price per 35 L of solution (USD)	Relative price
1	35.9%	0%	100%	0%	5.66	5.3	1
2	29%	7%	81%	19%	5.97	32.7	6.2
3	23%	14%	62%	38%	4.88	58.8	11.1
4	19%	21%	47%	53%	3.49	86.1	16.2
5	14%	28%	33%	67%	3.08	118.3	22.3
6	0%	45.8%	0%	100%	1.89	212.2	40

Figure 5.5 illustrates the measured humidity ratio and temperature of the LiCl-$MgCl_2$ mixtures superimposed on a psychrometric chart. The concentration of each salt in the mixture and the total concentration of the solution are shown in Figure 5.5.

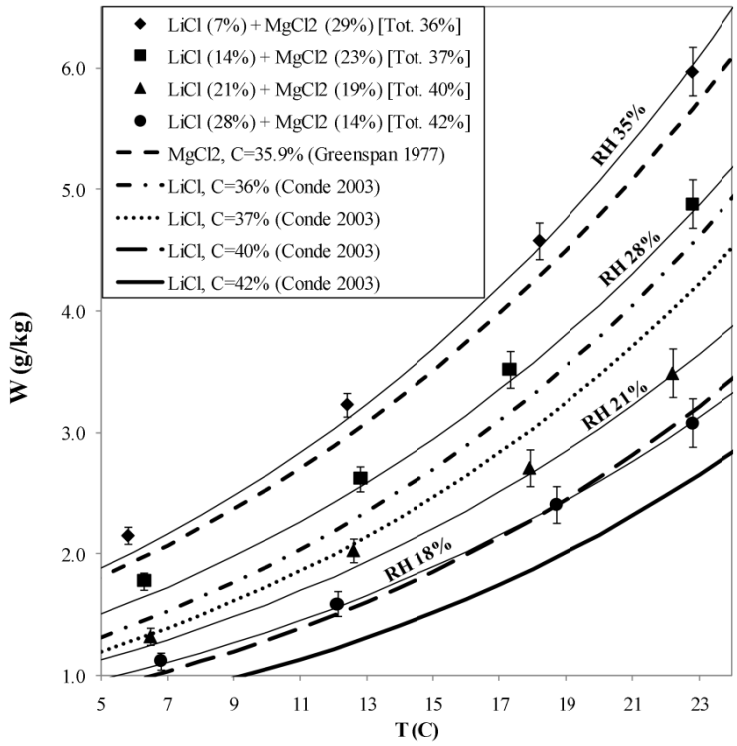

Figure 5.5: Equilibrium humidity ratio at the surface of LiCl-$MgCl_2$ mixtures with different mass combination ratios at different temperatures.

As seen in Figure 5.5, the humidity ratio clearly decreases as the mass ratio of LiCl increases in the mixture (i.e., from test number 1 to 6). Table 5.2 also shows that the addition of the first 53% of LiCl in the mixture (i.e., test number 4 in which mass ratio of LiCl is 53%) decreases the equilibrium humidity more than the addition of the next 47% (i.e., test number 6 in which the solutions is pure LiCl). For example at 23˚C, the equilibrium humidity ratio decreases from 5.66 g/kg for a saturated $MgCl_2$ solution

(C=35.9%) to 3.49 g/kg (i.e., a reduction of 2.2 g/kg in the equilibrium humidity ratio) after the addition of the first 50% of LiCl (test number 4) to the solution while the addition of the second 50% of LiCl to the mixture only reduces the equilibrium humidity ratio by 1.6 g/kg (test number 6). However the price of a pure saturated LiCl solution is more than twice the price of a $MgCl_2$-LiCl solution with 53% LiCl mass ratio and 47% $MgCl_2$ mass ratio for each salt in the solution.

A mixture with almost equal amounts of $MgCl_2$ and LiCl (i.e., C_{MgCl2}=19% and C_{LiCl}=21%) maintains the air humidity at approximately 21% RH which is 13% RH lower than the humidity at the surface of a saturated $MgCl_2$. A pure LiCl with 38.5% weight concentration is required to create an equilibrium humidity of 21% RH. The price of 35 L of the 38.5% LiCl solution is 125.2 USD which is more than 30% higher than the price of the mixture.

Figure 5.6 compares the critical humidity ratio lines of a roughly 1:1 mass ratio mixture of $MgCl_2$ and LiCl (C_{LiCl}=21% and C_{LiCl}=19%) with W_{cr} lines of pure $MgCl_2$ solution. As seen in Figure 5.6, the critical relative humidity of the mixture is 15% RH less than that of a pure $MgCl_2$ when the system operates in a building with 50% indoor RH. The reduction in the critical RH is approximately 12% RH when exhaust air relative humidity is 30% RH. During winter operating conditions, the mixture has no risk of crystallization if the exhaust air is at 50% RH, therefore, only the W_{cr} lines of 30% RH indoor condition are illustrated.

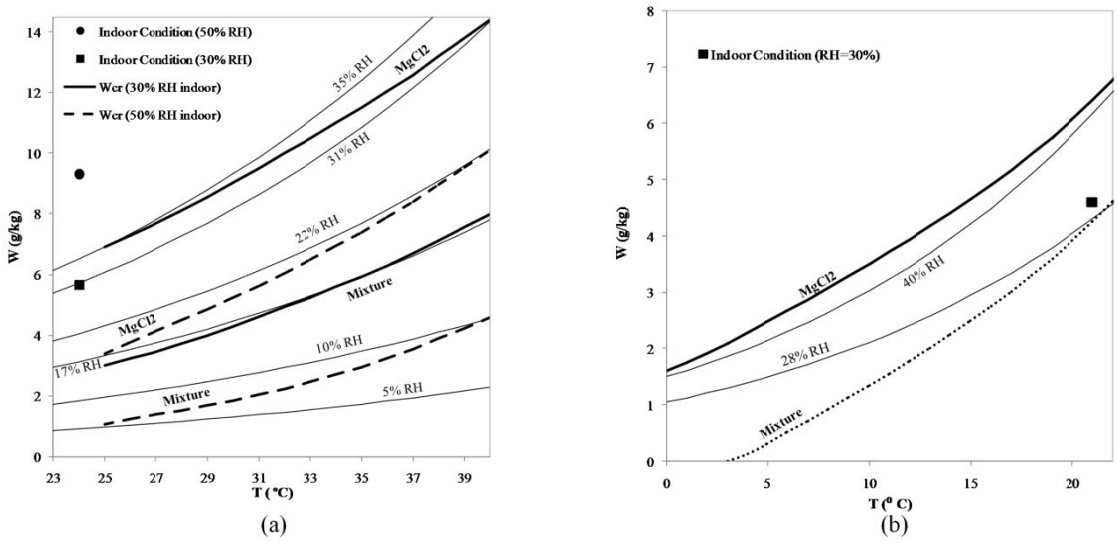

Figure 5.6: Critical humidity ratio lines of the LiCl-$MgCl_2$ mixture (C_{MgCl2}=19%, C_{LiCl}=21%) compared to pure $MgCl_2$ solution during (a) summer and (b) winter operating conditions.

The risk of crystallization of the LiCl-$MgCl_2$ mixtures with different mass combinations is illustrated in Figure 5.7 for three different cities located in the dry zone. As seen in Figure 5.7, the risk of crystallization reduces as the mass ratio of LiCl increases in the solution. Less than 2% of the year will be in the risk of crystallization in the driest North American climates if a $MgCl_2$ (19% wt)-LiCl (21% wt) mixture is used in the RAMEE with 50% RH exhaust air humidity. The risk will be less than 12% of the year for the same weight combination of the mixture if the exhaust air humidity is reduced to 30%.

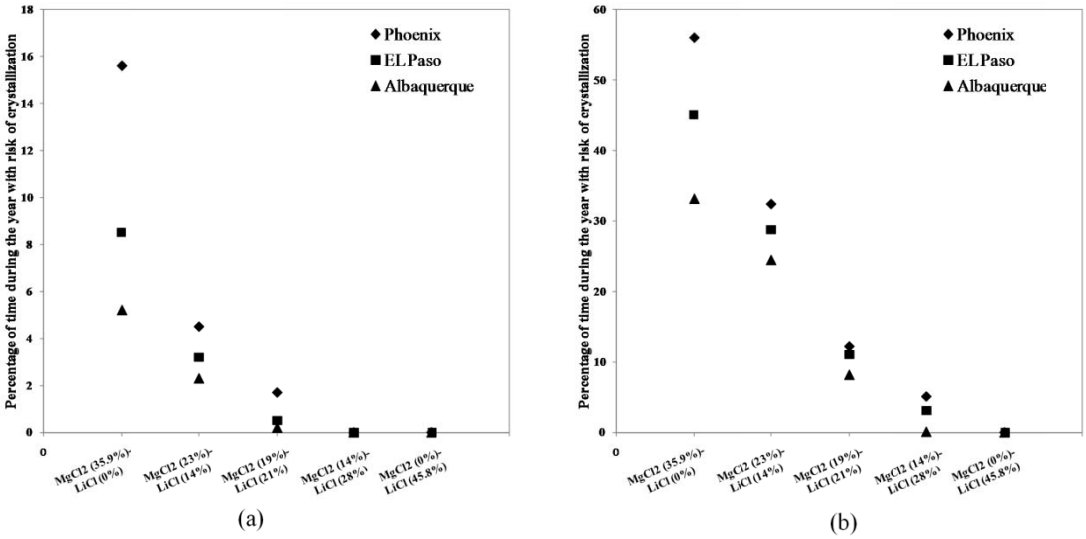

Figure 5.7: Percentage of the year in risk of crystallization in three different cities located in the dry climatic zone for different mass combinations of LiCl-$MgCl_2$ mixtures in a RAMEE operating with indoor humidity of (a) 50% RH and (b) 30% RH.

the 1:1 mass ratio $MgCl_2$-LiCl mixture combination has no risk of crystallization in climate zones except hot-dry, warm-dry and mixed-dry zones in both 30% RH and 50% RH indoor humidities and may be used as an alternative when $MgCl_2$ solution cannot be used.

5.5 Summary

In this chapter, experiments were performed on mixtures of LiCl and $MgCl_2$ with different weight combinations to measure the equilibrium humidity ratio at their interface with air. The purpose of these experiments was to investigate the possibility of replacing highly-priced LiCl or LiBr solutions with a more cost-effective desiccant that would have a low risk of crystallization.

The experiments showed that the addition of LiCl to a $MgCl_2$ solution reduces its equilibrium relative humidity. As the amount of LiCl increases in the mixture the equilibrium relative humidity at the surface of the mixture decreases. A mixture with 19% concentration $MgCl_2$ and 21% concentration LiCl (total concentration of 40%)

maintains the air relative humidity at approximately 21% RH. This mixture combination may be used in the RAMEE with very small risk of crystallization in all North American climate zones when the indoor humidity is 50% RH. However when indoor humidity is reduced to 30%, the hot, warm and mixed-dry climates may experience crystallization in less than 10% of the year.

CHAPTER 6

SUMMARY, CONCLUSIONS AND RECCOMMENDATIONS

6.1 Summary

The main objective of this study was to select an appropriate desiccant solution to use in a run-around membrane energy exchanger (RAMEE). Four widely used liquid desiccants in the HVAC industry (LiCl, LiBr, $CaCl_2$ and $MgCl_2$) were chosen to be investigated in this thesis. In chapter 2, a numerical model was presented that would calculate the properties at the liquid-membrane interface in each of the two liquid-to-air membrane energy exchangers (LAMEE) of the system.

The properties of the selected salt solutions were presented in Chapter 3, including the thermo-physical properties (i.e., density, viscosity, specific heat capacity, thermal conductivity, and diffusion coefficient), cost, safety and the RAMEE properties that result from the salt solution properties (i.e., pumping cost, storage tank size and effectiveness). Various property correlations to calculate the properties were compared and the most accurate correlations were selected for use in the numerical model.

Crystallization of the salt solution is a very important characteristic that must be considered when selecting an appropriate liquid desiccant. The risk of crystallization of the selected salt solutions as well as some recommendations to prevent salt crystallization in the RAMEE were presented in chapter 4.

In chapter 5, a new liquid desiccant (mixture of LiCl and $MgCl_2$ solutions) is introduced as a cost-effective alternative when the RAMEE operates in dry climates.

6.2 Conclusions

The following can be concluded from the research presented in this thesis:

1. Thermo-physical property correlations from more than seven different sources as well as several experimental measurements were compared in this thesis. These comparisons showed that more accurate correlations are available than those used by previous RAMEE researchers (Fan 2005; Vali 2009 and Seyed Ahmadi 2008) using the most accurate property correlations for the salt solution in the numerical model resulted in less than 1% change in the total effectiveness of the RAMEE.
2. Simulations showed that the total effectiveness of the RAMEE with AHRI operating conditions changes by less than 0.5% if different salt solutions are used in the RAMEE.
3. The prices of the liquid desiccants differ significantly from one another. LiCl solution is the most expensive among the selected solutions (i.e. $ 1.21/CFM of air flow through each LAMEE) and is followed by LiBr (i.e. $ 1.12/ CFM), $CaCl_2$ (i.e. $ 0.12/CFM) and $MgCl_2$ (i.e. $ 0.06/CF).
4. Storage tanks are unavoidable in a RAMEE is since the volume of the salt solution changes significantly during the year. Larger storage tanks are required in places where the outdoor air relative humidity changes more during the year. For example, the volume of a $MgCl_2$ solution will change by 27% in Phoenix (AZ) and by 17% in Saskatoon (SK).

5. Pumping costs differ for different salt solutions in the RAMEE. $MgCl_2$ solution requires the highest pumping power among the selected salt solutions and LiBr solution requires the least pumping power. The pumping cost of a RAMEE operating with $MgCl_2$ is approximately ¢ 7/CFM for yearly operation of the system (based on 12 hour operation daily throughout the year, 100 m piping). The initial and operational costs of the selected salt solutions are summarized in Table 6.1 with relative numbers. Number 1 in Table 6.1 indicates the salt solution with the lowest cost/smallest size and the other numbers are relative to this number.

Table 6.1: Initial and operating cost of the selected salt solutions in the RAMEE system. Value of 1 is assigned to the smallest size/lowest cost and other values are relative to this number.

Salt solution	Initial cost	Pumping cost	Storage tank size
LiCl	20	1.3	1.2
$CaCl_2$	2	1.9	1.3
LiBr	19	1	1.1
$MgCl_2$	1	3.3	1

6. The indoor and outdoor operating conditions were found to play an important role on the risk of crystallization of the salt in the RAMEE. The risk of crystallization increases as the outdoor or indoor humidity decreases. This finding shows that different salt solutions should be selected for different climates. For example in Phoenix (AZ) which is a dry climate, $MgCl_2$ has a risk of crystallization in more than 55% of the year (with 30% RH indoor condition) while LiCl has no risk of crystallization.
7. Crystallization may be prevented by increasing the solution flow rate when outdoor air humidity is close to the critical humidity of the particular salt

solution. Humidifying the dry outdoor air before it enters the supply LAMEE is another way to reduce the risk of crystallization in the RAMEE.

8. The risk of crystallization of the salt is very small during winter operating conditions. When outdoor humidity is 50% RH, there is no risk of crystallization of $MgCl_2$ for temperatures lower than 8˚C.
9. At an indoor humidity of 50% RH during summer operating conditions, $MgCl_2$ solution can be used in the RAMEE for most climates except in hot-dry and warm-dry climate zones (see Figure 6.1). When indoor humidity is reduced to 30% RH, $MgCl_2$ solution may only be used in Moist (A) and Marine (C) climate zones.
10. A mixture of $MgCl_2$ and LiCl (1:1 mass ratio mixture) can be used in dry climates (i.e., where $MgCl_2$ cannot be used due to high risk of crystallization) instead of highly priced pure LiCl or LiBr solutions. At 50% RH indoor humidity, this mixture has risk of crystallization in less than 2% of the year in Phoenix (i.e., the climate with the highest risk in North America) while its price is 30% less than the price of pure LiCl solution.
11. The recommended salt solutions to use in the RAMEE are shown in Figure 6.1 for different climates in the US for 50% RH and 30% RH indoor conditions during summer operating conditions.
    (a) $MgCl_2$ solution may be used as operating liquid desiccant in the RAMEE in most American climates except hot, warm and mixed-dry regions when indoor humidity is 50% RH. A mixture of $MgCl_2$-LiCl (1:1 mass

ratio mixture) can be used as the liquid desiccant in the hot, warm and mixed-dry regions (see Figure 6.1(a)).

(b) At an indoor humidity of 30% RH, $MgCl_2$ may be used in the RAMEE in Moist (A) and Marine (C) regions. $MgCl_2$-LiCl mixture (1:1 mass ratio mixture) can be used in the cool and cold-dry regions (5B and 6B). Finally, pure LiCl solution is recommended for hot, warm and mixed-dry (2B, 3B and 4B) climatic zones.

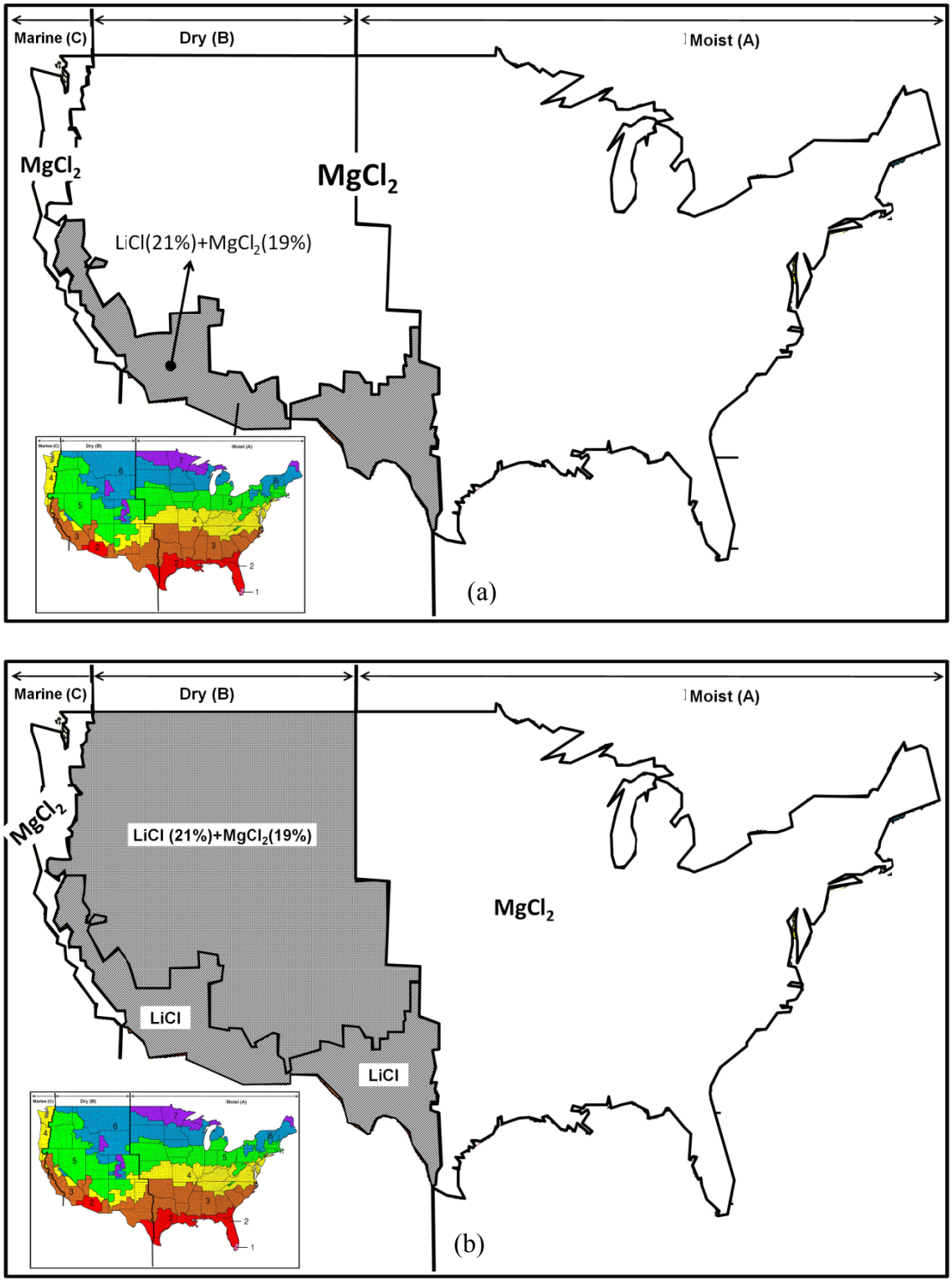

Figure 6.1: Recommended salt solution to use in the RAMEE system based on climate condition for (a) 50% RH indoor condition and (b) 30% RH indoor condition (summer operating conditions).

6.3 Recommendations for Future Work

The following can be recommended for future studies:

- The impact of maldistribution of the liquid flow in the channels on the risk of crystallization of the salt should be studied.
- The risk of crystallization should be investigated during the transient operation of the RAMEE.
- The salt solutions studied in this thesis were assumed to have no impurities, however, in reality the salt solutions may contain other chemicals. The impact of the impurities in the desiccant solution on the risk of crystallization or the properties of the solution should be studied.
- Frosting in the air channels of the LAMEEs should be investigated.
- Accurate correlations should be developed to predict the effectiveness of the RAMEEs with different design characteristics in different operating conditions.
- A more thorough economic analysis is required for the RAMEE.

REFERENCES

Ali, A., K. Vafai, and A.-R.A. Khaled. 2004. Analysis of heat and mass transfer between air and falling film in a cross flow configuration, *International Journal of Heat and Mass Transfer* 47: 743-755.

AHRI. 2005. ANSI/ARI Standard 1060, Standard for Rating Air-to-Air Exchangers for Energy Recovery Ventilation Equipment. Arlington, VA: Air-Conditioning & Refrigeration Institute.

ASHRAE, 2008. ASHRAE Handbook-Systems and Equipments, *American Society of Heating, Refrigerating and Air Conditioning, Engineers Inc.*, Atlanta, 2008.

ASHRAE, 2004. ANSI/ASHRAE Standard 62.1 Ventilation for Acceptable Indoor Air Quality. *ASHRAE*, Atlanta.

ASHRAE, 2004. ANSI/ASHRAE/IESNA Standard 90.1 Energy Standard for Buildings Except Low-Rise Residential Buildings. *ASHRAE*, Atlanta.

ASHRAE, 2005. ASHRAE Handbook-Fundamentals, *American Society of Heating, Refrigerating and Air Conditioning, Engineers Inc.*, Atlanta, 2005.

ASHRAE, 1996. ASHRAE Handbook-Systems and Equipments, *American Society of Heating, Refrigerating and Air Conditioning, Engineers Inc.*, Atlanta, 1996.

ASHRAE, 1989. ANSI/ASHRAE/IESNA Standard 90.1 Energy Standard for Buildings Except Low-Rise Residential Buildings. *ASHRAE*, Atlanta.

ASHRAE, 1981. ANSI/ASHRAE/IESNA Standard 90.1 Energy Standard for Buildings Except Low-Rise Residential Buildings. *ASHRAE*, Atlanta.

Asiedu, Y., R.W. Besant, and C.J. Simonson. 2005. Cost effective design of dual heat and energy recovery exchangers for 100% ventilation air in HVAC cabinet units, *ASHRAE Transactions*, 111(1): 857-872.

Bichowsky FR, Kelley GA. 1935. Concentrated solutions in air-conditioning, *Industrial and Engineering Chemistry,* 27: 879-882.

Boryta, D.A., A.J. Maas and C.B. Grant. 1975. Pressure–temperature–concentration relationship for system lithium bromide and water (40–70% lithium bromide), *J Chem Eng Data,* **20**(3): 316–319.

Bornehag C.G, J. Sundell, C.J. Weschler, T. Sigsgaard, B. Lundgren, M. Hasselgren, Hagerhed-Engman L. 2004. The association between asthma and allergic symptoms in children and phthalates in house dust: a nested case-control study. *Environ Health Perspect* 112(14):1393–7.

Briggs, R.S., R.G. Lucas, and Z.T. Taylor. 2003. Climate classification for building energy codes and standards: Part 1 - Development process, *ASHRAE Transactions*, 109(1): 109-121.

Chua H.T., H.K. Toh , A. Malek, K.C. Ng, K. Srinivasan, 2000. Improved thermodynamic property fields of LiBr+H_2O solution, *International Journal of Refrigeration*, 23: 412-429

Cisternas, L.A. and E.J. Lam. 1991. Analytic Correlation for the Vapour Pressure of Aqueous and Non-Aqueous Solutions of Single and Mixed Electrolytes. Part II. Application and Extension, *Fluid Phase Equilibria*, 62(1): 11-27.

Conde M. 2004. Properties of aqueous solutions of lithium and calcium chlorides: formulations for use in air conditioning equipment design, *International Journal of Thermal Sciences,* 43: 367–382

Conde-Petit, M. 2007. "Liquid desiccant-based air-conditioning systems—LDACS," *Proceedings of the 1st European Conference on Polygeneration*. stuttgart.de/sixcms/media.php/773/19_Conde_M.pdf

Conde-Petit, M., R. Weber, 2006. OPEN ABSORPTION SYSTEM FOR COOLING AND AIR CONDITIONING USING MEMBRANE CONTACTORS, *Federal Department of Environment, Transport, Energy and Communications (DETEC) Federal Office of Energy (SFOE)*, Switzerland.

Dieckmann J., K. Roth, J. Brodrick. 2008. Liquid Desiccant Air Conditioners, *ASHRAE Journal* 50(10): 90-95.

Engvall, K., P. Wickman, D. Norbäck. 2005. Sick building syndrome and perceived indoor environment in relation to energy saving by reduced ventilation flow during heating season: A 1 year intervention study in dwellings. *Indoor Air,* 15: 120–126.

Erb, B., C.J. Simonson, M. Seyed Ahmadi, and R.W. Besant. 2009. Experimental Measurements of a Run-Around Membrane Energy Exchanger (RAMEE) with Comparison to a Numerical Model, *ASHRAE Transactions*, 115(2).

Erb, B., 2006. Run-Around Membrane Energy Exchanger Performance and Operational Control Strategies, Department of Mechanical Engineering, University of Saskatchewan, Saskatoon, Saskatchewan

Erb, B., 2006. Designing and Testing a Run-Around Heat and Moisture Recovery System, Summer Work Report, Department of Mechanical Engineering, University of Saskatchewan, Saskatoon, Saskatchewan

Erb, B., 2007. Run-around membrane energy exchanger prototype 2 testing, Summer Work Report, Department of Mechanical Engineering, University of Saskatchewan, Saskatoon, Saskatchewan

Ertas, A., E.E. Anderson, and I. Kiris. 1992. Properties of a new liquid desiccant solution—lithium chloride and calcium chloride mixtures. Solar Energy 49(2):205-212.
Eto, H., C. Meyer. 1988. The HVAC costs of fresh air ventilation, *ASHRAE Juornal,* 30(9): 31-35

Fan, H., C.J.Simonson, R.W. Besant, and W. Shang. 2005. Run-around heat recovery system using cross-flow flat-plate heat exchangers with aqueous ethylene glycol as the coupling fluid. *ASHRAE Transactions* 111(1): 901-910.

Fan, H., 2005. Modelling a Run-Around Heat And Moisture Recovery System, Department of Mechanical Engineering, University of Saskatchewan.

Fang, L., G. Clausen and P.O. Fanger. 1998. Impact of temperature and humidity on the perception of indoor air quality, *Indoor Air,* 8: 80–90

Fanger, PO., 2006. What is IAQ?, *Indoor Air*, 16(5): 328–34.

Fauchoux, M., C.J.Simonson, and D.A. Torvi. 2007. The effect of energy recovery on perceived air quality, energy consumption and economics of an office building, *ASHRAE Transactions*, 113(2): 437-449.

Fauchoux, M., C.J.Simonson, and D.A. Torvi. 2009. Tests of a Novel Ceiling Panel for Maintaining Space Relative Humidity by Moisture Transfer from an Aqueous Salt Solution, *Journal of ASTM International*, 6(4).

Fox, R.W., and A.T., McDonald. 1988. Introduction to fluid mechanics, 4th ed., *J. Wiley*, New York.

Gabriel, K. 2007. Heat and energy wheels, Encyclopedia of Energy Engineering and Technology, Volume 2, Edited by Barney Capehart, *CRC Press*, Boca Raton, FL, 794-800.

Greenspan, L. 1977. Humidity Fixed Points of Binary Saturated Aqueous Solutions, *Journal of Research of the National Bureau of Standard*, 81A: 89– 96.

Hellmann, H.-M., and G. Grossman. 1996. Improved property data correlations of absorption working fluids for computer simulation of heat pump cycles. ASHRAE Transactions 102(1):980-997.

Hemingson, H.B. 2010. Run-Around Membrane Energy Exchanger: Performance Characteristics and Effectiveness Correlations. MSc. thesis (in progress). Department of Mechanical Engineering, University of Saskatchewan, Saskatoon.

Hemingson, H. 2005. Preliminary testing for run around heat and moisture exchanger, Summer Work Report, Department of Mechanical Engineering, University of Saskatchewan, Saskatoon, Saskatchewan.

Horvath, A.L. 1985. Handbook of aqueous electrolyte solutions, *ELLIS HORWOOD LIMITED*, Chichester, England.

Incropera, F.P. and Dewitt, D.P., 2002. Fundamentals of Heat and Mass Transfer, 5th ed. John Wiley & Sons, New York.

Izquierdo, M., M. Venegas, P. Rodriguez and A. Lecuona. 2004. Crystallization as a limit to develop solar air-cooled LiBr–H_2O absorption systems using low-grade heat, *Solar Energy Materials & Solar Cells*, 81: 205–216

Iyoki, S.; S. Iwasaki; T. Uemura, 1990. Vapor Pressure of the Water- Lithium Bromide-Lithium Iodide System, *J. Chem. Eng. Data,* 35: 429-433.

Iyoki, S.; S. Iwasaki; Y. Kuriyama; Uemura, T. 1993. Solubilities for the Two Ternary Systems Water + Lithium Bromide + Lithium Iodide and Water + Lithium Chloride + Lithium Nitrate at Various Temperatures. *J. Chem. Eng. Data,* 38: 396-398.

Kakac S., H. Liu. 2002. Heat exchangers selection, rating and thermal design, *CRC Press.*

Kawamata, K., Y. Nagasaka, and A. Nagashima, 1988. Measurements of the Thermal Conductivity of Aqueous LiBr Solutions at Pressures up to 40 MPa, *International Journal of Thermophysics,* 9(3): 317-329.

Kettleborough, C.F., and D.G. Waugaman. 1995. Alternative desiccant cooling cycle*, Journal of Solar Energy Engineering—Transactions of the ASME*, 117(3): 251.

Kim, D.S., and C.A. Infante Ferreira. 2009. Air-cooled LiBr–water absorption chillers for solar air conditioning in extremely hot weathers, *Energy Conversion and Management* 50: 1018–1025.

Koo, K.K., Lee, H.R., Jeong, S., Oh, Y.S., Park, D.R., Baek, Y.S. 1999a. Solubilities, Vapor Pressures and Heat Capacities of the (Water + Lithium Bromide + Lithium Nitrate + Lithium Iodide + Lithium Chloride) System. *Int. J. Thermophys,* 20: 589-600.

Larson, M.D., C.J. Simonson, R.W. Besant, and P.W. Gibson. 2007. The elastic and moisture transfer properties of polyethylene and polypropylene membranes for use in liquid-to-air energy exchangers. *Journal of Membrane Science*, 302: 136-149.

Larson, M.D., 2006. The performance of membrane in a newly proposed run-around heat and moisture exchanger, M.Sc. Thesis, Department of Mechanical Engineering, University of Saskatchewan, Saskatoon, Saskatchewan

Lee, R.J.. R.M. DiGuilio. S.M. Jeter, and A.S. Teja. 1990. Properties of Lithium Bromide-water solutions at high temperatures and concentrations. IL Density and Viscosity. *ASHRAE Transactions* 96(1):709-7I4.

Lenard, J.L.Y., S.M. Jeter, and A.S. Teja. 1992. Properties of lithium bromide-water solutions at high temperatures and concentrations—Part 4: Vapor pressure. *ASHRAE Transactions* 98(1):1-6.

Liao, X., and R. Radermacher. 2007. Absorption chiller crystallization control strategies for integrated cooling heating and power systems, *International Journal of Refrigeration*, 30: 904-911.

Lower, H. 1961. *Kaltetechnik*, 13(5). 178-83

Mahiuddin, S., and K. Ismail. 1983. Concentration Dependence of the Viscosity of Aqueous Electrolytes. A Probe into Higher Concentration, *J. Phys. Chern.*, 87: 5241-5244.

Mahmud, K. 2009. Design and testing of a laboratory RAMEE system with counter flow exchangers to transfer heat and water vapor between supply and exhaust air flows. University of Saskatchewan.

McNeeley, L.A. 1978. Thermodynamic properties of aqueous-solutions of lithium bromide. ASHRAE Journal 20(12):54-55.

Mei, L., and Y.J. Dai. 2008. A technical review on use of liquid-desiccant dehumidification for air-conditioning application, *Renewable and Sustainable Energy Reviews,* 12: 662–689.

Mesquita, L.C.S., S.J. Harrison, and D. Thomey. 2006. Modeling of heat and mass transfer in parallel plate liquid desiccant dehumidifiers, *Solar Energy*, 80: 1475-1482.

MINI-1200, 2004. Two-pressure humidity generator, operation and maintenance manual. New Mexico: *Thunder Scientific Corporation*.

MSDS, 2005. Lithium Chloride-Water Solution, MSDS No. 9417003, *SCHOLAR CHEMISTRY*.

MSDS, 1993. Magnesium Chloride Solution, MSDS No. 4998821, *DOW CHEMICAL CANADA INC*: Sarnia, Ontario.

Naterer, G.F. 2007. Heat and energy wheels, Encyclopedia of Energy Engineering and Technology, Volume 2, Edited by Barney Capehart, *CRC Press*, Boca Raton, FL, 794-800.

National Renewable Energy Laboratory, NREL, TMY2 weather data file, http://rredc.nrel.gov/solar/old_data/nsrdb/tmy2/, Aug. 26 2009.

National Board of Energy of Canada, NBE, http://www.neb.gc.ca/clf-nsi/rnrgynfmtn/prcng/lctrct/crrntmrktcndtn-eng.html, Mar. 26 2010.

Niu, J.L. and Zhang, L.Z., 2001. Membrane-based Enthalpy Exchanger: Material considerations and clarification of moisture resistance, *Journal of membrane science,* **189**(2): 179-191.

Patil, K.R., et al. 1990. Thermodynamic properties of aqueous-electrolyte solutions.1. Vapor-pressure of aqueous-solutions of Licl, Libr, and Lii. Journal of Chemical and Engineering Data 35(2):166-168.

Phang 1., and R.H. Stokes, 1980. Density, Viscosity, Conductance, and Transference Number of Concentrated Aqueous Magnesium Chloride at 25C, *Journal of Solution Chemistry,* 9(7): 497-505.

Reay D., Kew P. 2006. Heat pipes theory, design and applications. *Batterwoth-Heinemann*. Burlington, MA.

Seppanen, O, W.J. Fisk, and Q.H. Lei. 2006. Ventilation and performance in office work, *Indoor Air,* 16: 28–36

Shang, W. and Besant, R.W. 2008. Theoretical and Experimental Methods for the Sensible Effectiveness of Air-to-Air Energy Recovery Wheels, *HVAC&R Research.*, 14 (3), 373-396.

Simonson, C.J. 2007. Heat and energy wheels, Encyclopedia of Energy Engineering and Technology, Volume 2, Edited by Barney Capehart, *CRC Press*, Boca Raton, FL, 794-800.

Simonson, C.J., and R.W. Besant. 1999. Energy wheel effectiveness: part I - development of dimensionless groups, *International Journal of Heat and Mass Transfer*, 42: 2161-2170.

Stabat, P., and D. Marchio. 2009. Heat and mass transfer modeling in rotary desiccant dehumidifiers, *Applied Energy* 86(5): 762-771.

Uemura, T., S. Hasaba. 1964. Studies on the lithium bromide-water absorption refrigerating machine. *Tech. Rep. Kansai Uniniv.*, (6) 31-55.

VAISALA Operating Manual. 1998. *HMP 230 series transmitters operating manual*, Woburn, MA.

Vali, A., C.J. Simonson, R.W. Besant, and G. Mahmood, 2009. Numerical model and effectiveness correlations for a run-around heat recovery system with combined counter and cross-flow exchangers, *International Journal of Heat and Mass Transfer*, 52(25-26): 5827-5840.

Vali, A. 2009. Modeling a Run-around Heat and Moisture Exchanger System Using Two Counter/Cross Flow Exchangers. University of Saskatchewan.

Wargocki, P., D.P. Wyon, J. Sundell, G. Clausen and P.O. Fanger. 2000. The effects of outdoor air supply rate in an office on perceived air quality, Sick Building Syndrome (SBS) symptoms and productivity, *Indoor Air,* 10: 222–237.

Waugaman, D.G., A. Kini, and C.F. Kettleborough. 1993. A review of desiccant cooling systems, *J. Energy Resour. Technol.* 115: 1–8.

White, F.M., 2003. Fluid mechanics, *McGraw-Hill*, Boston.

Wimby, J.M., and T.S. Berntsson. 1994. Viscosity and density of aqueous-solutions of Libr, Licl, Znbr2, Cacl2, and Lino3.1. Single salt-solutions. *Journal of Chemical and Engineering Data*, 39(1):68-72.

Zeng, Y.Y.; Besant, R.W.; Rezkallah, K.S. 1992. Performance of a run-around system using a two-phase, gas-liquid coupling fluid, *ASHRAE Transactions*, 98: 563-573.

Zhang, Y., Jiang, J., Zhang, L. Z., Deng, Y. and Jin, Z., 2000. Analysis of thermal performance and energy savings of membrane based heat recovery ventilator, *Energy,* **25:** 515–527

Zaytsev I. D., and G.G. Aseyev. 1992. Properties of Aqueous Solutions of Electrolytes, *CRC Press,* Boca Raton, FL.

APPENDIX A

CORRELATIONS OF SOLUTION PROPERTIES

A.1 Vapor pressure

Cisternas and Lam (1991) proposed a correlation to calculate the equilibrium VP of several electrolytes in a range of concentrations and temperatures. Their correlation requires a single *"K"* value for each salt and five other parameters for the solvent. Cisternas and Lam (1991) reported *K* values of 111 different electrolytes in their research paper.

This correlation is presented as:

$$\mathrm{L}og\, P_{sol} = KI\left[\mathrm{A} - B/\left(T - 39.53\right)\right] + \left[C - D/\left(T - 39.53\right)\right] \tag{A-1}$$

where for solutions with water as solvent:

$$A = -0.021302 + 3.60591 \times 10^{-4} I + M_s/2303 \tag{A-2}$$

$$B = -5.390915 + 1.382982 I - 0.031185 I^2 \tag{A-3}$$

$$C = 7.192959 - 3.99334 \times 10^{-3} I - 1.11614 E - 4 I^2 + M_s I\left(1 - \chi\right)/2303 \tag{A-4}$$

$$D = 1730.2857 + 0.138481 I + 0.027511 I^2 - 1.79277 \times 10^{-3} I^3 \tag{A-5}$$

$$\chi = 2\left(\nu_+ + \nu_-\right)/\left(\nu_+ Z_+^2 + \nu_- Z_-^2\right) \tag{A-6}$$

where

P_{sol} is the vapor pressure at the solution-air interface [kPa],

T is temperature [K],

M_s is the molecular mass of water [kg/mol],

K is the electrolyte parameter (see Table A.1),

I is ionic strength of the solution (see Table A.1),

ν_+ is the number of moles of cation in one mole of the salt solution,

ν_- is the number of moles of anion in one mole of the salt solution, and

Z_+ denotes the valency of cation and Z_- the valency of anion.

The *K* values of some selected electrolytes are listed in Table A.1.

Table A.1: *K* values, in Equation (A-1).

Component	*K*	*I*
$CaCl_2$	0.32138	2
LiBr	1.00000	1
LiCl	0.72567	1
LiI	1.54354	1
$MgCl_2$	0.37678	2

Conde (2004) introduced a general equation which may be used to predict vapor pressure of solutions of LiCl and $CaCl_2$ in water. This equation can be used for concentrations up to saturation concentration of the mentioned salt solutions for a temperature range of 25-100 ˚C.

Conde (2004) established an accurate formula for prediction of vapor pressure of LiCl and $CaCl_2$ in one specific temperature and then correlated it for other temperatures. This formula may be expressed as:

$$\pi \equiv \frac{P_{sol}(c,T)}{P_{H_2O}(T)} = \pi_{25} f(c,\theta) \tag{A-7}$$

Where c is the weight concentration of the salt in the solution and θ is the reduced temperature by critical temperature of water. The function f is:

$$f(c,\theta) = A + B\theta \tag{A-8}$$

$$A = 2 - \left[1 + \left(\frac{c}{\pi_0}\right)^{\pi_1}\right]^{\pi_2} \tag{A-9}$$

$$B = \left[1 + \left(\frac{c}{\pi_3} \right)^{\pi_4} \right]^{\pi_5} - 1 \tag{A-10}$$

$$\pi_{25} = 1 - \left[1 + \left(\frac{c}{\pi_6} \right)^{\pi_7} \right]^{\pi_8} - \pi_9 e^{-\frac{(c-0.1)^2}{0.005}} \tag{A-11}$$

The π parameters for LiCl and $CaCl_2$ solutions are shown in Table A.2.

Table A.2: π_i parameters in Equations (A-7)-(A-11).

	LiCl	$CaCl_2$
π_0	0.28	0.31
π_1	4.30	3.698
π_2	0.60	0.60
π_3	0.21	0.231
π_4	5.10	4.584
π_5	0.49	0.49
π_6	0.362	0.478
π_7	-4.75	-5.20
π_8	-0.40	-0.40
π_9	0.03	0.018

Several investigations have been performed to correlate equilibrium vapor pressure (or humidity ratio) at the surface of saturated salt solutions (Greenspan, 1977; Wexler, 1954). Humidity ratio at the saturated salt solutions surface is particularly required to investigate the crystallization of salts in the RAMEE system.

Here, an empirical correlation proposed by Greenspan (1977) is introduced that may be applied to calculate the relative humidity at the liquid-air interface of some salt solutions:

$$RH = \sum_{i=0}^{3} A_i t^i \tag{A-12}$$

where:

RH is the relative humidity [%],

t is temperature [˚C], and

A_i coefficients are listed in Table A.3 for the selected salt solutions.

Table A.3: Coefficients in equation (A-12).

Component	A_0	A_1	A_2	A_3
LiBr	7.75437	−0.0654994	-0.420737×10^{-3}	
LiCl	11.2323	−0.00824245	-0.214890×10^{-3}	
$MgCl_2$	33.6686	−0.00797397	-0.108988×10^{-2}	0.761055×10^{-4}

A.2 Viscosity

Zaytsev and Aseyev (1992) correlated the experimental data available for the dynamic viscosity of some binary salt solutions. They proposed the following correlation to calculate the dynamic viscosity coefficient of salt solutions:

$$\log\mu = \log\mu_o + Dc \tag{A-15}$$

where:

μ is dynamic viscosity [Pa.s]

μ_0 is viscosity of pure water [Pa.s]

D is a coefficient given in Equation (A-17), and

c is the weight concentration of the salt solution ($kg_{salt}/kg_{solution}$).

Viscosity of pure water can be calculated using Slott equation (Zaytsev and Aseyev, 1992):

$$\mu_o = 0.59849(43.252 + t)^{-1.5423} \quad for\ t = (0,100\ ^o C) \tag{A-16}$$

The D coefficient depends on the type of salt used in the solution and is calculated from the dependences:

$$D_i = d_0 + d_1 t + d_2 t^2 \tag{A-17}$$

The d_i coefficients are listed for the selected salt solutions in Table A.4. Equation (A-15) is valid for temperatures between 0 and 100 ˚C.

Table A.4: d_i coefficients in Equation (A-17).

Component	$d_0 \times 10^2$	$d_1 \times 10^4$	$d_2 \times 10^5$
$CaCl_2$	148.7	−17.2	0
LiBr	74.5	23.3	0
LiCl	173.7	2.8	0
$MgCl_2$	206.9	−22.5	0

Conde (2004) correlated experimental data available for LiCl-water and $CaCl_2$-water solutions. His correlation is valid for concentrations up to saturation and may be used to calculate the dynamic viscosity at subzero temperatures (as low as -20 ˚C). This correlation is expressed as follows:

$$\mu = \mu_0 e^{\mu_1 C'^{3.6} + \mu_2 C' + \mu_3 \frac{C'}{\theta} + \mu_4 C'^2} \tag{A-18}$$

where C' is defined as:

$$C' = \frac{C}{(1-C)^{\frac{1}{0.6}}} \tag{A-19}$$

The μ_i parameters are shown for two salt solutions (LiCl-water and $CaCl_2$-water) in Table A.5.

Table A.5: μ_i parameters in Equation (A-18).

	LiCl-water	$CaCl_2$-water
μ_1	0.090481	-0.169310
μ_2	1.390262	0.817350
μ_3	0.675875	0.574230
μ_4	-0.583517	0.398750

Muhiuddin and Ismail (1983) have recommended the following correlation to describe the concentration dependence of the viscosity of a $MgCl_2$ solution:

$$\mu = a_0 \exp(b_0 m + c_0 m^2)/1000 \quad \text{(A-21)}$$

where:

m is the concentration of the salt solution [molality], and

a_0, b_0 and c_0 coefficients are listed in Table A.6 at four different temperatures.

Table A.6: a_0, b_0 and c_0 coefficients in Equation (2.20).

T (°C)	a_0	b_0	c_0
15	1.1617	0.3506	18.6401
25	0.9108	0.3574	14.3925
35	0.7408	0.3581	10.8796
50	0.5596	0.3751	3.8780

Correlation of Lee et al. (1990) may be expressed as:

$$\ln\mu = [A_1 + A_2/(T + A_3 \ln T)]/1000 \quad \text{(A-22)}$$

where A_1, A_2 and A_3 coefficients are:

$$A_1 = 16.3967C\text{-}0.14511C^2\text{-}494.122 \quad \text{(A-23)}$$

$$A_2 = 28606.4\text{-}934.568C\text{+}8.52755C^2 \quad \text{(A-24)}$$

$$A_3 = 70.3848\text{-}2.35014C\text{+}0.0207809C^2 \quad \text{(A-25)}$$

A.3 Density

The following equation was developed by Zaytsev and Aseyev (1992) to calculate the density of the salt solutions:

$$\log\rho = \log\rho_0 + (b_0 + b_1 t + b_2 t^2)c \quad \text{(A-26)}$$

where:

ρ is the density of the salt solution [kg/m^3],

ρ_0 is the density of pure water [kg/m^3], and

b_0,b_1 and b_2 coefficients are listed in Table A.7.

Density of pure water may be calculated using the following relation (Zaytsev and Aseyev, 1992).

$$\rho_0 = 1000 - 0.062t - 0.00355t^2, t = (0,100\ ^oC) \quad \text{(A-27)}$$

Table A.7: b_0,b_1 and b_2 coefficients in Equation (A-26).

Component	$b_0.10^4$	$-b_1.10^6$	$b_2.10^8$
$CaCl_2$	3627.0	0.0	14.0
LiBr	3525.0	-229.2	-137.6
LiCl	2452.0	0	1.9
LiI	3743.9	-125.7	-116.1
$MgCl_2$	3523.8	-34.5	0

Correlation of Conde (2004):

$$\rho = \rho_0 \sum_{i=0}^{3} \rho_i \left(\frac{C}{1-C} \right)^i \quad \text{(A-28)}$$

where ρ_i coefficients are listed in Table A.8.

Table A.8: ρ_i coefficients in Equation (A-28).

	$CaCl_2$	LiCl
ρ_0	1.0	1.0
ρ_1	0.836014	0.540966
ρ_2	-0.436300	-0.303792
ρ_3	0.105642	0.100791

Correlation of Novotny and Sohnel (1988):

$$\rho = \rho_0 + A\xi + B\xi t + C\xi t^2 + D\xi^{3/2} + E\xi^{3/2}t + F\xi^{3/2}t^2 \quad \text{(A-29)}$$

where A to F coefficients are listed in Table A.9.

Table A.9: A to F coefficients in Equation (A-29).

	$MgCl_2$	LiBr
$A\times10^{-2}$	0.8099	0.6032
-B×10	1.877	0.0044
$C\times10^3$	2.315	0.2329
-D	6.029	0.6188
$E\times10^2$	7.449	-2.448
$-F\times10^4$	8.305	-1.773

A.4 Specific Heat Capacity

Corrolation of Zaytsev and Aseyev (1992):

$$c_p = (c_{p,0} + B_1 + B_2 C + B_3 t + B_4 t^2) C \tag{A-30}$$

where

c_p is the heat capacity [J/(kg·K)]

B_i coefficients are listed in Table A.10 and

$c_{p,0}$ is the heat capacity of pure water and can be calculated from:

$$c_{p,0} = 4217.591 - 371.6753t + 1436.422t^2 - 3043.413t^3 + 3819.384t^4 - 2538.933t^5 + 696.99867t^6 \tag{A-31}$$

Table A.10: B_i coefficients in Equation (A.30).

Component	$-B_1$	B_2	B_3	$-B_4 \times 10^3$
$CaCl_2$	6360.2	4706.8	7.2	12.5
LiBr	5277.4	2568.4	2.8	16.1
LiCl	5016.3	4248.9	-3.4	15.9
$MgCl_2$	6304.3	3082.9	7.9	13.9

Correlation of Conde (2004):

$$c_p = c_{p,0} (1 - f_1(C) \times f_2(\theta)) \tag{A-31}$$

where:

$$f_1(C) = A_a C + B_a C^2 + C_a C^3 \tag{A-32}$$

$$f_2(\theta) = F_a \theta^{0.02} + G_a \theta^{0.04} + H_a \theta^{0.06} \tag{A-33}$$

where:

$$\theta = \frac{T}{228} - 1 \tag{A-34}$$

A_a to H_a coefficients are listed in Table A.11.

Table A.11: Parameters in Equations (A.32) and (A.33).

Component	A_a	B_a	C_a	D_a	G_a	H_a
$CaCl_2$	1.63799	-1.69002	1.05124	58.225	-105.6343	47.7948
LiCl	1.43980	-1.24317	-0.12070	58.522	-105.6343	47.7948

A.5 Thermal Conductivity

Correlation of Zaytsev and Aseyev (1992):

$$k = k_0(1-\beta C) \tag{A-35}$$

where:

k is the thermal conductivity of the solutions [W/(m·K)]

β coefficients are listed in Table A.12.

k_0 is the thermal conductivity of pure water [W/(m·K)] and can be calculated from:

$$k_0 = 0.5545 + 0.00246t - 0.00001184t^2 \tag{A-36}$$

Table A.12: β coefficients in Equation (A-37) for the selected salt solutions.

Component	β
$CaCl_2$	182.1
LiBr	526.1
LiCl	344.5
$MgCl_2$	477.9

Correlations of Conde (2004):

The thermal conductivity of LiCl and $CaCl_2$ solutions may be calculated using the *"equivalent thermal conductivity depression (α_R)"* term:

$$\alpha_R = \frac{k_0 - k}{C_{eq}} \tag{A-37}$$

where:

C_{eq} is the "equivalent ionic concentration" and can be calculated from:

$$C_{eq} = \frac{C \times \rho \times I}{M} \tag{A-38}$$

where:

M is the molar mass of the salt solution [kg/mol],

I is the ionic strength of the solution, and

ρ is the density of the salt solution [kg/m^3]

The equivalent thermal conductivity depression may then be calculated from:

$$\alpha_R = \alpha_0 + \alpha_1 C \tag{A-39}$$

where:

α_i coefficients are listed in Table A.13.

Table A.13: α_i coefficients in Equation (A-39) for the selected salt solutions.

Component	α_0	α_1
$CaCl_2$	5.9473×10^{-3}	-1.3988×10^{-3}
LiCl	10.8958×10^{-3}	-11.7882×10^{-3}

A.6 Diffusion Coefficient

Correlation of Conde (2004):

$$D = D_0 \left\{ 1 - \left[1 + \left(\frac{\sqrt{C}}{\delta_1} \right)^{\delta_2} \right]^{\delta_3} \right\} \tag{A-40}$$

where:

D is the diffusion coefficient of water into the salt solution [m^2/s]

D_0 is the self diffusion coefficient of water [m^2/s]

δ_i coefficients are δ_1=0.52, δ_2= -4.92, δ_3= -0.56 for solutions of LiCl δ_1=0.55, δ_2= -5.52, δ_3= -0.56 for solutions of $CaCl_2$.